Simulation Study on the Running Behavior of the 4L Bogie

Project Report

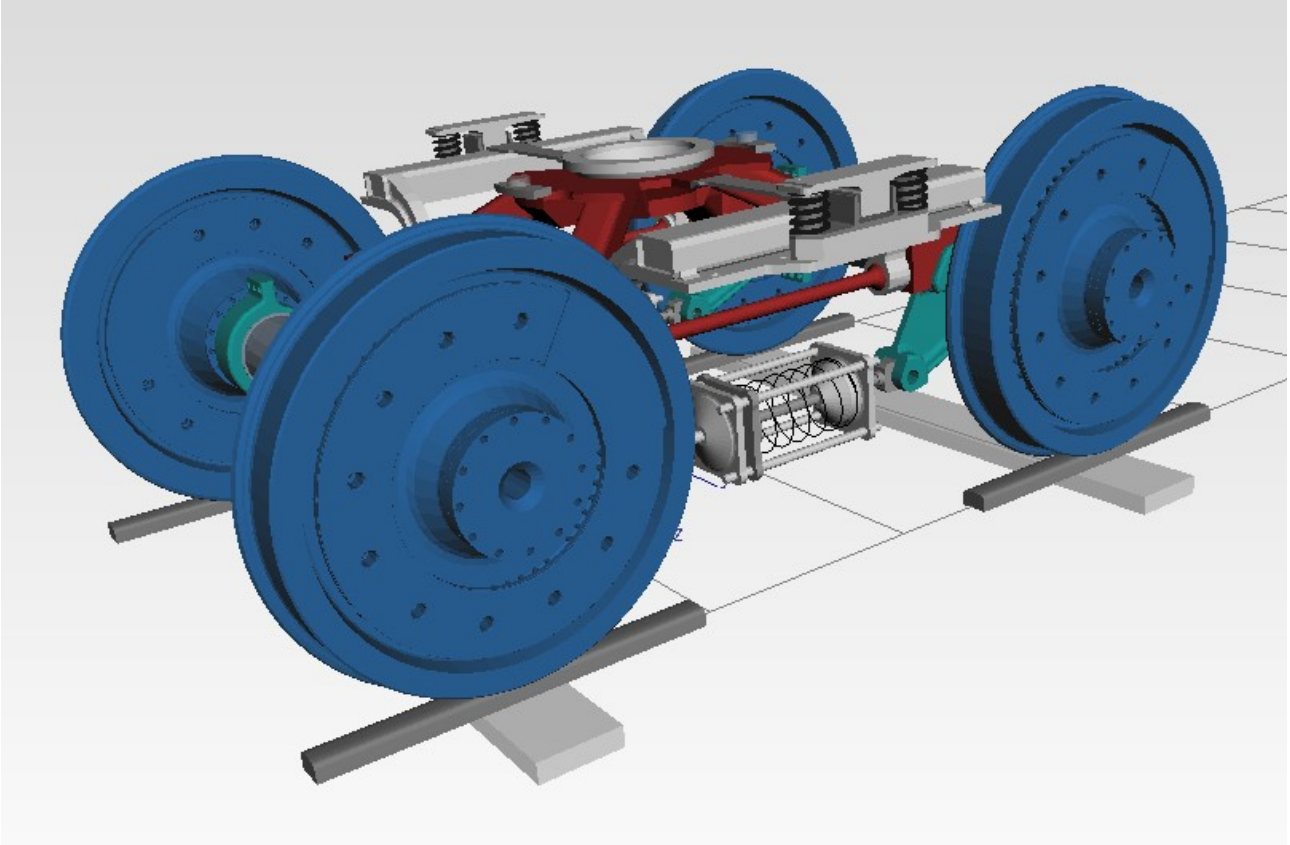

12. Apr. 2021

DLR

German Aerospace Center (DLR)
Institute of System Dynamics and Control (SR)
Robotics and Mechatronics Center (RMC)
Head of Institute: Prof. Dr.-Ing. Johann Bals
Münchner Straße 20, Geb. 135
82234 Weßling, GERMANY
Tel +49 (0)8153/28-2461
Fax +49 (0) 8153/28-1441

Dr.-Ing. Gerhard Hippmann
Tel +49 (0)8153/28-4646
E-Mail gerhard.hippmann@dlr.de

Alexander Poßeckert, M. Sc.
Tel +49 (0)8153/28-1740
E-Mail alexander.posseckert@dlr.de

Title	4L Bogie: Project Report	
Keywords		
Accesses	DLR; Swiss Federal Office for the Environment (BAFU)	
Authors	Dr. Gerhard Hippmann, Alexander Poßeckert	
Contribution	Dr. Andreas Heckmann	
Version	**Commentary**	**Date**
2.1	Report with corrected fig. 25 and 26	12. Apr. 2021
2.0	Final report	9. Apr. 2021
1.1	Report preview	6. Apr. 2021
1.0	Interim report complete	17. Dec. 2020
0.1	Interim report preview	11. Dec. 2020
Last saved	12. Apr. 2021 by Gerhard Hippmann	

Table of Contents

1 Introduction

The 4L Bogie is a new freight wagon bogie concept which promises reduced noise and wear compared to the standard Y25 Bogie. Its main features are inside frame wheelsets, a suspension system with coupled swinging axle bridges and a rather light weight "four leg" (therefrom "4L") frame which contributes flexibility to the system. Today there are several publications about the 4L Bogie design [9][11][10] and it is available as CAD model, but real world prototypes do not yet exist.

The Swiss Federal Office for the Environment (BAFU) is interested in the 4L Bogie for lower freight train noise emissions and considers to join the project. As a precondition its running characteristics is examined by a simulation study in this work.

This report is structured in three parts. In chapter 2 the simulation model is described. Chapter 3 documents the simulation scenarios and presents the simulation results. And chapter 4 evaluates the simulation results.

2 Simulation Model

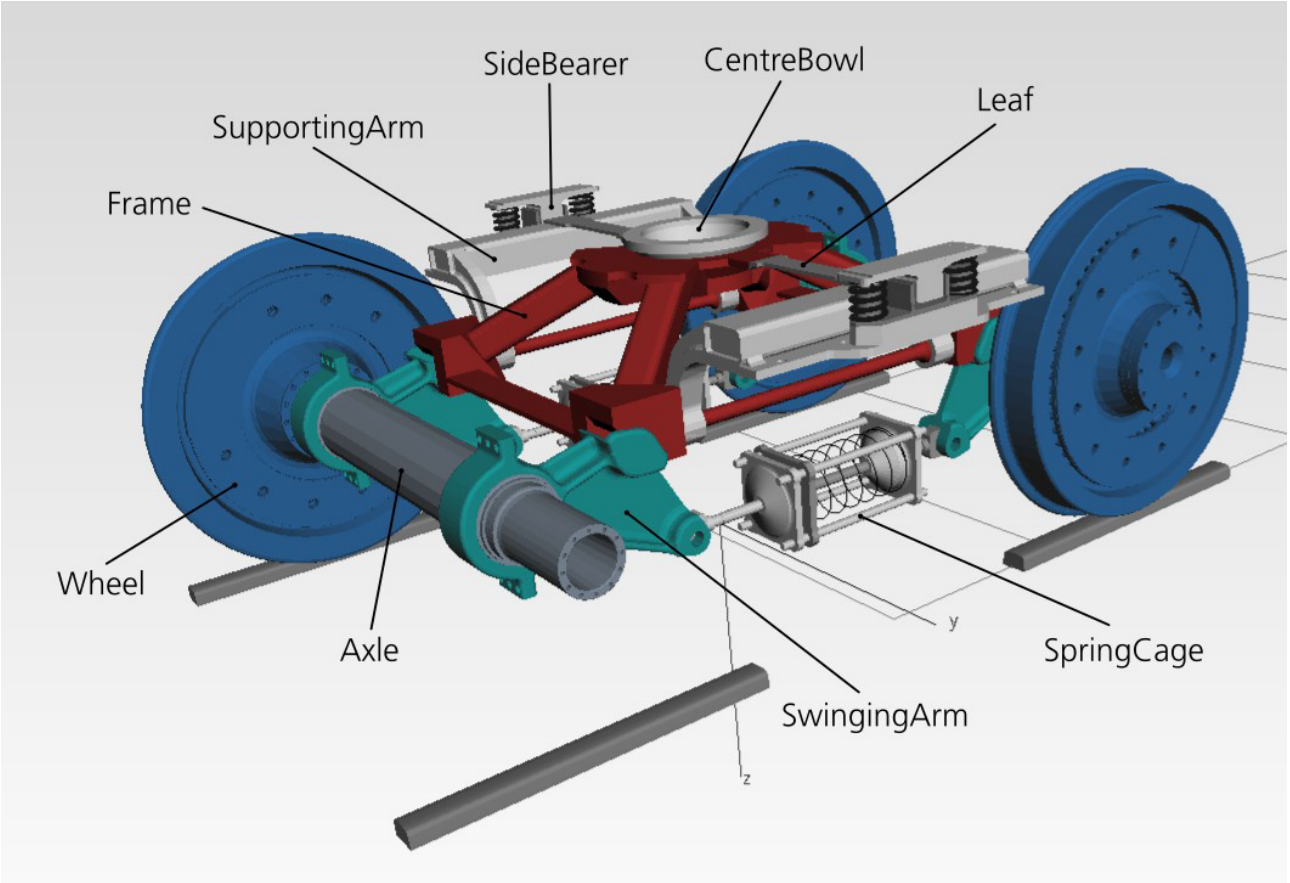

Figure 1: Components of the 4L Bogie.

The 4L Bogie and hence its simulation model is composed of a quite small number of components (Figure 1):

- The Frame is the central platform of the system.
- Each of the two Axles is connected to the frame by two SwingingArms with hinges.
- The Wheels are connected to the Axles by rolling bearings. Left and right Wheel can be coupled by a rigid shaft (standard wheelset) or with a torque limiter (AIR wheelset [8]).
- SpringCages on both sides act as compliant suspension elements converting tension loads into compressive spring forces.
- Two SupportingArms carry the SideBearers and the BrakeCallipers. Each of them is connected to the Frame by two hinges and a tension rod called Leaf.
- The CentreBowl resides on the top of the Frame.

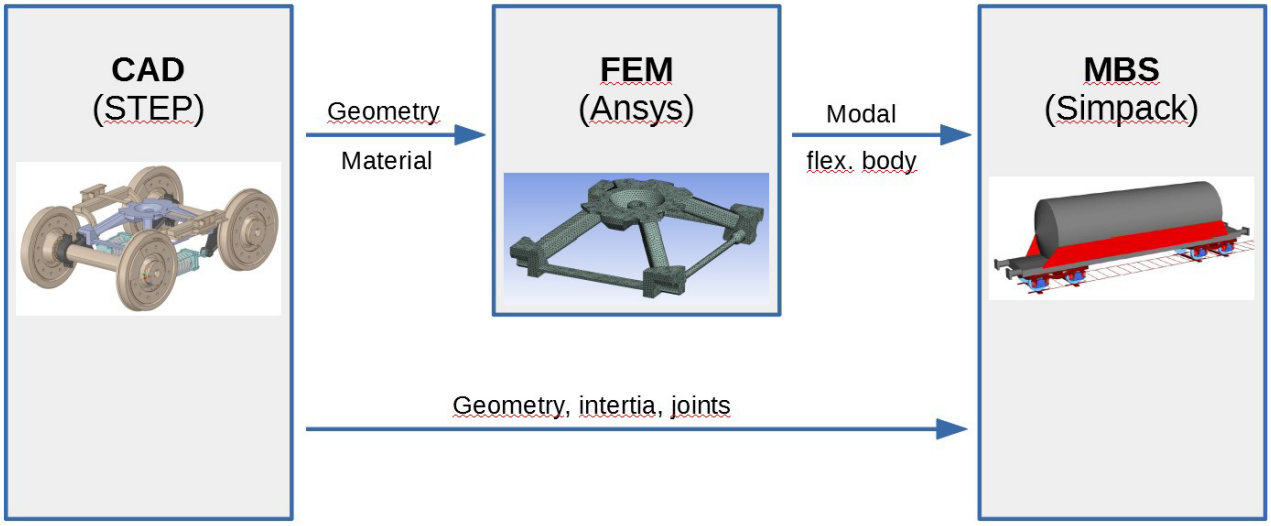

Figure 2: Process of creating an MBS model containing a flexible body.

The steps for building up the multibody system (MBS) model are illustrated in Figure 2. CAD data was kindly provided by the University of Florence. From this, input data such as geometry, inertia and positions of connecting points (markers) have been exported and implemented in the MBS software Simpack [15]. For the bogie Frame, an intermediate step using the Finite Element Method (FEM) was necessary due to the requirement of flexible body modeling.

2.1 Frame FEM Model

This section explains the procedure of including the flexible bogie frame into the MBS. In three subsections the essential operations are described: Meshing, modal analysis and the reduction of the FE-Model.

The frame is made of S355 steel [11]. A Young's modulus of 200 GPa and a Poisson's ration of 0.3 was chosen.

2.1.1 Meshing

Before performing a Finite Element Analysis, the bogie Frame had to be meshed, see Figure 3. This has been done using tetrahedral solid elements (element type SOLID187 [14]). The elements have an average edge length of 10 mm, which corresponds to the wall thickness of the Frame legs. This resulted in a FEM model with approximately 1.2 M degrees of freedom.

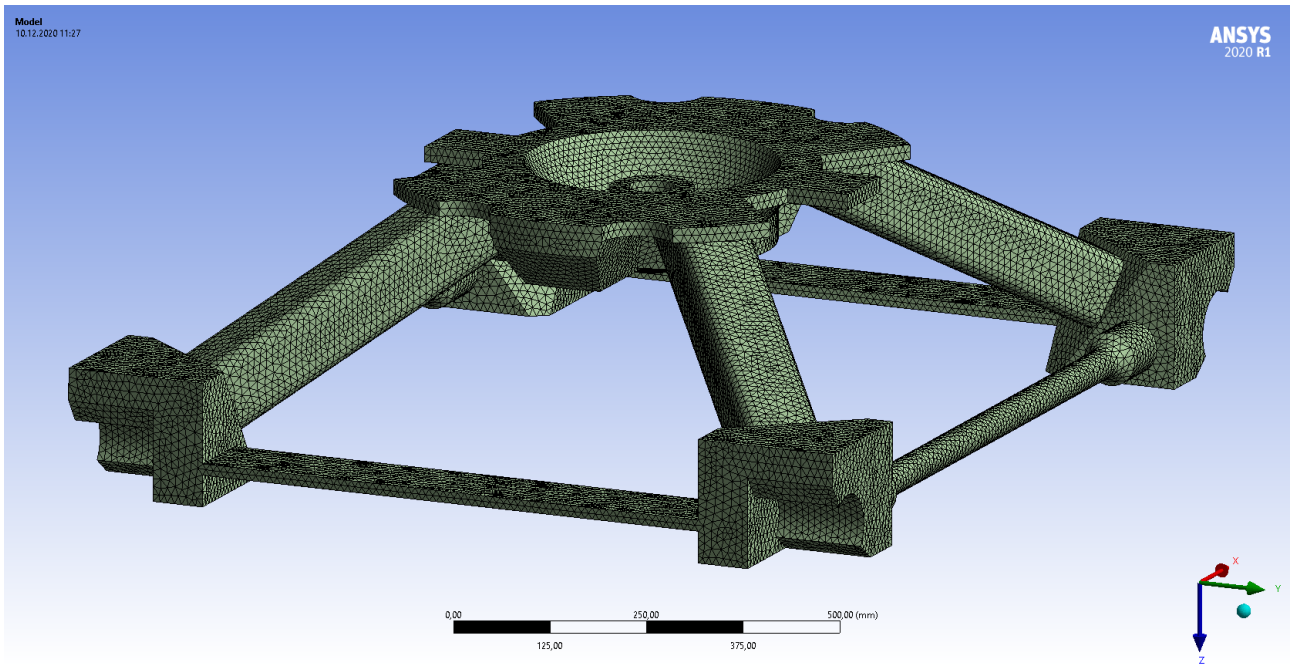

Figure 3: Meshed bogie-frame.

To check convergence, the analysis described in this section has been repeated with an element edge length of 5 mm. Up to a frequency of 800 Hz, no larger differences of the calculated natural frequencies were detected (error <1 %). It is assumed that the excitation of the bogie due to track irregularities at a frequency that is higher than 800 Hz can be neglected. Therefore a finer mesh has not been considered.

2.1.2 Modal Analysis

The model described in section 2.1.1 has been used to perform a modal analysis in order to determine eigenfrequencies and eigenmodes. Since the bogie is not fixed anywhere, six rigid body modes appear.

The top image of Figure 4 shows the 7th eigenmode (the first one above the rigid body modes). The Frame twists around the x-axis, which is equivalent to the running direction. Due to the structure of the bogie, this kind of deformation is necessary when driving along a twisted track. Otherwise one of the wheels could be relieved more than allowed raising the risk of derailment. The smaller images of Figure 4 show the normal modes starting from No. 8 to No. 13.

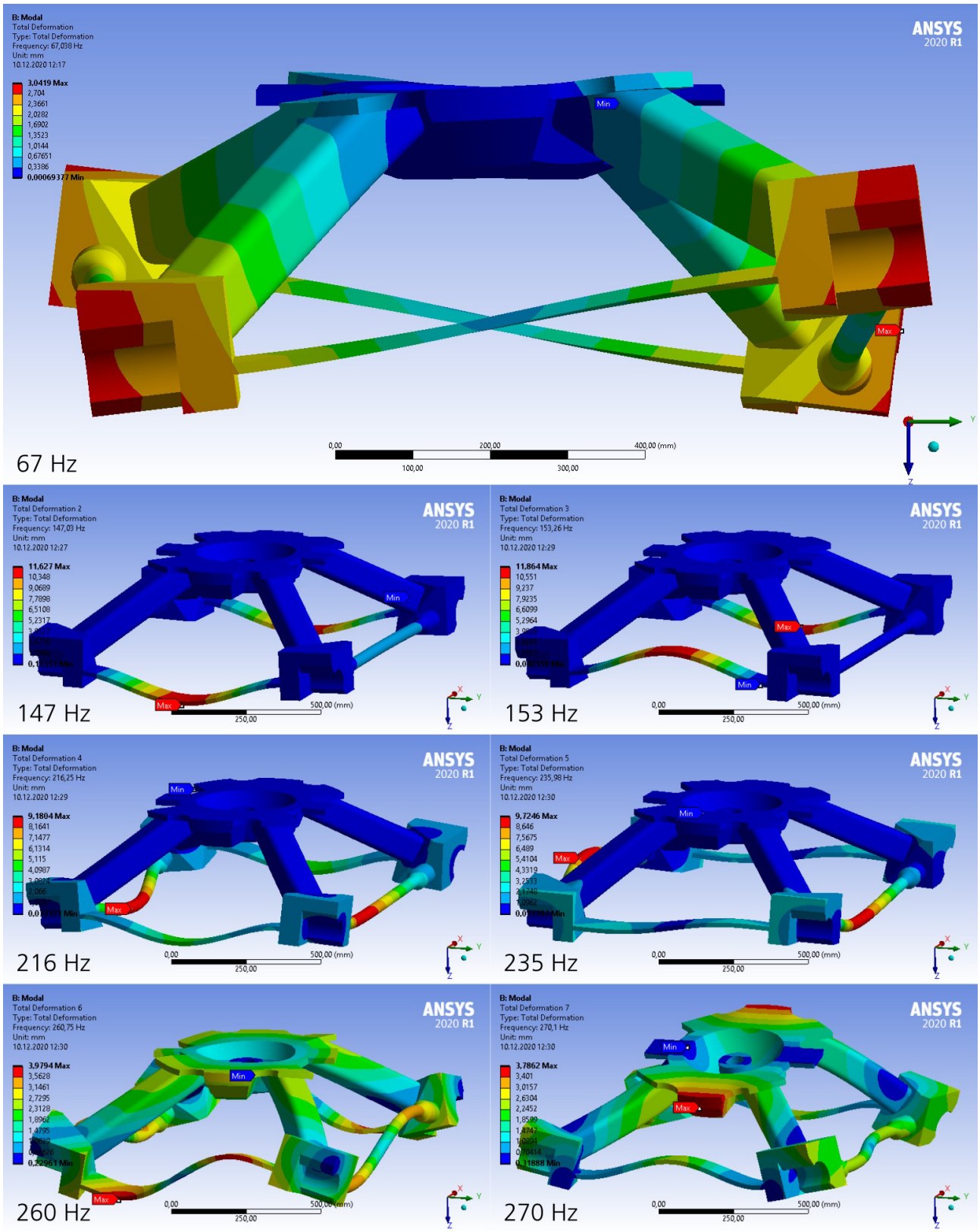

Figure 4: Frame eigenmodes No. 7 to No. 13. Driving direction (x-axis) is normal to the image.

2.1.3 Reduction of FE-Model

The model presented in section 2.1.1 cannot be used in multibody simulation software directly because of its large number of degrees of freedom. In order to reduce the computational effort, the model has been condensed using the Craig-Bampton method.

To do so, the following steps have been performed:

1. Definition of interface nodes that serve as links to the MBS model. These nodes are needed at each connection of the bogie to other components (e.g. SwingingArms, SupportingArms, etc.).
2. Definition of couplings to connect interface nodes to the bogie. For example Figure 5 shows an interface node which is located on the axis of rotation between the Frame and a SwingingArm. A coupling between node and the bogie surface is established via force distributing constraint element [13].

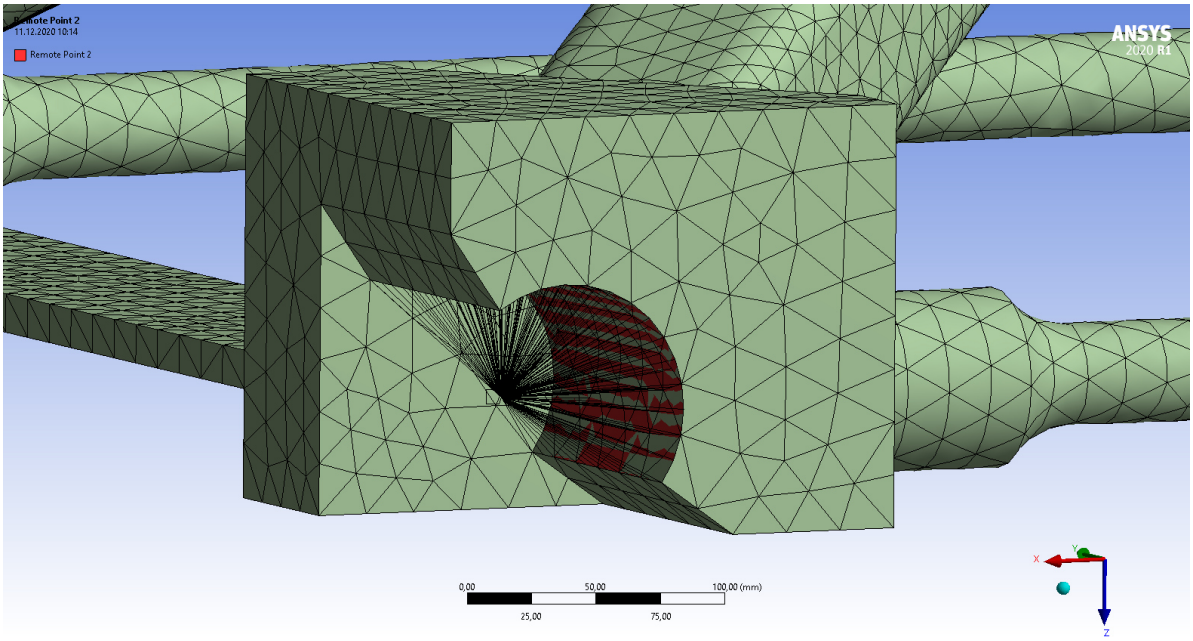

Figure 5: Interface node for SwingingArm hinge.

3. Perform Craig-Bampton method [1]. Besides the constraint modes, which are determined by the definition of interface nodes, one has to select the number of dynamic modes to be computed (here 30 modes were selected).

The condensed model can be imported in the MBS software. To verify the reduction process, the eigenfrequencies of the condensed model have been compared to those which were calculated using the full scale model of section 2.1.2. Up to 500 Hz, no larger differences have been detected.

2.2 Bogie MBS Model

2.2.1 MBS Structure

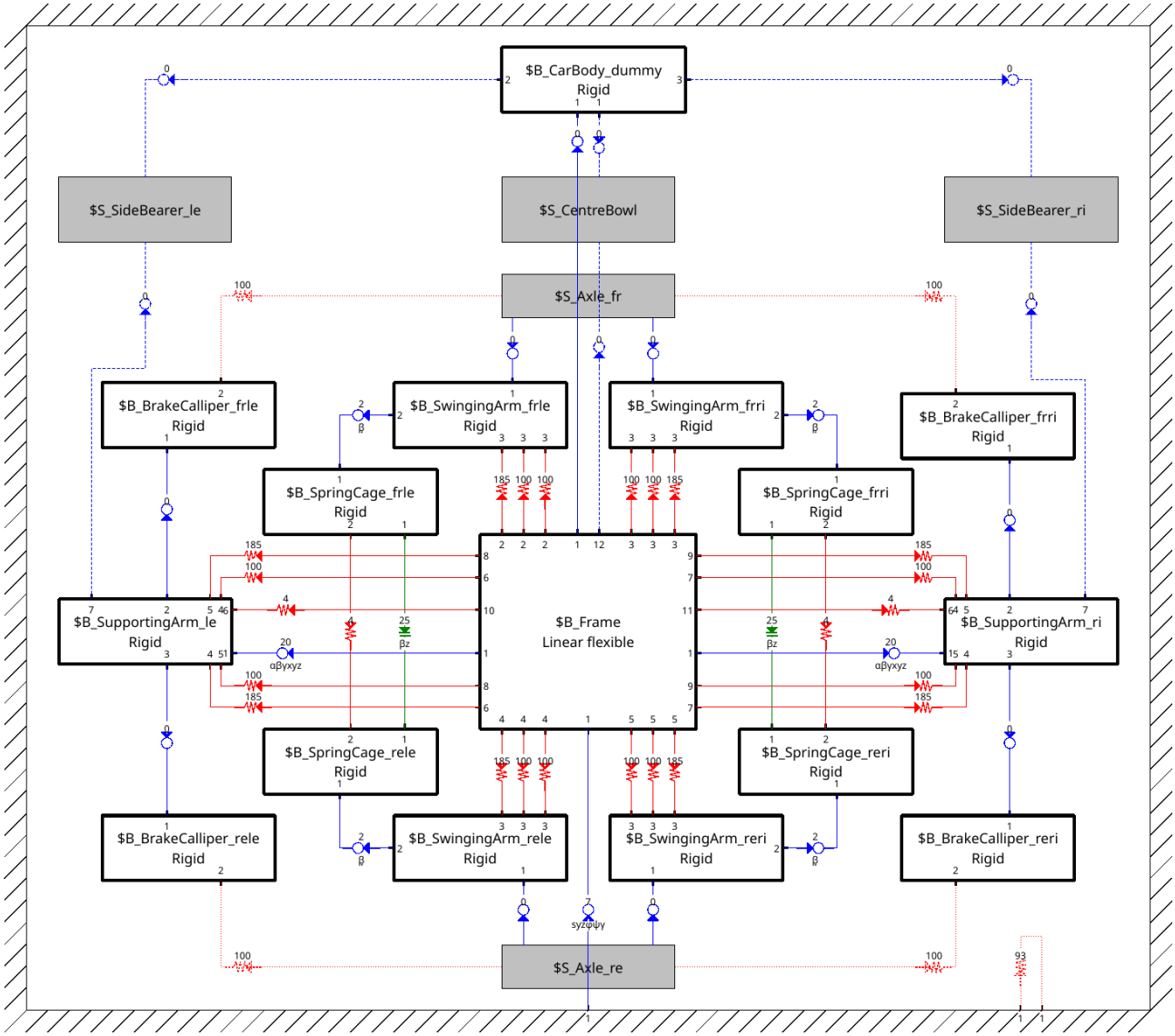

Figure 6: 2D view of the 4L Bogie MBS model.

The structure of the MBS model is visualized as 2D view in Figure 6. White boxes represent bodies, blue and green lines kinematic connections and red lines force elements. Gray boxes are used for substructures which are MBS models themselves.

The bodies are similar to those in Figure 1. However, the SpringCages consist of two bodies (front and rear part) and there are additional BrakeCallipers (not visualized in Figure 1) and a massless dummy Body which simplifies connecting the bogie to the CarBody. Only the Frame is modeled as modal flexible body, all other bodies are rigid.

2.2.2 Geometry

MBS models use markers which represent positions and orientations on bodies as virtual coordinate frames. Other MBS elements like kinematic connections, force elements or sensors always refer to markers (represented by numbers in the body boxes of Figure 6). So markers are essential for the geometry definition of MBS models.

For this project the markers required for the MBS model have been identified resp. defined in the CAD model and their coordinates have been introduced as parameters (substitution variables) in the MBS. This geometry data is listed in appendix A.1.

2.2.3 Mass Properties

MBS simulation is based on the equations of motion of the system. As a consequence the mass properties of the bodies play a prominent role. Translational dynamics of a body requires its mass and its center of gravity position, rotational dynamics its moments and products of inertia.

Similar to the geometry data, the mass properties have been exported from the CAD model. For this the density of all bodies has been set to the value of steel (7.86 g/cm³). Since the BrakeCallipers were not available as volume parts, their mass and center of gravity have been taken from an engineering drawing of the manufacturer [7]. The resulting mass properties data is listed in appendix A.2.

2.2.4 Connections

Connections are used to define interactions of the bodies. Kinematic connections represent ideal joints which lock certain translational and/or rotational relative motions. They do not convert potential or dissipative energy. On the other hand force elements can be used to model compliant connections which may introduce clearance, damping and/or friction. The parameter values of the force elements are listed in appendix A.3.

Frame – SwingingArm

The hinges between the Frame and the SwingingArms are important for the running behavior of the bogie since they play a central role in the suspension system. They are modeled by three force elements:

- A cylindrical bushing introduces compliant restrictions in radial and axial directions of the hinge. The stiffness values have been estimated such that full load (ca. 100 kN) results in a negligible deformation of 0.1 mm. In axial direction clearance of 2 mm is defined such that free flexible deformation corresponding to the elastic limit of the Frame is enabled. The axial distance of the SwingingArm markers is chosen 0.228 mm (i.e. static Frame elongation at 75 % loaded wagon) larger than at the Frame to consider improved load distribution caused by bearing wear.

- Two friction elements model regularized Coulomb friction for the rotational and axial motion of the hinge. The applied friction coefficient of 0.3 has been taken from [10].

Since the axle bridges (consisting of the rigidly connected bodies Axle, left and right SwingingArm) behave like rigid bodies, their rotations in the y-plane are restricted by the lateral moment arm of the two hinges. So no rotational stiffness is required in the force elements and according flexible deformations of the Frame are not interfered.

Frame – SupportingArm

The SupportingArms are also connected to the Frame by a pair of hinges. These are modeled similar to those of the SwingingArms. The main difference is that axial contact is only considered at the outer side of the hinges.

- The cylindrical bushing is modeled with axial clearance of 2 mm again.
- A friction element introduces regularized Coulomb friction in axial direction.

Leaf

The rotation of the SupportingArms is restricted by Leafs which are designed as slightly compliant pull rods. These are modeled as spring-damper force elements. Their stiffness value has been calculated assuming a steel rod of 70 mm x 10 mm cross section area of 290 mm length.

BrakeCallipers

The BrakeCalliper units are connected to the SupportingArms by rigid connections.

SpringCage

The front and rear parts of the SpringCages are connected to the SwingingArms by ideal rotational joints. Another kinematic connection represents the prismatic guidance of the SpringCage. A force element with non-linear force law (Figure 7) due to [11] models the compression spring of the suspension.

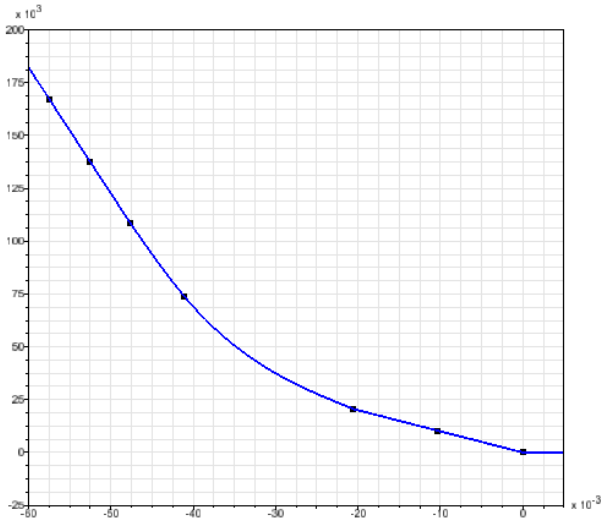

Figure 7: Suspension spring force [N] vs. deflection [m].

2.2.5 Substructures

Axle

In the Axle submodel the Wheels are connected to the Axles by ideal rotational joints. As described in [8] there are two options for the rotational connection between left and right Wheels:

- A rigid shaft results in a conventional wheelset.
- A shaft with torque limiter yields an Apparently Independently Rotating (AIR) wheelset which promises improved wear and running behavior in small radius curves.

Since no torque limiter force element is available in Simpack, a user element has been implemented. Its characteristics represents a rotational spring which changes its unloaded torsion angle when the maximum torque is exceeded. Figure 8 shows the force law by a sinusoidal angle excitation for a limit torque of 4 kNm and rotational stiffness of 882 kNm/rad.

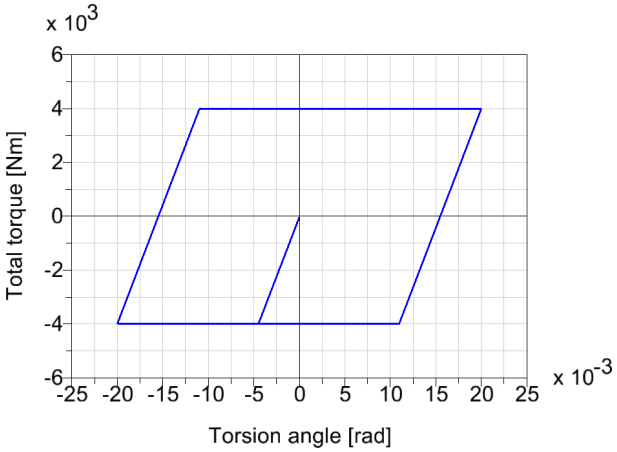

Figure 8: AIR torque limiter force law.

SideBearer

The 4L Bogie provides the same CarBody interface as the standard Y25 Bogie, i.e. a center bowl and two lateral side bearers. So these components have been taken over from a former freight bogie project [3] to avoid duplicate modeling and validation work.

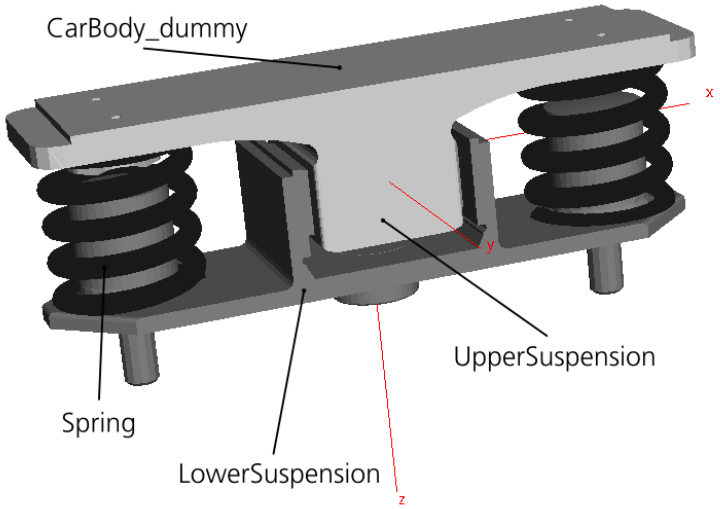

Figure 9: SideBearer MBS submodel.

The SideBearer submodel consists of three parts (Figure 10): The lower suspension body is fixed at the SupportingArm of the bogie. It carries the upper suspension body by two vertical springs. A third dummy body is fixed to the CarBody and represents its planar contact to the side bearer.

The springs of the suspension are modeled by a bushing force element. In addition bumps stops in vertical and longitudinal direction are represented by unilateral spring-dampers. Another force element introduces regularized Coulomb friction with a friction coefficient of 0.22 between CarBody and side bearer top.

CentreBowl

The CentreBowl submodel is also based on [3]. It approximates the spherical contact between the lower hollow half sphere on the bogie Frame and the upper half sphere at the CarBody by three contact pair definitions. Each of them uses a downsized virtual sphere surface on the CarBody side such that the areal contact of the center bowl is modeled by three well defined points contacts (Figure 10). Unilateral contact force elements introduce normal and tangential forces. Again a friction coefficient of 0.22 is assumed.

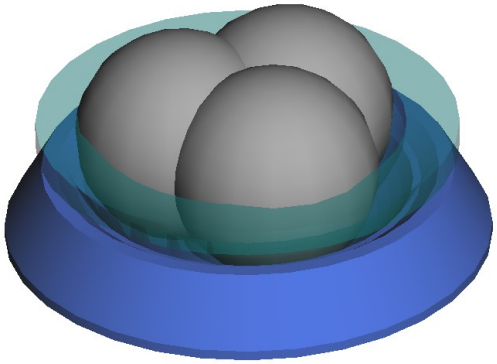

Figure 10: Three point contact of the CentreBowl submodel.

In addition rotational compliance of the upper part with respect to the CarBody is modeled by a spherical joint and a rotational bushing in parallel.

As a particularity the suspension system of the 4L Bogie does not prevent pitch motion of the Frame. So two different pitch locking mechanisms are proposed in [12], i.e. four side bearers in rectangular arrangement or pitch bearers as centre bowl extension. The latter solution has been implemented in the CentreBowl submodel as additional unilateral point contacts at the front and rear (Figure 11). Their clearance is chosen such that it almost vanishes when the wagon is fully loaded. In case of contact a friction coefficient of 0.22 is considered.

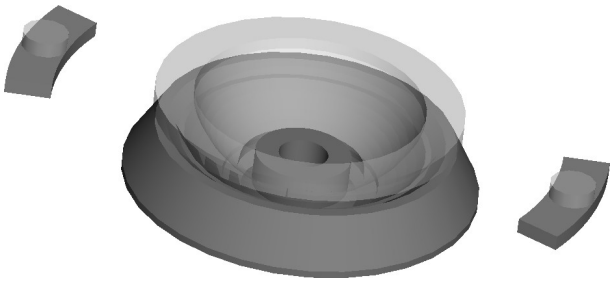

Figure 11: CentreBowl with pitch bearers.

2.3 Wheel, Rail and Track

2.3.1 Rail-Wheel Contact

In all simulations of this study a standard configuration of the contact between rails and wheels is used. The rails are modeled with UIC 60 profile and a cant value of 1/40. The wheels have a nominal radius of 460 mm and S 1002 profile.

The normal contact forces are calculated by Simpack's "Discrete Elastic Contact" method [15] which is based on [2]. The Young's modulus is 210 GPa, the Poisson number 0.28 and the

reference damping value 100 kNs/m. For the tangential forces the FASTSIM method is used with a discretization of 11x11 elements. The friction coefficient is 0.4.

2.3.2 Track

The track gauge is 1435 mm. Compliance and inertia of the track bed are modeled by ballast bodies beneath each wheelset. Simpack's standard values are used for mass properties (A.2.10), stiffness and damping (A.3.7) [15].

2.3.3 Rail Irregularities

In most simulation scenarios of this study the vehicle is excitated by rail irregularities defined by "ERRI B176 high" [15]. For this according predefined power spectral densities are used to calculate generic irregularity signals in lateral, vertical and roll direction and gauge by inverse Fourier transformation with 417 equidistant frequencies in the range of 1/25 m to 1/3 m. Finally the resulting signals are applied as track-related irregularities between track ballast bodies and rails.

For comparison with DIN EN 14363 [6] the track-related irregularities have been converted to rail-related. So standard deviations of 1.97 mm in vertical and 1.22 mm in lateral direction have been determined. These values comply with the proposed ranges of the norm, i.e. 1.80..2.50 mm in vertical and 1.05..1.45 mm in lateral direction.

2.4 Freight Wagon MBS Model

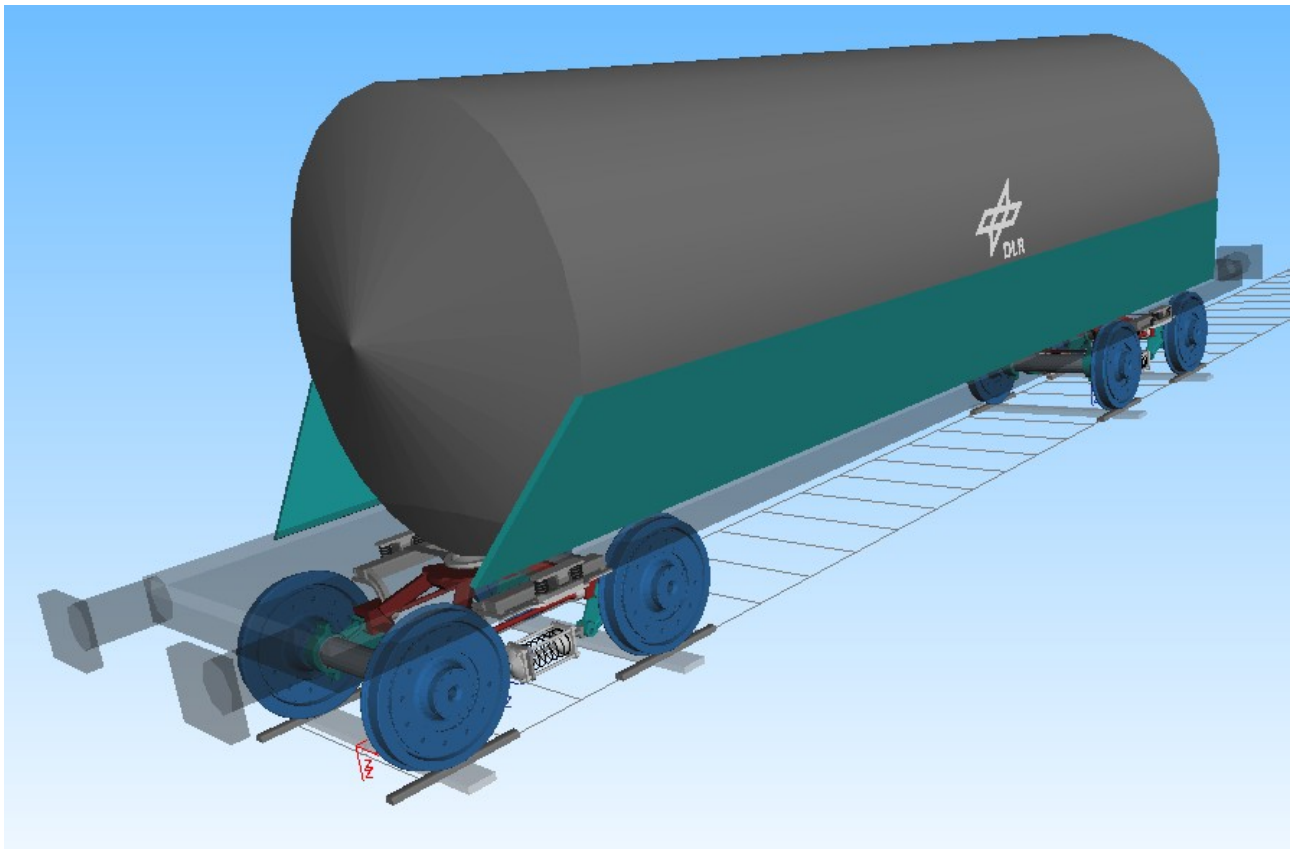

Figure 12: Tank wagon MBS model with 4L Bogies.

For running behavior analyses always a complete rail vehicle is considered. Hence the simulation model must consist of a full freight wagon with two 4L Bogies. Again suitable data from [3] has been reused, i.e. a rigid car body model of a standard 57 m³ tank wagon with a center bowl distance of 8.8 m which normally is carried by Y25 Bogies.

The CarBody is parameterized with a load factor that allows to approximate its mass properties. So arbitrary loading conditions resp. axle loads can be adjusted as required for the running behavior simulation study.

In all simulation scenarios the wagon is tested standalone, i.e. coupling forces of adjacent vehicles are neglected. Its velocity resp. driving force is considered by kinematic guiding of the CarBody in longitudinal direction while the point of attack is located in the center of the wagon, 1.0 m above the rails.

3 Simulation Scenarios and Results

Two different loading conditions are used in the simulation scenarios: In "tare" state the load factor is chosen such that the axle load is 5.75 t, i.e. the total wagon weight is 23 t. And "laden" stands for an axle load of 22.25 t resp. wagon weight of 89 t. The corresponding mass properties are listed in A.2.11.

3.1 Suspension Preloads

The CAD model represents the bogie in its nominal state. The preload determination described in this section yields the preloads of the suspension springs such that the bogie is in static equilibrium for the tare wagon.

For this a modified bogie submodel with an additional test body has been used. The body has half of the tare CarBody mass (i.e. 7480.7 kg) and is fixed to the CentreBowl at the center of the bogie. With this configuration a preload simulation has been executed resulting in suspension spring forces of 24350 N. An inverse evaluation of the non-linear spring force law (Figure 7) yielded a corresponding spring deflection of 22.951 mm. This value is used as nominal force parameter of the suspension spring force elements in all simulations.

3.2 Braking Tests

Braking scenarios have been simulated to study the dynamics of the 4L Bogie when braking in tare and laden state on a straight track without irregularities. For this wheel disc brakes have been modeled by force elements which apply Coulomb friction forces between the brake pads and discs with a friction coefficient of 0.39.

Figure 13 shows the assumed brake pad normal force (16 kN resp. 45 kN building up within 3 s) and the resulting vehicle velocity over time starting at 120 km/h. Constant deceleration stops the wagon after 27 resp. 34 seconds.

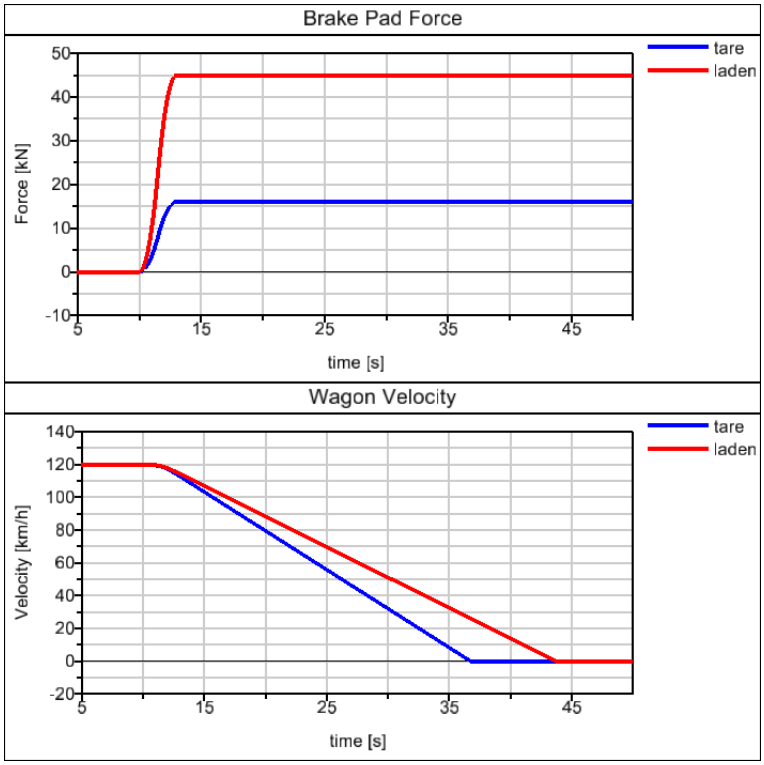

Figure 13: Brake pad force and wagon velocity of the braking tests.

As already mentioned in 2.2.5 braking is of interest for the 4L Bogie because it is equipped with additional pitch bearers at the CentreBowl to avoid large pitch motion of the Frame. During braking the reaction forces of the CarBody, axle bridges and BrakeCallipers result in a moment that aims to raise the Frame at the front. This motion is blocked by the pitch bearers pictured in Figure 11.

The upper plot of Figure 14 shows the relative pitch angles between front and rear bogie Frame and the CarBody. The lower plot shows the normal forces at the front pitch bearers. The simulation results verify the functionality of the pitch bearers and give an estimate of their – quite high – quasistatic loads.

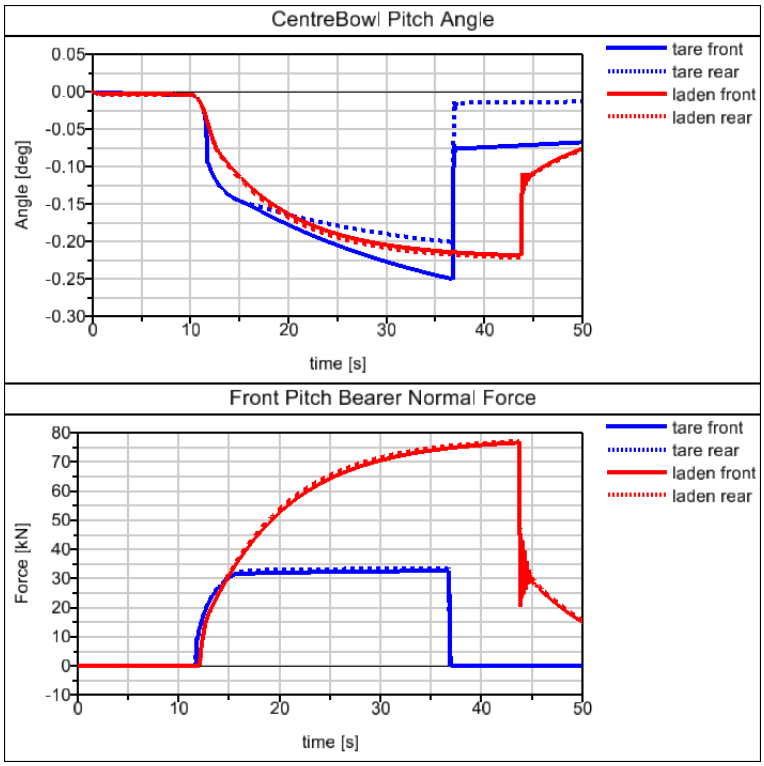

Figure 14: CentreBowl pitch angle and pitch bearer normal force of the braking tests.

3.3 Derailment Tests

The 4L Bogie's safety against derailment has been tested on a twisted track according to DIN EN 14363 [6] chapter 6 method 1. For this the wagon runs slowly (5 km/h) through a small radius curve (150 m) varying the outer rail superelevation from positive (+45 mm) to negative (-45 mm) cant within 30 m. In this scenario no rail irregularities have been considered.

Assessment is made for the maximum wheel lift and derailment coefficient values of the front axle outer wheels. The test is successful if wheel lift does not exceed 5 mm

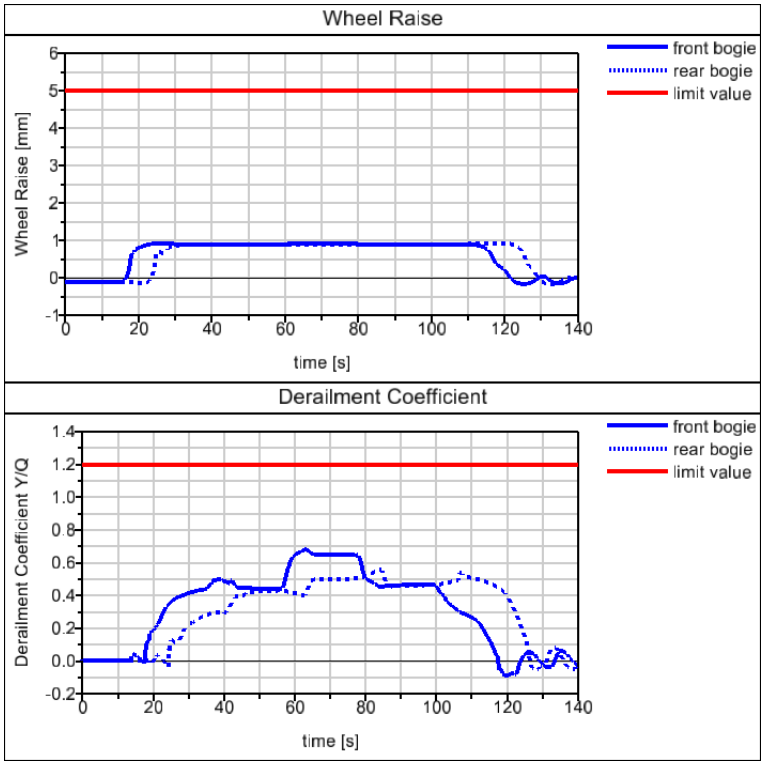

Figure 15: Front outer wheel lift and derailment coefficient of the tare derailment test.

and derailment coefficient does not exceed a limit value of 1.2.

The derailment test has been simulated in tare and laden condition. Figure 15 and Figure 16 show the results for both cases. Obviously the vehicle stays clearly below the limit values. As expected all other wheels yield even lower values. Interestingly the results in tare and laden conditions are very similar.

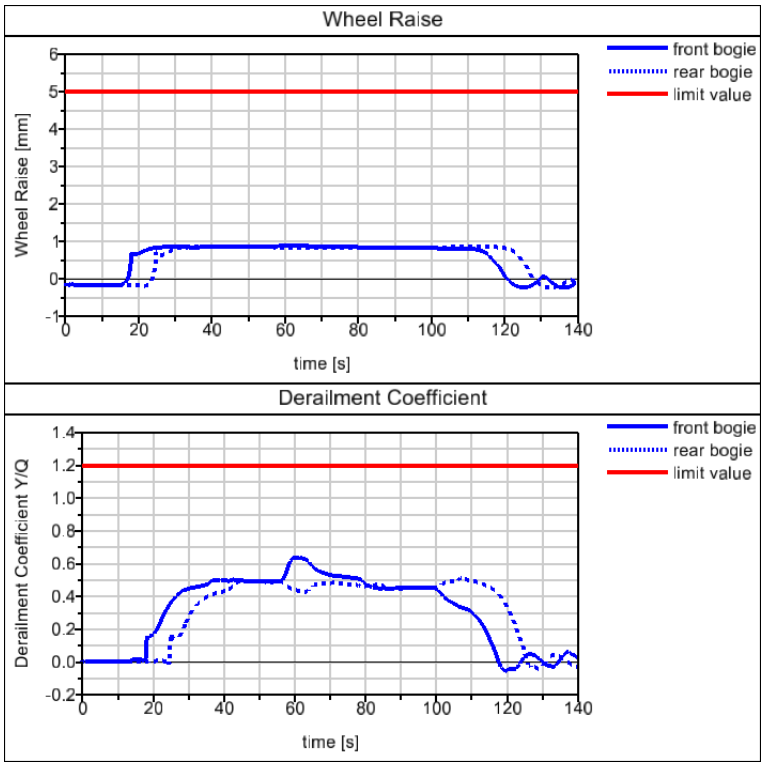

Figure 16: Front outer wheel lift and derailment coefficient of the laden derailment test.

This test result verifies that the flexible Frame model works as designed, because longitudinal torsion of the bogie axles can only develop from flexible deformation of the Frame. The test has also been performed with brakes enabled as in 3.2 to check the influence of the pitch bearer friction forces on the derailment qualities. No significant changes have been observed in this case.

3.4 Running Stability Tests

Running stability of the 4L Bogie has been assessed according to DIN EN 14363 [6] chapter 7 while on-track tests have been replaced by simulations. For this the vehicle runs on tangent track and very large radius curves at 10 % above its admissible velocity. In this study the latter is assumed as 120 km/h, so a test speed of 132 km/h has been chosen for the stability assessment.

A synthetic test track constructed of two curves with radii of -/+11 km and a long straight section has been used. The wagon covers a distance of 10.4 km in 283.6 s. As described in 2.3.3 rail irregularities according to "ERRI B176 high" are considered. The test has been performed in tare and laden condition.

The stability of the vehicle is assessed by limit values for the sum of the lateral wheel-rail forces of each wheelset. The simulation yields time histories of this quantity with a sampling frequency of 200 Hz. As proposed in [6] a band pass filter with cut-off frequencies 0.4 Hz and 4.4 Hz has been applied to the signals. After this sliding RMS values with window lengths of 100 m have been calculated for the whole test.

[6] defines limit values for the resulting RMS values depending on the axle load of the vehicle, i.e. 12.2 kN in tare and 35.2 kN in laden condition. Table 1 shows the results of the tare wagon and Table 2 of the laden wagon.

Table 1: Running stability assessment of the tare wagon.

Wheelset	Lateral Force RMS [kN]	Limit Value 12.2 kN Exploitation [%]
Front bogie front axle	4.6	38
Front bogie rear axle	10.4	85
Rear bogie front axle	3.6	30
Rear bogie rear axle	10.6	87

Table 2: Running stability assessment of the laden wagon.

Wheelset	Lateral Force RMS [kN]	Limit Value 35.2 kN Exploitation [%]
Front bogie front axle	14.5	41
Front bogie rear axle	31.3	89
Rear bogie front axle	11.7	33
Rear bogie rear axle	32.8	93

All evaluation results are below the limit values, so the simulation verifies running stability for an admissible velocity of 120 km/h. Remarkably the values of the rear axles are much higher. This phenomenon also occurs in the running safety and track loading tests at high velocities resp. large curve radii.

3.5 Running Safety and Track Loading Tests

Running safety and track loading of the 4L Bogie has also been assessed by simulations according to DIN EN 14363 [6] chapter 7. The assessment consists of four test zones, i.e. tangent track and very large radius curves (test zone 1), large radius curves (test zone 2), small radius curves (test zone 3) and very small radius curves (test zone 4). For each test zone simulations in tare and laden condition have been performed.

Test zone 1 is the same scenario as the stability test described in 3.4, only the evaluation is different based on 27 track sections of 100 m length. In test zones 2 through 4 the wagon also runs on artificial tracks which consist of 30 curves according to the specifications in [6]: In zone 2 the radius range is 700..1400 m, in zone 3 400..600 m and in zone 4 250..390 m. Rail irregularities according to "ERRI B176 high" are applied in all tests.

Cant deficiency is a measure for horizontal accelerations of curving rail vehicles. It expresses the centrifugal acceleration by the additional superelevation value which would eliminate quasi-static lateral forces between track and wheelsets. In [6] an admissible cant deficiency of 130 mm is proposed for freight wagons. From this a range of 91..149.5 mm follows for the test scenarios.

In test zone 2 the vehicle runs at a constant velocity of 132 km/h. As a consequence, the superelevation of the track has to be chosen such that the resulting cant deficiency lies in the specified range. Appendix A.4.1 lists the used curve radii, superelevation and cant deficiency values. For the assessment 30 track sections of 100 m length located in the middle of the curves are evaluated.

In test zones 3 and 4 the superelevation of the curves is predefined with usual values and the wagon velocity is varied. Again random values are used that result in cant deficiency values within the range specified by [6]. The curve velocity is changed in the middle of the straight track sections and kept constant in clothoid and curve sections. The used curve radii, superelevation values and vehicle velocities are listed in Appendices A.4.2 and A.4.3. In both scenarios 30 track sections in the middle of the curves are evaluated, 100 m long in test zone 3 and 70 m long in test zone 4.

The total track lengths and simulation times are 15.8 km / 430.9 s in test zone 2, 15.8 km / 587 s in zone 3 and 12.8 km / 607 s in zone 4.

For running safety assessment the sum of the wheel-rail guiding forces of each wheelset and the derailment coefficients (quotient of lateral and vertical force) are used. As specified in [6] the signals are output by the simulation with a sampling rate of 200 Hz and filtered by a 20 Hz low pass and a sliding mean filter with a window length of 2 m. In the next step the 0.15 % and 99.85 % percentiles are determined from the cumulative curve of the signal and converted depending on the curve direction for each track section. So one scalar value results for each section and an estimated maximum value (confidence level 99 %) can be determined for the whole test. These results are assessed against the respective limit values.

The wheelset guiding forces are used as criterion for safety against track shifting. [6] defines limit values of 24.5 kN for tare and 70.3 kN for laden condition of the wagon. The derailment coefficient is used to quantify safety against derailment with a limit value of 0.8. In Appendix A.5.1 the results of all running safety simulations are presented.

Figure 17 gives an overview on the maximum estimated wheelset guiding forces as percentage of the limit values. In tare condition the

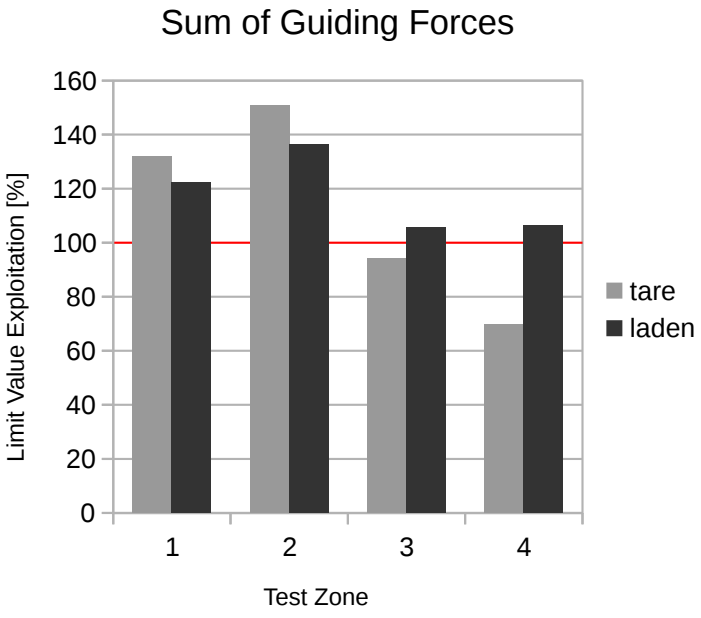

Figure 17: Limit value exploitation of max. wheelset guiding forces.

limits are exceeded up to 51 % in test zones 1 and 2. For the laden wagon the limit value is exceeded in all test zones about 6 to 36 %. Figure 18 summarizes the assessment of the derailment coefficient. In test zone 2 the limit value is reached for the tare wagon, but no exceedance occurs in any scenario. So the simulation predicts a clear failure in running safety because of inadmissible high lateral wheelset forces, in particular on tangent track and large radius curves at maximum velocity.

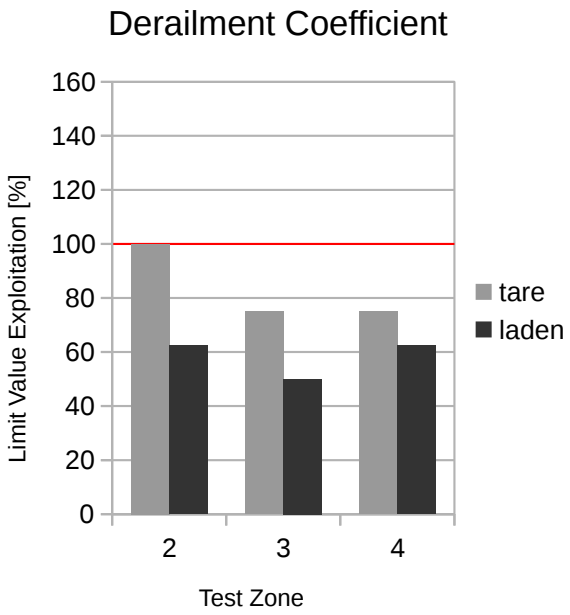

Figure 18: Limit value exploitation of derailment coefficients.

For track loading assessment the quasi-static guiding and vertical wheel forces and the maximum vertical wheel forces are used. Again the simulation results are first filtered with a 20 Hz low pass. The quasi-static forces are evaluated with 50 % percentiles of the outer wheels in test zones 2 through 4 only. For the maximum vertical forces 99.85 % percentiles are used per wheelset in test zone 1 and for the outer wheels in the other zones, and estimated maximum values with a confidence level of 95 % are determined for each track section.

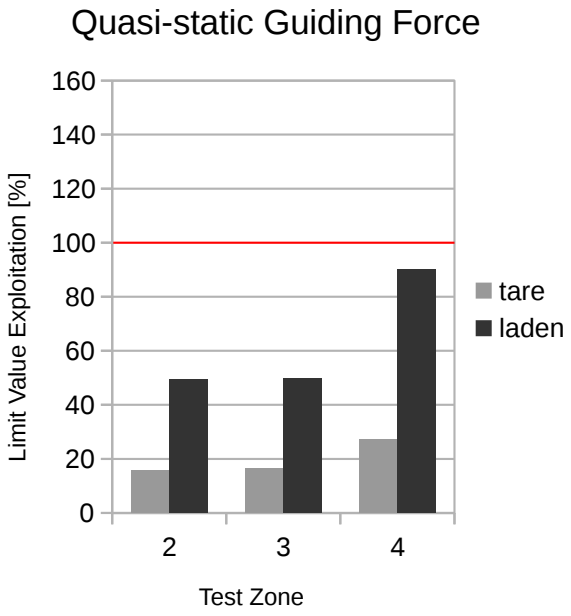

Figure 19: Limit value exploitation of quasi-static guiding forces.

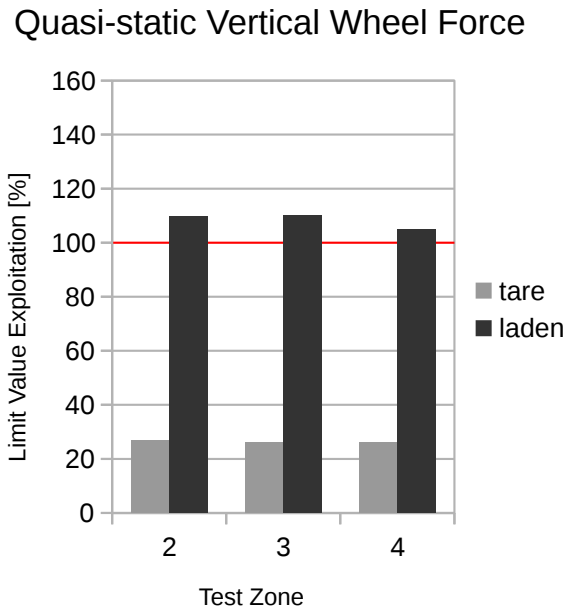

Figure 20: Limit value exploitation of quasi-static vertical wheel forces.

The respective limit values are 60 kN for the quasi-static guiding force, 145 kN for the quasi-static vertical force and 118.2 kN (tare) resp. 199.1 kN (laden) for the maximum vertical force. All assessment results are presented in Appendix A.5.2.

Figure 19 summarizes the assessment of the quasi-static guiding forces. Expectedly the laden wagon running through very small curve radii is the most critical scenario where 90 % of the limit value is reached. The result of the quasi-static vertical wheel forces is shown in Figure 20. Again this assessment is only relevant in laden condition where the limit value is exceeded by 5 to 10 % in all test zones. Finally Figure 21 gives an overview on the maximum vertical wheel forces assessment. For the tare wagon only up to 50 % of the limit value is reached, but in laden state the limit is exceeded up to 20 %. As a consequence, due to the simulation results a failure of the track loading assessment is expectable.

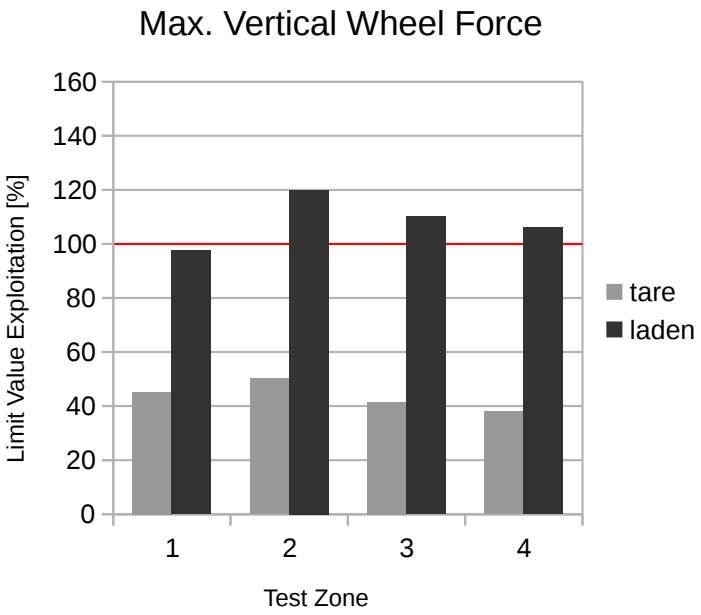

Figure 21: Limit value exploitation of maximum vertical wheel forces.

3.6 AIR Wheelset Tests

The AIR wheelset concept is presented in [5][8] and its usage for the 4L Bogie is proposed in [11]. The idea is to reduce rail wear in small radius curves by a torque limiter which limits the torque between left and right wheel of the wheelset. Regarding only longitudinal rail-wheel forces, the torque limit has the effect of a maximum friction coefficient for given wheel radius and vertical load, i.e. torque limit = friction coefficient × load × radius. As a consequence wear, usually measured by the product of friction

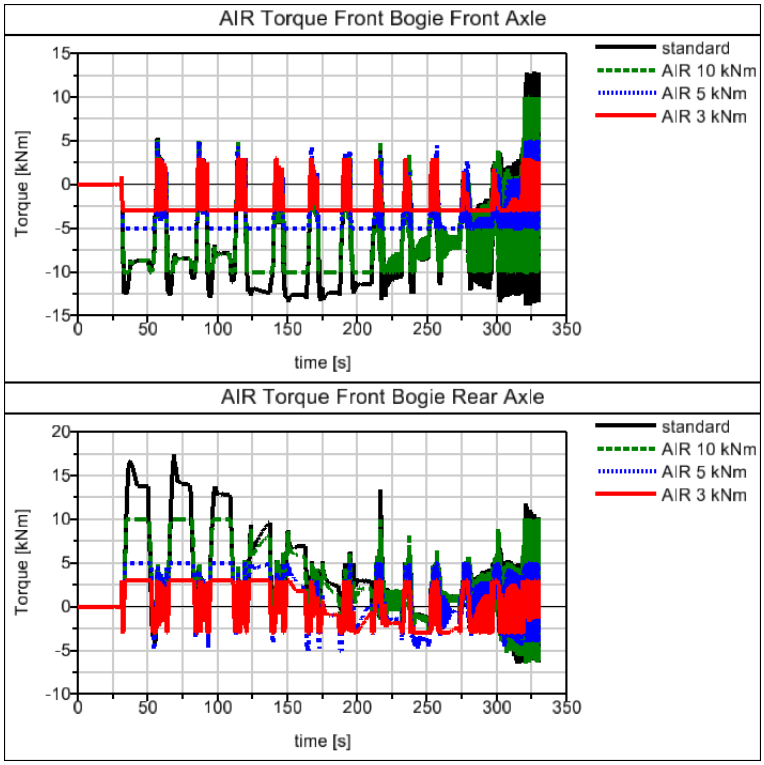

Figure 22: Torque between left and right wheel for standard and different AIR wheelsets.

force and creepage (wear number), can be reduced. However, as stated in [5] the overall benefit of AIR wheelsets is limited because as a side effect they reduce the steering capability of the bogie resulting in higher lateral wear.

In this study the influence of AIR wheelsets on the running behavior of the 4L Bogie is analyzed. This is done in two steps: First a scenario with curve radii between 250 m and 2000 m and cant deficency values in the range of 0 to 150 mm (see Appendix A.4.4) is simulated with AIR torque limits in the range from 2 kNm to 20 kNm to scan the general effect of AIR wheelsets on the test wagon. After this the scenarios large radius curves (test zone 2) and very small radius curves (test zone 4) are simulated with torque limits of 5 kNm and 10 kNm and the results are compared to the standard wheelset test of 3.5.

Intending a certain longitudinal friction coefficient limit, the torque limit scales with the vertical wheel load. As a consequence, the torque limit has to be designed for the laden vehicle and has no significant effect in tare condition. So all simulation scenarios in this section have been performed with the laden wagon.

Figure 22 shows the torques between left and right wheels of the front bogie axles. With standard wheelsets torques up to 17.4 kNm

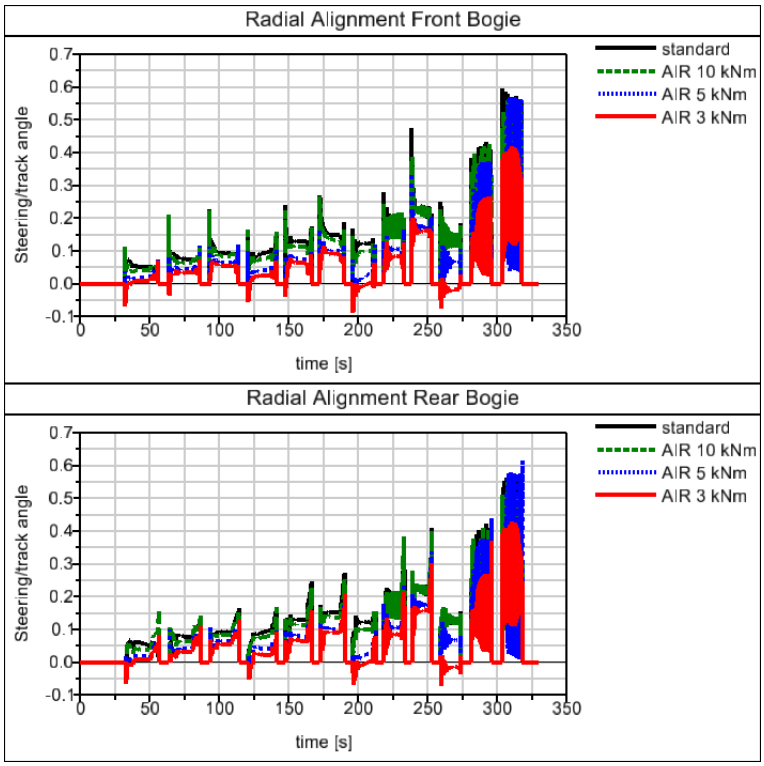

Figure 23: Curving capability with standard and AIR wheelsets.

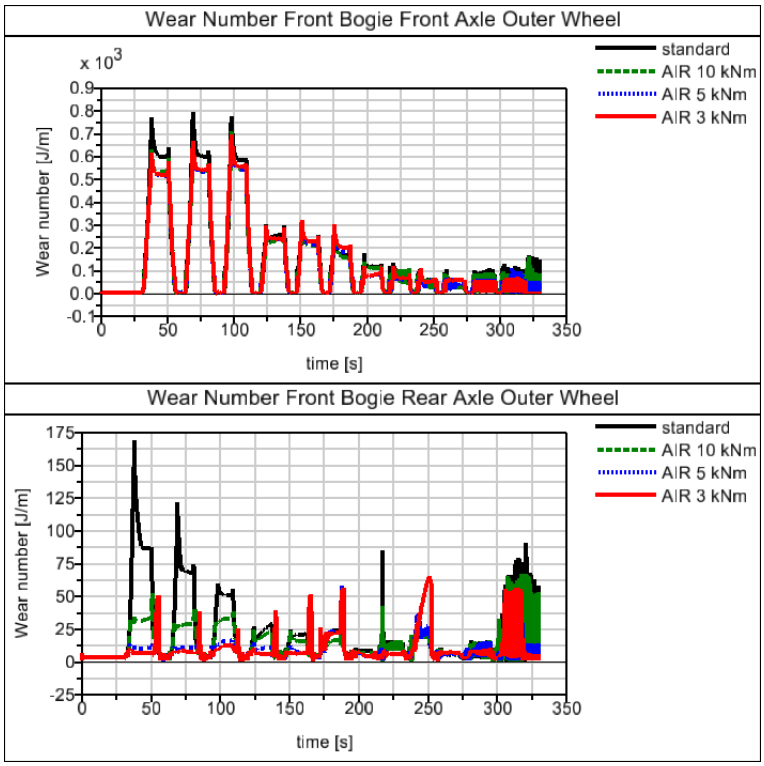

Figure 24: Outer wheel wear number with standard and AIR wheelsets.

arise in the 250 m curves. The colored plots present the effect of AIR wheelsets with torque limits of 10, 5 and 3 kNm. In the end phase of the test oscillations occur because of running instability at high velocities.

In Figure 23 the radial alignment of the bogies is shown. For this the steering angle (about the vertical direction) between front and rear wheelset axles is divided by the track direction angle difference, i.e. a value of 1.0 represents ideal alignment. As expected the curving capability is improved by larger curve radii, higher cant deficiency and greater AIR torque limit. Obviously a limit torque of 10 kNm is not very relevant, whereas 3 kNm has a significant negative effect in all curve radius/cant deficiency combinations.

The goal of AIR wheelsets is to reduce the wear number of the wheel-rail contact. Figure 24 shows the wear numbers of the outer wheels of the front bogie. As expected the highest values appear in small radius curves at the front wheel. Unfortunately AIR wheelsets can reduce them only about 15 % because friction mainly occurs in lateral direction. The reduction is already present for a limit torque of 10 kNm and lower limits have nearly no additional effect. At the rear axis longitudinal friction dominates, so the effect of AIR wheelsets is significant. In the extreme case of 250 m curve radius and zero cant deficiency a torque limit of 5 kNm reduces the wear number about more than 90 %. The same behavior is presented and explained in [5].

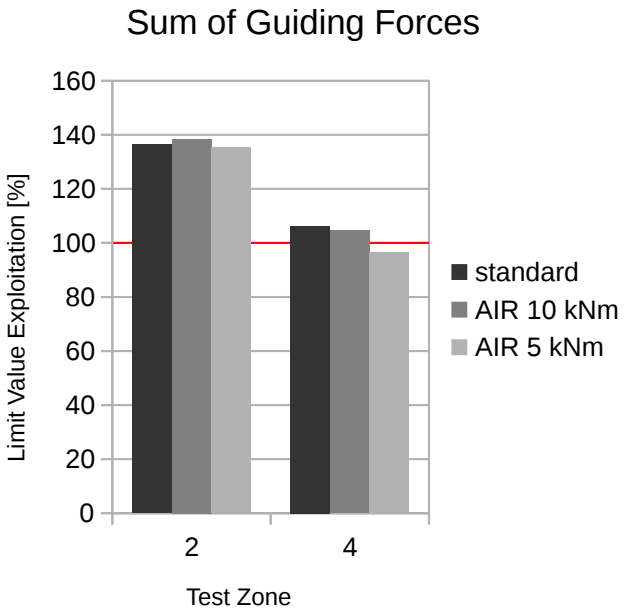

Figure 25: Max. guiding forces limit value exploitation with AIR wheelsets.

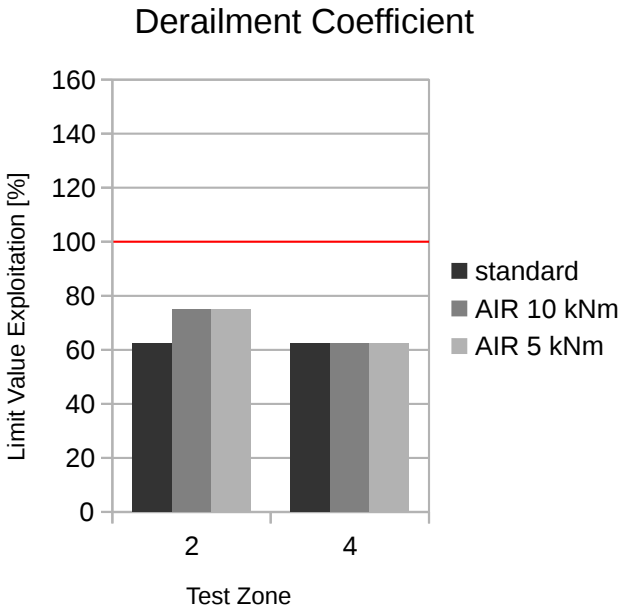

Figure 26: Derailment coefficient limit value exploitation with AIR wheelsets.

After verification of the basic AIR wheelset functionality selected running dynamics tests have been performed for comparison with the results of standard wheelsets. For this the scenarios large radius curves (test zone 2) and very small radius curves (test zone 4) have been simulated again in laden condition with AIR limit torques of 10 kNm and 5 kNm corresponding to longitudinal friction coefficient limits of 0.2 and 0.1.

Figure 25 shows the effect of AIR wheelsets on the wheelset guiding forces. In small radius curves the results are slightly improved, but the changes are not significant.

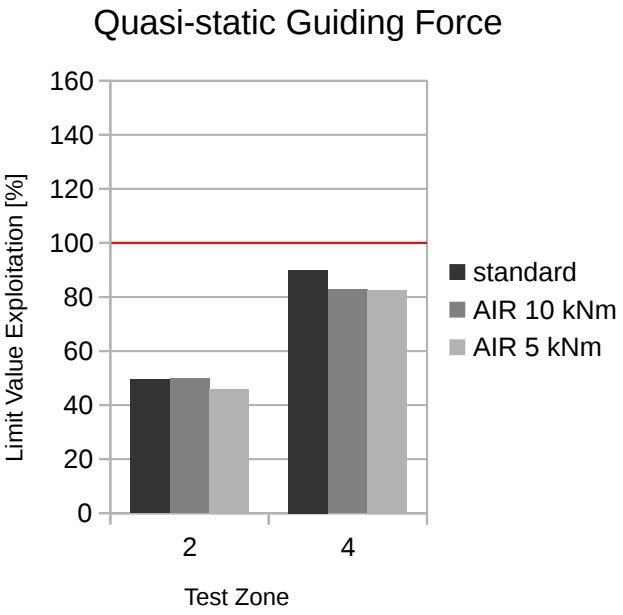

Figure 27: Quasi-static guiding force limit value exploitation with AIR wheelsets.

Figure 26 through Figure 29 show the comparison of derailment coefficient and track loading assessments. Obviously AIR wheelsets do not have a significant effect on any of the evaluation quantities.

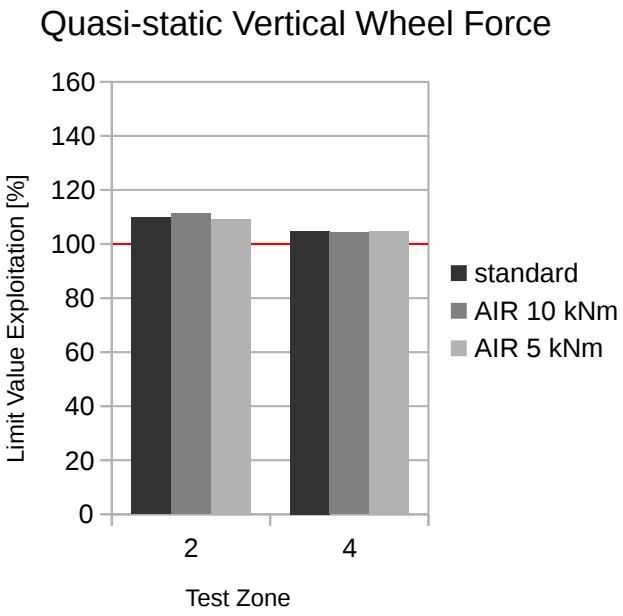

Figure 28: Quasi-static vertical wheel force limit value exploitation with AIR wheelsets.

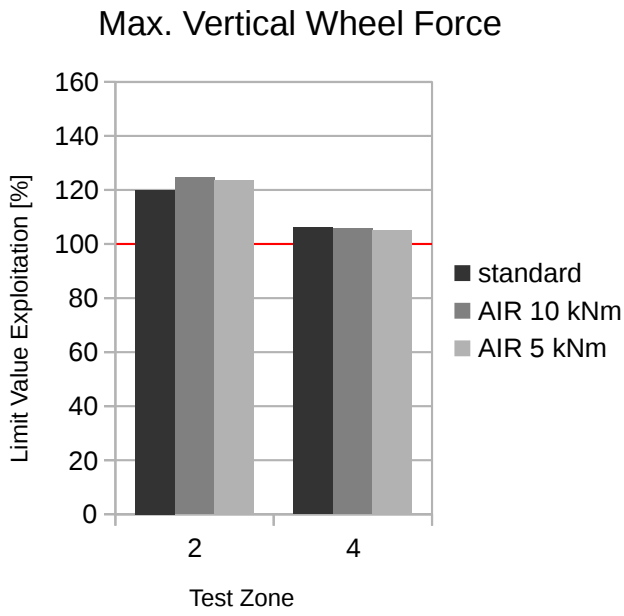

Figure 29: Max. vertical wheel force limit value exploitation with AIR wheelsets.

4 Interpretation and Conclusions

4.1 Bogie Concept

Increased operating speed and improved track friendliness are the major design goals of the 4L Bogie. The basic idea of the concept is to conduct the car body load as directly as possible from the center bowl to the wheel contact patches by a framework-like pyramidal inboard bearings frame. This allows to reduce the bogie weight about 15 % and its yaw moment of inertia about 30 % compared to the standard Y25 bogie.

The suspension system of the 4L Bogie is based on two axle boxes connected by swinging arms with hinges to the frame. So vertical translation and pitch rotation are the kinematic degrees of freedom between wheelsets and frame. Two progressive helical springs are used as compliant suspension components and load dependent damping is provided by friction of the hinges. However, the latter functionality is weakened by the relationship of the levers of the swinging arms and the hinge contact surfaces, resulting in proportionately lowered frictional power.

A special feature of the 4L Bogie concept is intended flexible deformation of the frame, i.e. non-parallel wheelset axes are only possible in case of load induced frame deformation. In case of twisted track, torsion about the longitudinal direction enables balanced vertical wheel forces. And increased outer wheel loads caused by cant deficiency (centrifugal forces in curves) induce torsion about the vertical direction resulting in partly radial alignment of the axes and therefore improved curving performance. However, this effect appears limited because of the comparatively low deformation capability of the frame.

4.2 Simulation Results

The simulation results of the braking tests described in 3.2 did not expose any issues. As intended by the design, moments induced by braking forces were supported by the pitch bearers so that the frame does not rotate significantly about the lateral direction.

The 4L Bogie also showed problem-free behavior in the quasi-static derailment assessment according to DIN EN 14363 presented in 3.3. Both, wheel raise and derailment coefficient remained clearly below the limit values.

Running stability has been tested according to DIN EN 14363 as described in 3.4. Assuming an admissible vehicle velocity of 120 km/h, the dynamic lateral forces of all wheelsets did not exceed the limit values, so running stability is verified.

Running safety and track loading have also been assessed as proposed by DIN EN 14363, see 3.5. For running safety the estimated max. wheelset guiding forces and derailment coefficients have been evaluated. In six of eight scenarios the guiding forces exceed the limit

values up to 50 %, foremost on tangent track and large curve radii at maximum speed. The calculated derailment coefficient values do not exceed the limit value.

For track loading assessment the quasi-static guiding and vertical wheel forces and the maximum vertical wheel forces have been evaluated. For the tare wagon all results are clearly below the limit values. But in laden condition the quasi-static and maximal vertical forces exceed them up to 20 %.

In 3.6 the performance of the 4L Bogie with Apparently Independently Rotating (AIR) wheelsets is analyzed. For this curving behavior and rail wear have been studied for varied curve radii and cant deficiency values. The results agree with [5] and show that wear numbers in the rail-wheel contacts can be reduced for the laden wagon in small radius curves. In addition large and very small radius curve scenarios of the running safety and track loading tests have been re-run with two AIR configurations. The results show that AIR wheelsets do not have a significant impact on running dynamics.

4.3 Result Assessment

In this pure virtual study the 4L Bogie basically worked in all scenarios. No problems occurred in the braking, derailment, stability and AIR wheelset tests. However, according to DIN EN 14363 the vehicle would be rejected because of exceeded limit values in running safety and track loading assessments.

Of course simulation models cannot exactly represent reality, but limit value exceedance up to 50 % clearly indicates a problem in the system design. During modeling and simulation many iterations and double-checks have been made to get as close as possible to the available design data and information and to eliminate modeling errors. In particular clearance and friction of the hinges and side bearers have been improved several times. An admissible vehicle velocity of 120 km/h (instead of 140 km/h as targeted in [11]) has been assumed in the dynamic tests to avoid critical conditions.

The simulation scenarios have also been double-checked. Running freight wagons on a track with “ERRI high” irregularities at up to 132 km/h and cant deficiency values up to 150 mm is unquestionable a demanding requirement. It should also be noted that [6] does not specify roll and gauge irregularities as used in the simulations, but of course these are also present in real life tests which are the main topic of the norm. However, the equivalent standard deviations of vertical and lateral irregularities of the scenarios do not exceed the ranges proposed in [6].

In the simulation animations quite large roll motions of the car body are apparent. This phenomenon might be the main cause of the exceeding lateral wheelset and vertical wheel forces in the running dynamics assessment. In fact informative simulation samples with disabled roll irregularities yielded significantly reduced results below the limit values. The direct flux of force between center bowl and wheels without any lateral suspension enables the

lightweight design of the bogie, but it appears to be problematic concerning running dynamics.

The running behavior of the 4L Bogie has also been analyzed by MBS simulation in [9]. A similar model in a different simulation environment has been used to verify running stability and track friendliness. For the running stability assessment, the same method based on DIN EN 14363 has been applied, but measured rail irregularities have been used. The results are very similar in tare condition. However, in laden condition the limit value is not exceeded up to more than 170 km/h, while in this study a limit value exploitation of 93 % has been determined at 132 km/h. Unfortunately, no other assessments according to DIN EN 14363 are presented in [9].

In [4] the running behavior of the Spectrum freight vehicle is analyzed. In the Spectrum project similar design goals, i.e. increased operating velocity up to 160 km/h, improved ride quality and track friendliness have been targeted. Regarding the running safety and track loading results of this study it is interesting that acceptable running stability of the Spectrum bogie could not be achieved unless a swing link arrangement had been introduced as secondary lateral suspension system between center bowl and bogie frame. This information might guide the way to improve the 4L Bogie concept for high speed operation.

A Appendix

A.1 Geometry

The geometry data (for the nominal state of the bogie) is represented by position vectors with respect to the bogie reference frame. As usual the bogie reference frame is located at the top of rail in the center of the bogie/center bowl. Its z-axis points vertically to the ground, the x-axis horizontally to the front and the y-axis to the right (gray in Figure 1). Since the bogie design is symmetrical in the horizontal directions, front/right is interchangeable with rear/left. All lengths are given in mm.

A.1.1 Basics

Wheel base: 1800
Nominal wheel radius: 460

A.1.2 Marker Positions

All markers have the same orientation as the bogie reference frame.

Frame – CentreBowl: x = 0 ; y = 0 ; z = -802.5
Frame – left/right Leaf: x = 0 ; y = -/+300 ; z = -825
Frame – SupportingArm: front/rear x = +/-413.915 ; left/right y = -/+ 481 ; z = -535
Frame – SwingingArm: front/rear x = +/-588.915 ; left/right y = -/+481 ; z = -535
SupportingArm – Leaf: x = 0 ; left/right y = -/+716.85 ; z = -825
SupportingArm – SideBearer: x = 0 ; left/right y = -/+850 ; z = -850
SupportingArm – BrakeCalliper: front/rear x = +/-275 ; left/right y = -/+750 ; z = -727
SwingingArm – Axle: front/rear x = +/-900 ; left/right y = -/+481 ; z = -460
SwingingArm – SpringCage: front/rear x = +/-440.735 ; left/right y = -/+481 ; z = -262.708
Axle – Shaft: front/rear x = +/-900 ; y = 0 ; z = -460
Axle – Wheel: front/rear x = +/-900 ; left/right y = -/+750 ; z = -460
Pitch bearer contact point: front/rear x = +/-360 ; y = 0 ; z = -850
BrakePad contact point: front/rear x = +/-596 ; left/right y = -/+750 ; z = -512

A.2 Mass Properties

All lengths are given in mm. The moments and products of inertia are given in kgm² at the center of mass with respect to the bogie reference frame (except for Wheel, track ballast and CarBody).

A.2.1 Frame

Mass: 320.1 kg
Center of mass: x = 0 ; y = 0 ; z = -654.5
Moments of inertia: x = 41.781 ; y = 60.098 ; z = 93.841
Products of inertia: xy = 0 ; yz = 0 ; zx = 0

A.2.2 SwingingArm

Mass: 50.9 kg
Center of mass: front/rear x = +/-745 ; left/right y = -/+484 ; z = -431
Moments of inertia: x = 0.617 ; y = 2.254 ; z = 1.746
Products of inertia: front left/right xy = -/+0.024 ; left/right yz = -/+0.016 ; front/rear zx = 0.354

A.2.3 SupportingArm

Mass: 95.4 kg
Center of mass: x = 0 ; y = -/+705 ; z = -741
Moments of inertia: x = 1.679 ; y = 8.586 ; z = 9.473
Products of inertia: xy = 0 ; left/right yz = -/+0.436 ; zx = 0

A.2.4 Axle

Mass: 153.0 kg
Center of mass: front/rear x = +/-900 ; y = 0 ; z = -460
Moments of inertia: x = 40.550 ; y = 1.036 ; z = 40.550
Products of inertia: xy = 0 ; yz = 0 ; zx = 0

A.2.5 Wheel

Center of mass, moments and products of inertia are given with respect to the wheel reference frame located at marker Axle – Wheel.

Mass: 616.8 kg
Center of mass: x = 0 ; left/right y = +/-27.8 ; z = 0
Moments of inertia: x = 39.9 ; y = 62.525 ; z = 39.9
Products of inertia: left/right xy = 0 ; yz = 0 ; zx = 0

A.2.6 Front SpringCage

Includes half of Spring inertia.

Mass: 27.8 kg
Center of mass; x = -12.9 ; left/right y = -/+481 ; z = -262.7
Moments of inertia: x = 0.17 ; y = 0.765 ; z = 0.764
Products of inertia: xy = 0 ; yz = 0 ; zx = 0

A.2.7 Rear SpringCage

Includes half of Spring inertia.

Mass: 46.3 kg
Center of mass: x = -24.9 ; left/right y = -/+481 ; z = -262.7
Moments of inertia: x = 0.351 ; y = 1.958 ; z = 1.957
Products of inertia: xy = 0 ; yz = 0 ; zx = 0

A.2.8 BrakeCalliper

Mass: 91.0 kg
Center of mass: front/rear x = +/-346 ; front left/rear right y = -/+755 ; front right/rear left y = +/-745 ; z = -529
Estimated moments of inertia: x = 1.5 ; y = 2.4 ; z = 2.6
Estimated products of inertia: xy = 0 ; yz = 0 ; zx = 0

A.2.9 Total Bogie

Mass: 4019.3 kg
Center of mass: x = 0 ; y = 0 ; z = -487.9
Moments of inertia: x = 2012.46 ; y = 2794.86 ; z = 4461.5
Products of inertia: xy = 0.63 ; yz = 0 ; zx = 0.68

A.2.10 Track Ballast

Mass: 330 kg ; Moment of inertia: x = 10

A.2.11 CarBody

Center of mass, moments and products of inertia are given with respect to the CarBody reference frame located at the top of rail in the center of the wagon.

Tare (Axle Load 5.75 t)

Mass: 14961.4 kg
Center of mass: x = 0 ; y = 0 ; z = -1777
Moments of inertia: x = 23824.1 ; y = 214246.8 ; z = 210631.7
Products of inertia: xy = 0 ; yz = 0 ; zx = 0

Laden (Axle Load 22.25 t)

Mass: 80961.4 kg
Center of mass: x = 0 ; y = 0 ; z = -2362
Moments of inertia: x = 88611.3 ; y = 733137.2 ; z = 728494.8
Products of inertia: xy = 0 ; yz = 0 ; zx = 0

A.3 Force Elements

A.3.1 Frame – SwingingArm

Radial (zx)

Stiffness: 1000 kN/mm ; Damping: 2 kNs/mm
Friction coefficient: 0.3 ; Friction radius: 50 mm

Axial (y)
Stiffness: 1000 KN/mm ; Damping: 2 kNs/mm
Clearance: +/-1.0 mm
Axial position increase at SwingingArm: left/right y = -/+0.114 mm

A.3.2 Frame – SupportingArm

Radial (yz)
Stiffness: 1000 kN/mm ; Damping: 2 kNs/mm
Friction coefficient: 0 ; Friction radius: 35 mm

Axial (x)
Stiffness: 1000 kN/mm ; Damping: 2 kNs/mm
Clearance: +/-1.0 mm
Friction coefficient: 0.3

A.3.3 Leaf

Stiffness: 483 kN/mm ; Damping: 966 Ns/mm ; Unloaded length: 416.85 mm

A.3.4 Suspension Spring

Stiffness: Non-linear ; Damping: 10 Ns/mm
Nominal length: 316 mm ; Nominal deflection: 22.951 mm ; Preload: 24350 N

A.3.5 SideBearer

Vertical Bushing (z)
Stiffness: 570 N/mm ; Damping: 1 Ns/mm ; Preload: 16 kN

Vertical Bump Stop (z)
Stiffness: 100 kN/mm ; Position: 12 mm

Horizontal Bushing (xy)
Stiffness: 380 N/mm ; Damping: 1 Ns/mm

Longitudinal Bump Stop (x)
Stiffness: 100 kN/mm ; Position: +/-1 mm

Lateral Rotational Bushing (beta)
Stiffness: 12 kNm/rad ; Damping: 21 Nms/rad

Vertical Rotational Bushing (gamma)
Stiffness: 8 kNm/rad ; Damping: 21 Nms/rad

Horizontal Friction (xy)
Friction coefficient: 0.22

A.3.6 CentreBowl

Spherical Contacts
Stiffness: 1000 kN/mm ; Damping: 2 kNs/mm ; Friction coefficient: 0.22

Pitch Bearer Contacts
Stiffness: 1000 kN/mm ; Damping: 2 kNs/mm ; Friction coefficient: 0.22

Rotational Bushing (alpha, beta, gamma)
Stiffness: 10000 kNm/rad ; Damping: 10 kNms/rad

A.3.7 Track Ballast

Lateral (y)
Stiffness: 40 kN/mm ; Damping: 98 Ns/mm

Vertikal (z)
Stiffness: 150 kN/mm ; Damping: 188 Ns/mm

Roll (alpha)
Stiffness: 84375 kNm/rad ; Damping: 105.75 kNms/rad

A.4 Tracks

A.4.1 Large Radius Curves (Test Zone 2)

Each curve is 200 m long and lies between 100 m long clothoids transitioning to straight sections of 100 m. Cant is defined by random superelevation values chosen such that cant deficiency lies within the range of 91 mm to 149.5 mm.

Section	Radius [m]	Superelevation [mm]	Velocity [km/h]	Cant Deficiency [mm]
11	700	150	132	143.7
21	-700	-148	132	145.7
31	-750	-150	132	124.1
41	750	136	132	138.1
51	-800	-108	132	149.0
61	800	143	132	114.0
71	850	109	132	132.9
81	-850	-93	132	148.9
91	900	107	132	121.4
101	-900	-98	132	130.4
111	-950	-90	132	126.4
121	950	84	132	132.4
131	1000	60	132	145.6
141	-1000	-91	132	114.6
151	1050	81	132	114.8
161	-1050	-48	132	147.8
171	1100	60	132	126.9
181	-1100	-84	132	102.9
191	1150	65	132	113.8
201	-1150	-87	132	91.8
211	1200	54	132	117.3
221	-1200	-64	132	107.3
231	-1250	-45	132	119.5
241	1250	57	132	107.5
251	1300	61	132	97.1
261	-1300	-28	132	130.1
271	1350	9	132	143.3
281	-1350	-10	132	142.3
291	1400	43	132	103.8
301	-1400	-14	132	132.8

A.4.2 Small Radius Curves (Test Zone 3)

Each curve is 200 m long and lies between 100 m long clothoids transitioning to straight sections of 100 m. Velocity is defined by random values chosen such that cant deficiency lies within the range of 91 mm to 149.5 mm.

Section	Radius [m]	Superelevation [mm]	Velocity [km/h]	Cant Deficiency [mm]
11	600	90	102,6	117,1
21	-600	-90	96,3	92,2

31	-580	-120	105,0	104,5
41	580	120	113,0	139,9
51	-560	-120	108,6	128,4
61	560	120	103,5	105,8
71	550	120	109,0	135,1
81	-550	-120	110,5	141,9
91	540	120	110,6	147,0
101	-540	-120	105,2	121,6
111	-520	-150	111,5	131,9
121	520	150	109,0	119,6
131	500	150	106,9	119,8
141	-500	-150	105,6	113,3
151	480	150	109,2	143,2
161	-480	-150	105,4	122,9
171	460	150	105,6	136,1
181	-460	-150	104,8	131,5
191	455	120	93,0	104,4
201	-455	-120	90,6	92,7
211	450	90	92,4	133,9
221	-450	-90	92,8	135,8
231	-440	-120	98,9	142,0
241	440	120	88,8	91,3
251	420	120	94,6	131,6
261	-420	-90	90,5	139,9
271	400	90	84,7	121,6
281	-400	-90	87,0	133,1
291	440	60	88,0	147,7
301	-440	-60	76,4	96,6

A.4.3 Very Small Radius Curves (Test Zone 4)

Each curve is 150 m long and lies between 75 m long clothoids transitioning to straight sections of 100 m. Velocity is defined by random values chosen such that cant deficiency lies within the range of 91 mm to 149.5 mm.

Section	Radius [m]	Superelevation [mm]	Velocity [km/h]	Cant Deficiency [mm]
11	390	130	87,5	101,5
21	-390	-90	84,2	124,7
31	350	150	87,4	107,5
41	370	120	90,5	141,2
51	-360	-120	84,9	116,0
61	-350	-120	84,8	122,5
71	340	120	80,5	104,6
81	-340	-120	82,3	114,8
91	340	120	83,4	121,2
101	-320	-120	77,7	102,7
111	320	70	76,7	147,0
121	310	80	67,6	93,8
131	-310	-80	73,6	126,3

141	300	90	69,9	102,4
151	-300	-90	72,3	115,7
161	-290	-100	78,0	147,4
171	290	95	72,8	120,6
181	-285	-120	74,1	107,2
191	280	120	73,8	109,3
201	-280	-120	73,6	108,4
211	275	90	66,1	97,2
221	-275	-90	65,3	93,2
231	-270	-120	74,2	120,8
241	260	120	74,0	128,4
251	255	120	74,9	139,4
261	-250	-150	74,5	111,8
271	250	150	78,3	139,1
281	-260	-120	70,7	106,8
291	260	120	72,1	116,2
301	-335	-60	66,4	95,4

A.4.4 AIR Wheelset Test

Each curve lies between 100 m long clothoids transitioning to straight sections of 100 m. Velocity is defined such that the predefined cant deficiency values follow.

Length [m]	Radius [m]	Superelevation [mm]	Velocity [km/h]	Cant Deficiency [mm]
200	250	150	56,4	0,0
200	250	100	60,9	75,0
200	250	50	65,1	150,0
300	500	150	79,7	0,0
300	500	100	86,1	75,0
300	500	50	92,1	150,0
400	1000	150	112,8	0,0
400	1000	100	121,8	75,0
400	1000	50	130,2	150,0
500	2000	100	130,2	0,0
500	2000	50	130,2	50,0
500	2000	0	130,2	100,0

A.5 Dynamic Performance Results

A.5.1 Running Safety Assessment

Tangent Track / Very Large Radius Curves (Test Zone 1)

Tangent track / very large radius curves, tare	**Running safety**	Mean value Standard deviation

Sum of guiding forces

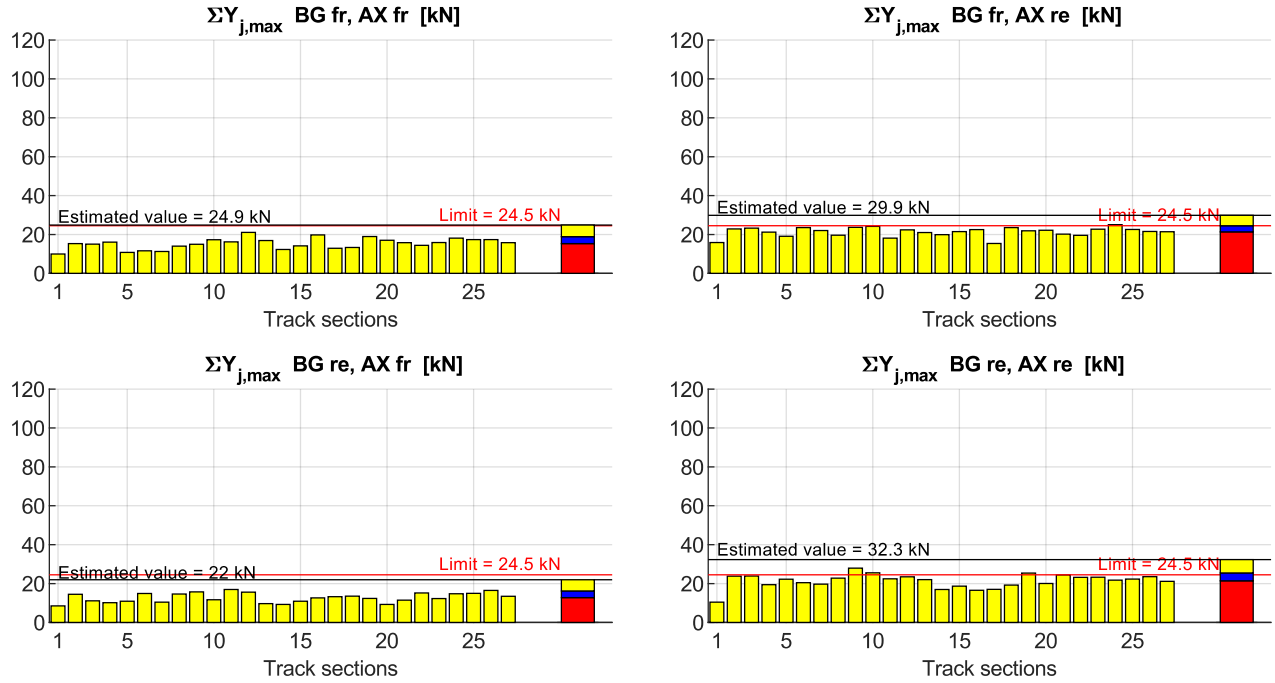

Tangent track / very large radius curves, laden	**Running safety**	Mean value Standard deviation

Sum of guiding forces

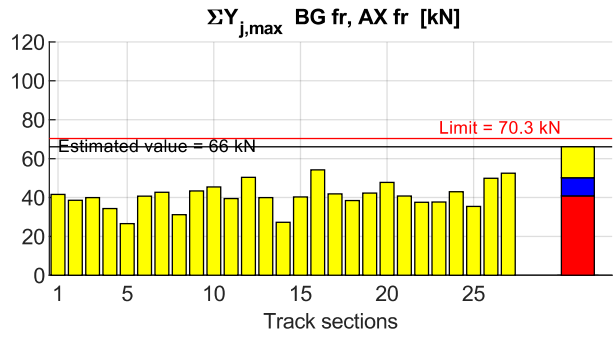

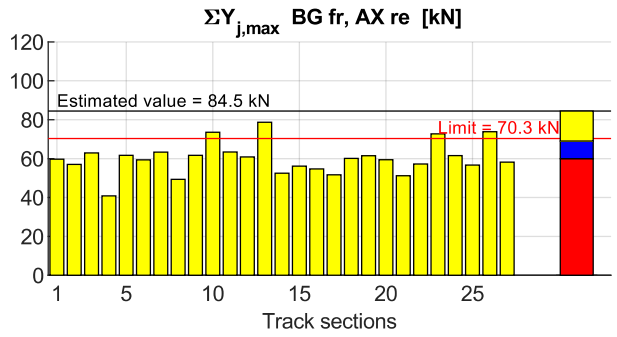

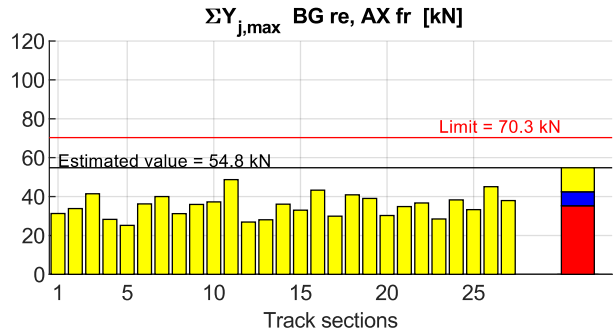

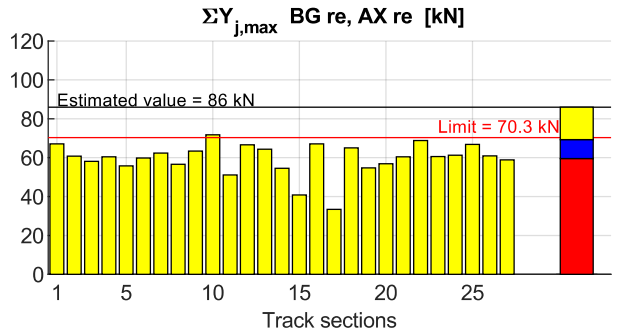

Large Radius Curves (Test Zone 2)

Large radius curves, tare	**Running safety**	Mean value Standard deviation

Sum of guiding forces

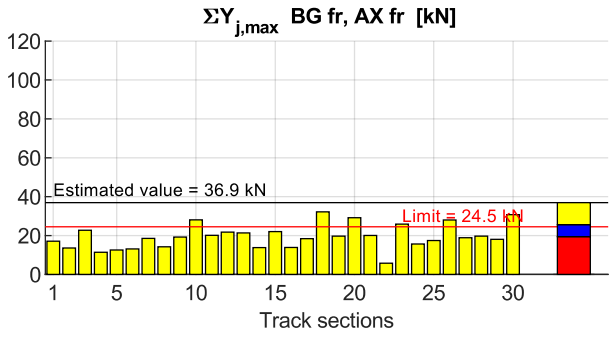

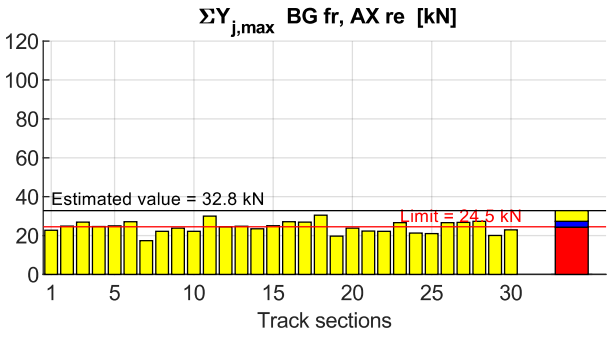

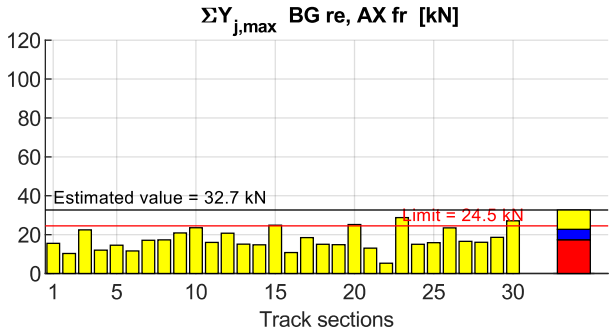

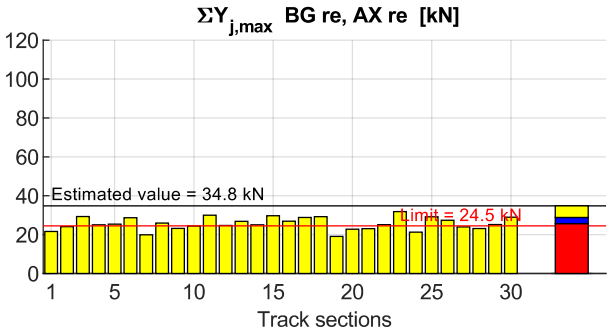

Quotient of lateral and vertical wheel force

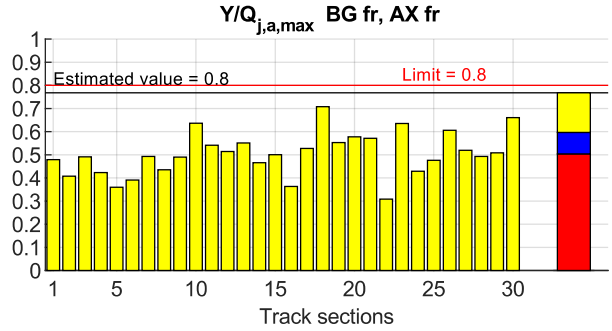

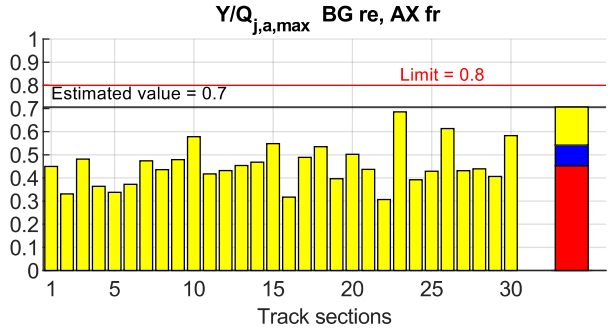

Large radius curves, laden	**Running safety**	Mean value Standard deviation

Sum of guiding forces

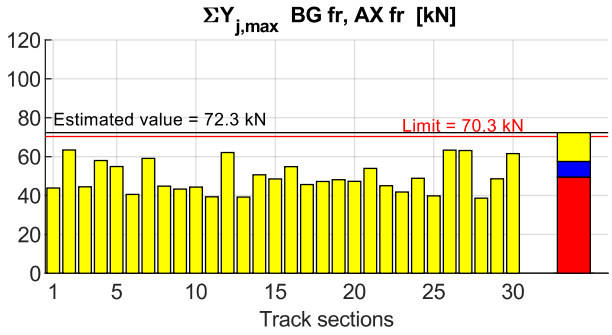

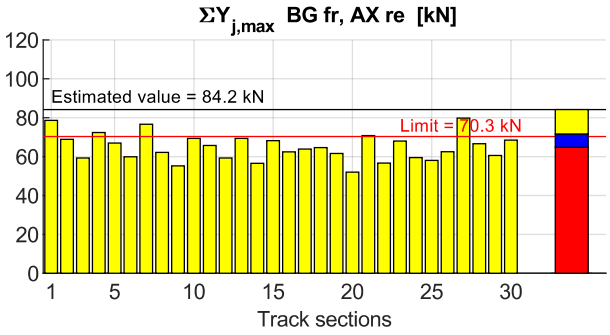

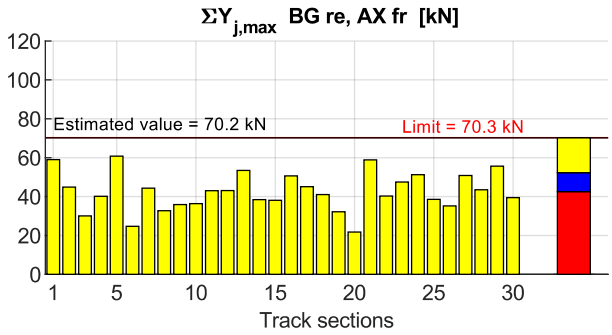

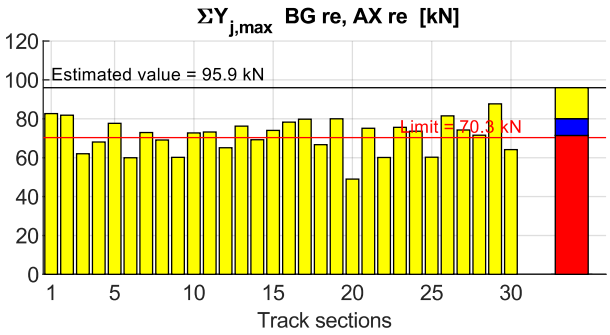

Quotient of lateral and vertical wheel force

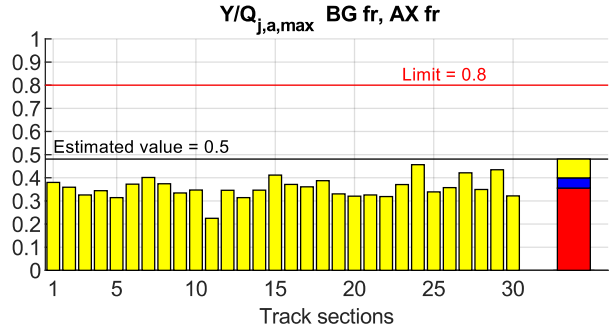

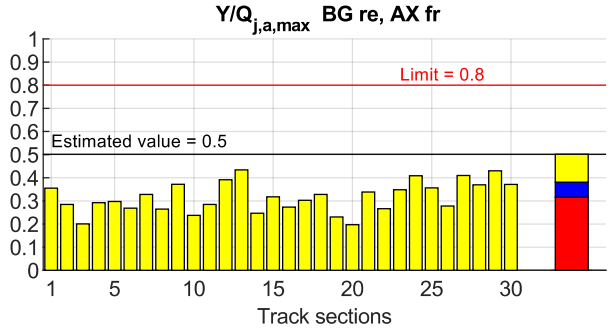

Large radius curves AIR 10 kNm	**Running safety**	Mean value Standard deviation

Sum of guiding forces

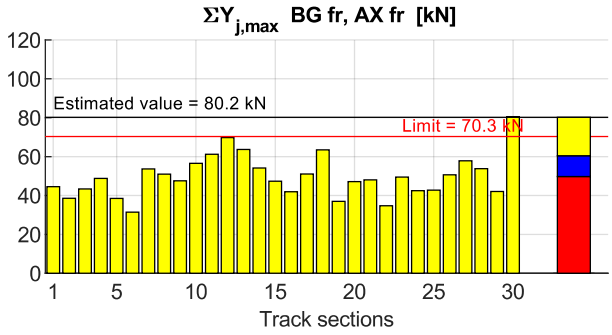

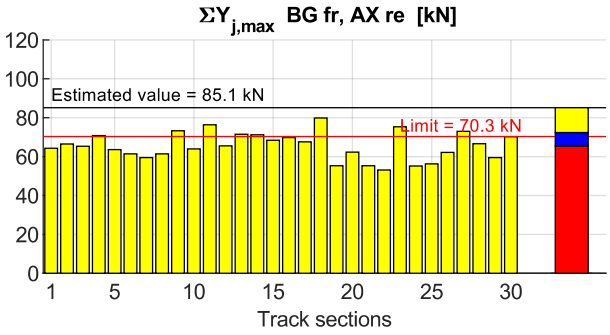

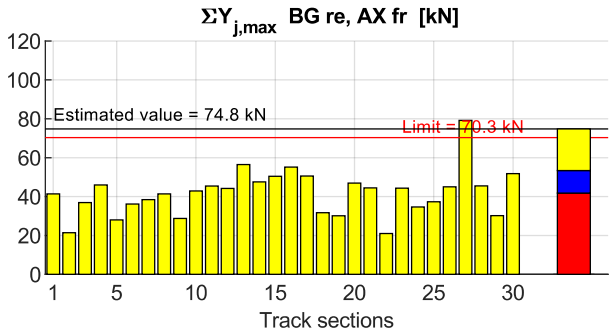

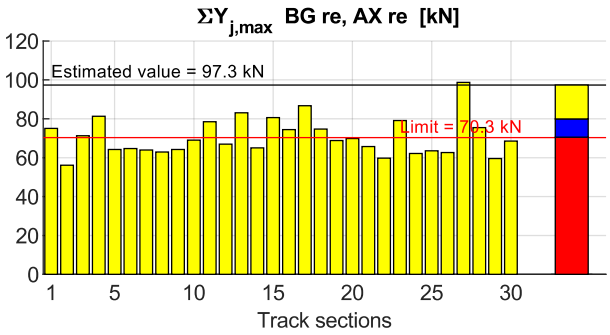

Quotient of lateral and vertical wheel force

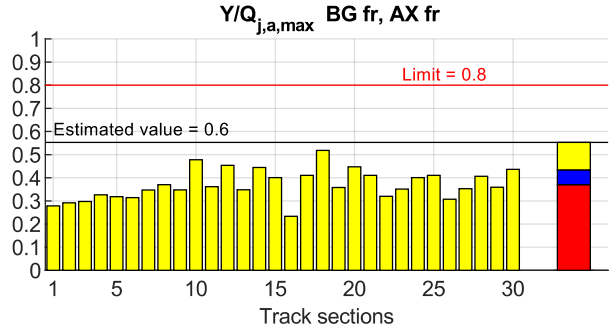

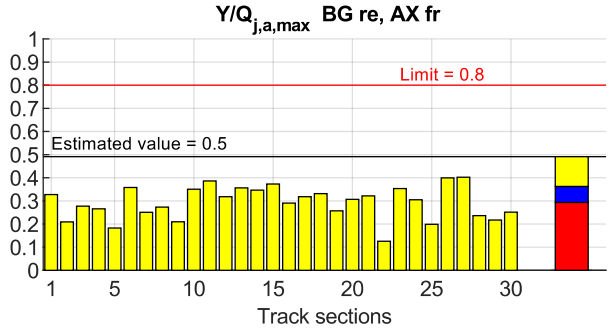

Large radius curves AIR 5 kNm	**Running safety**	Mean value Standard deviation

Sum of guiding forces

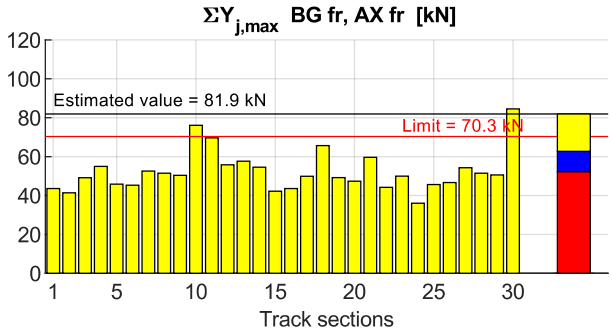

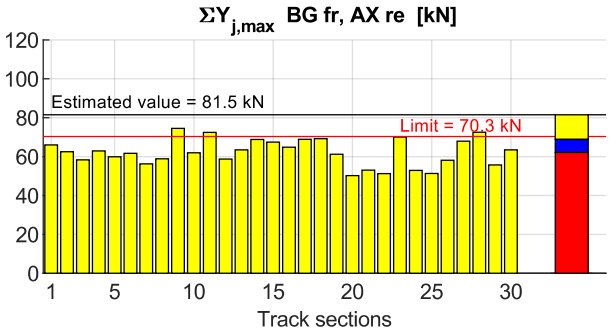

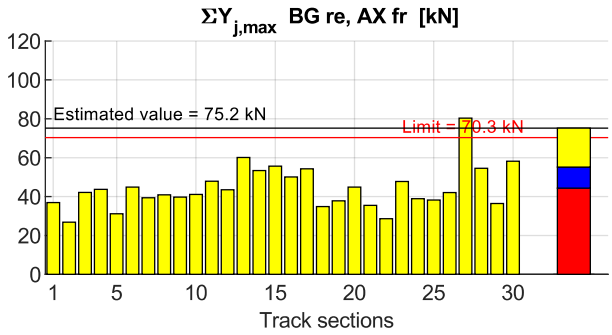

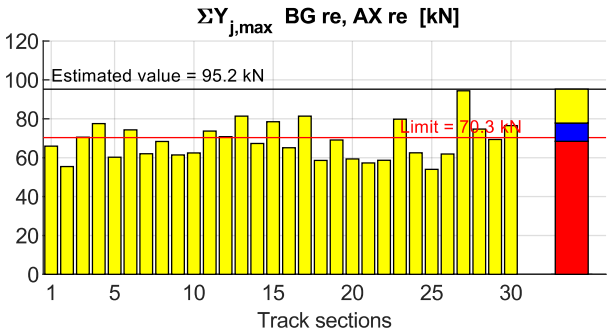

Quotient of lateral and vertical wheel force

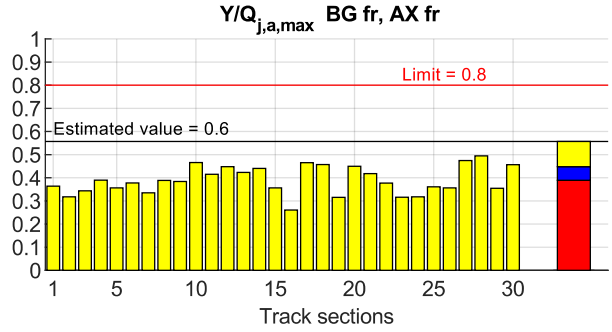

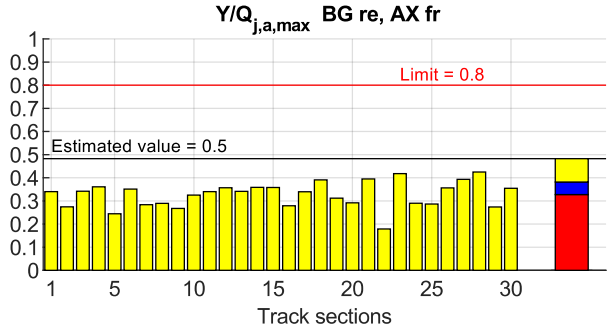

Small Radius Curves (Test Zone 3)

Small radius curves, tare	**Running safety**	Mean value Standard deviation

Sum of guiding forces

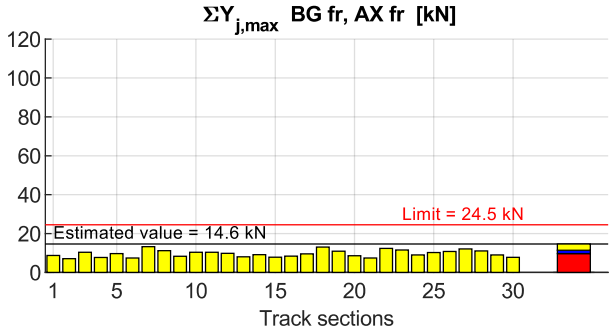

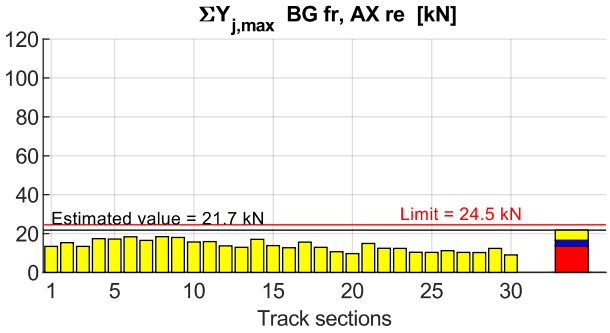

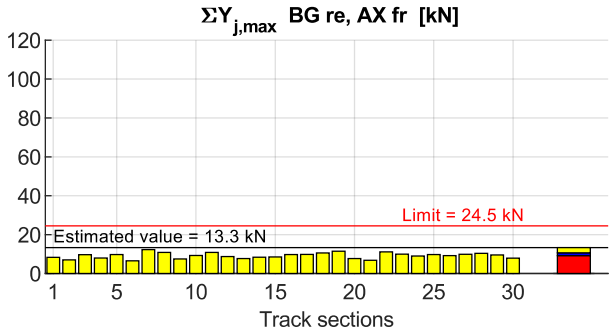

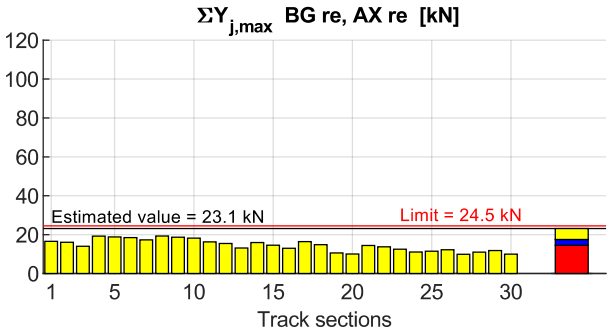

Quotient of lateral and vertical wheel force

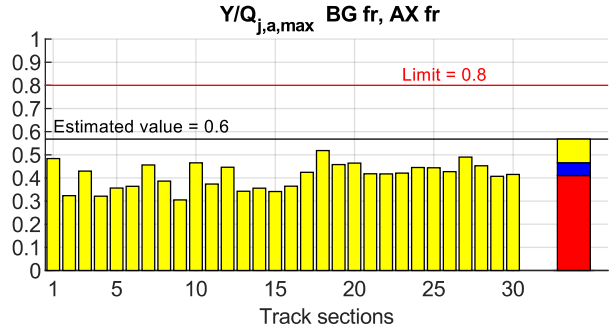

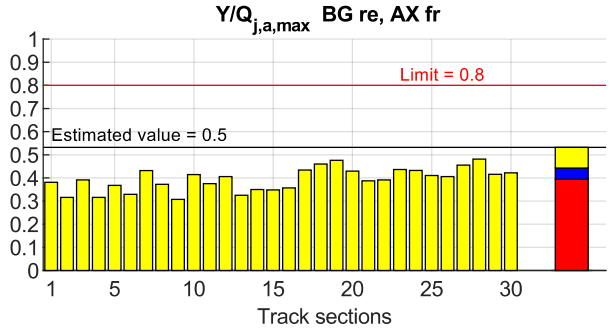

Small radius curves, laden	**Running safety**	Mean value Standard deviation

Sum of guiding forces

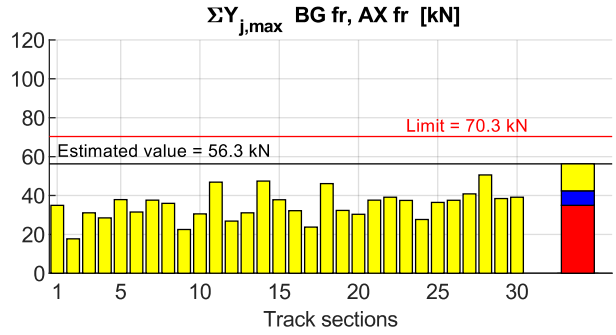

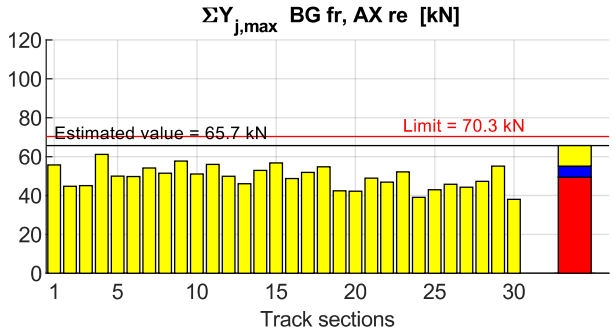

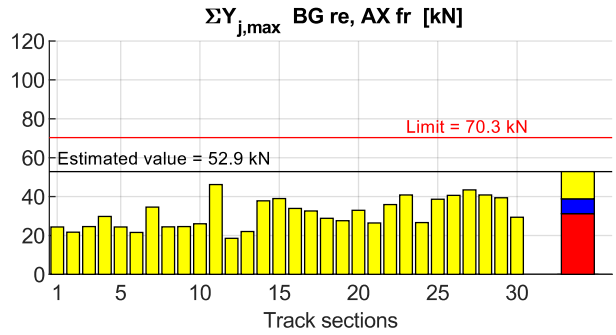

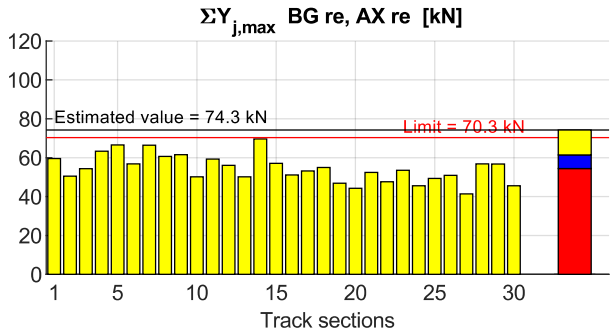

Quotient of lateral and vertical wheel force

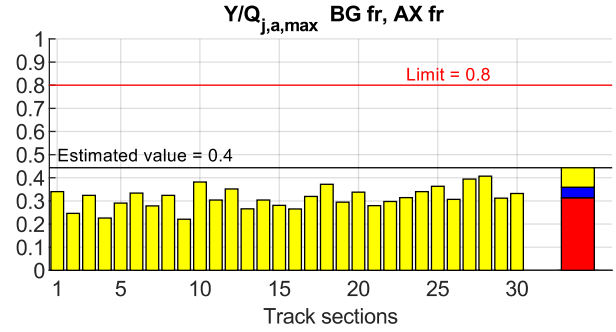

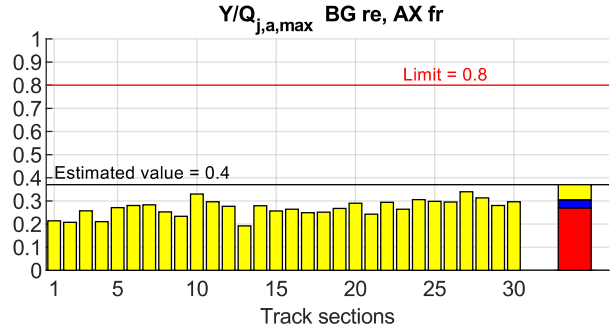

Very Small Radius Curves (Test Zone 4)

Very small radius curves, tare	**Running safety**	Mean value Standard deviation

Sum of guiding forces

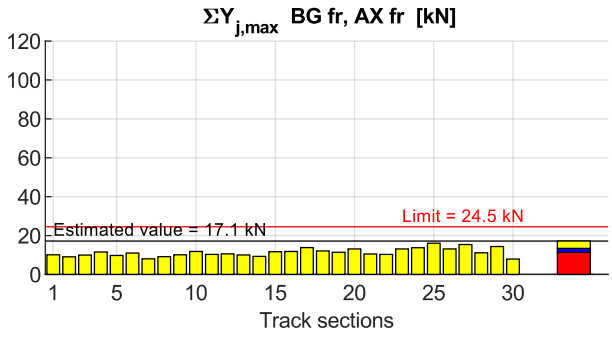

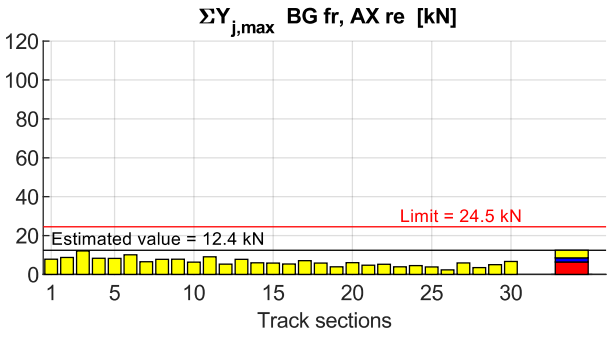

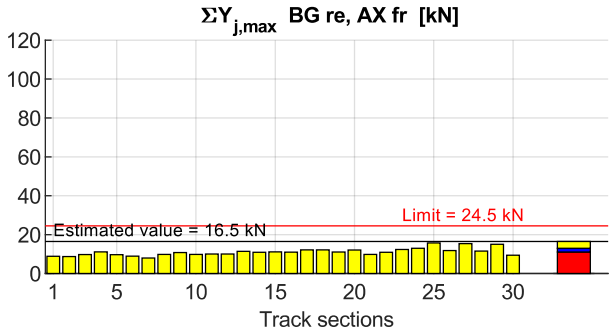

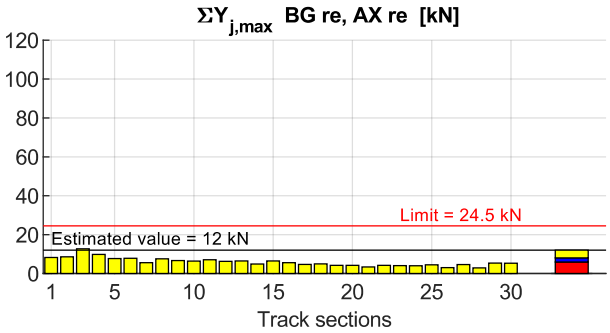

Quotient of lateral and vertical wheel force

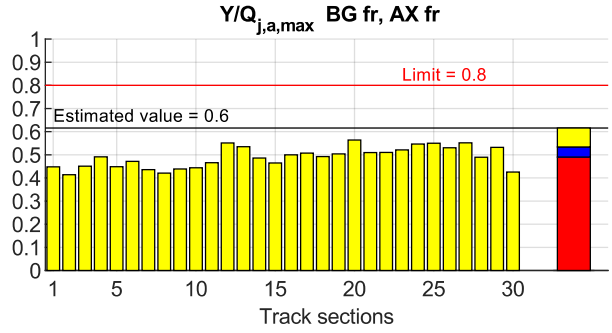

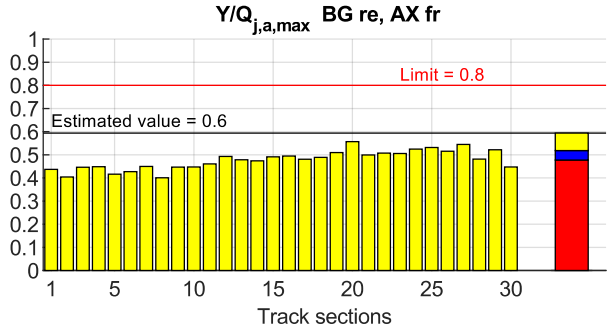

Very small radius curves, laden	**Running safety**	Mean value Standard deviation

Sum of guiding forces

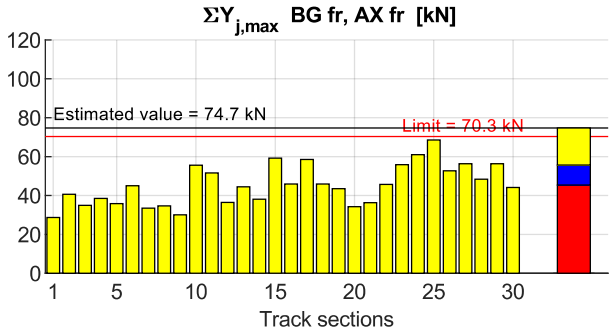

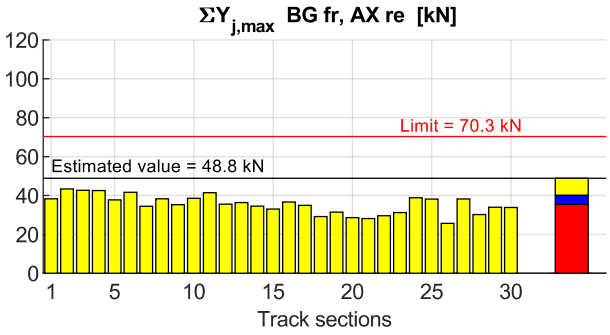

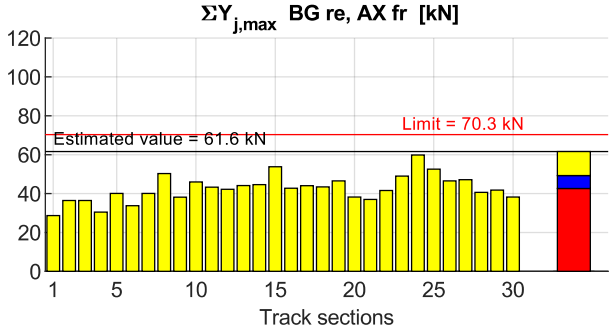

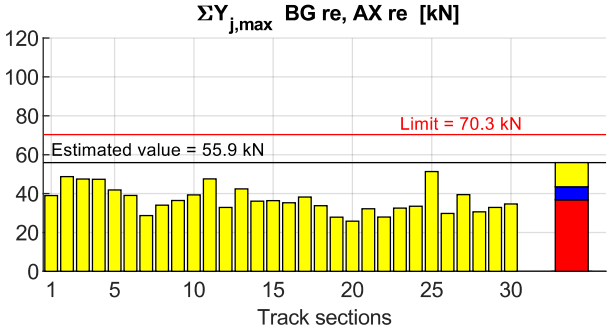

Quotient of lateral and vertical wheel force

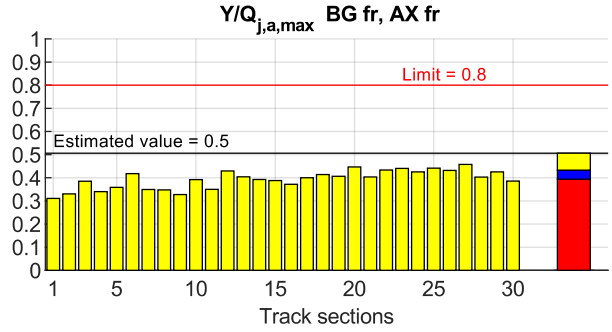

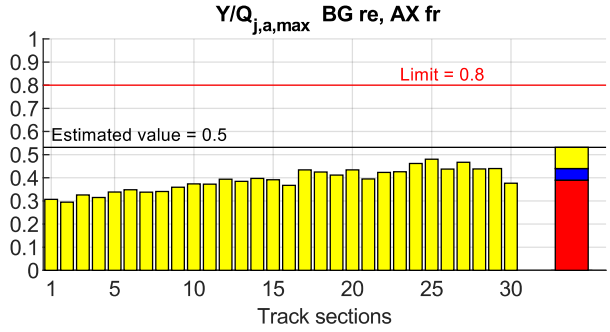

Very small radius curves, AIR 10 kNm	**Running safety**	Mean value Standard deviation

Sum of guiding forces

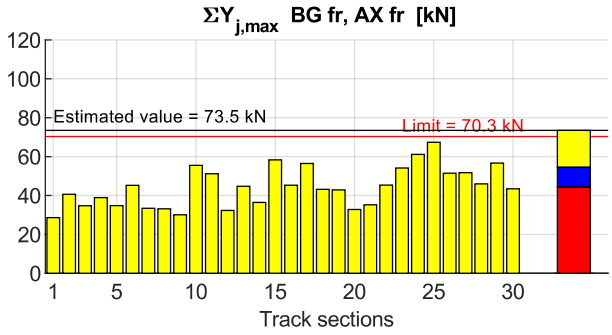

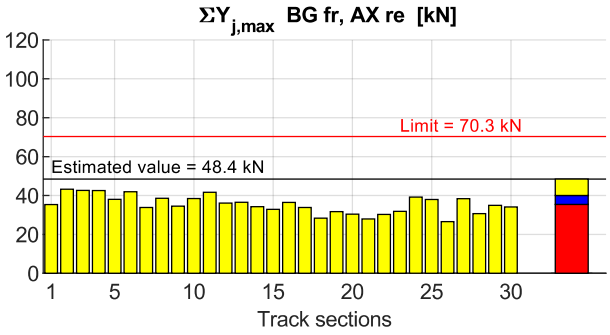

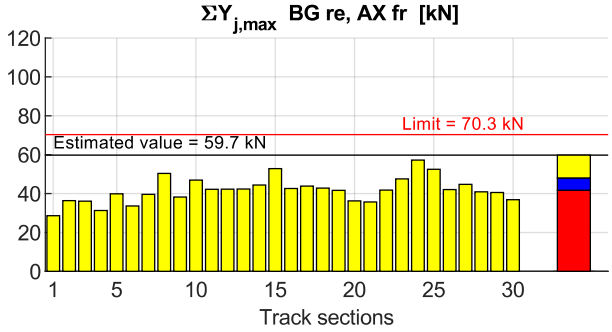

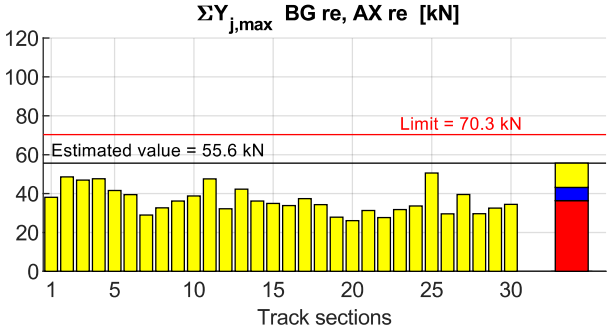

Quotient of lateral and vertical wheel force

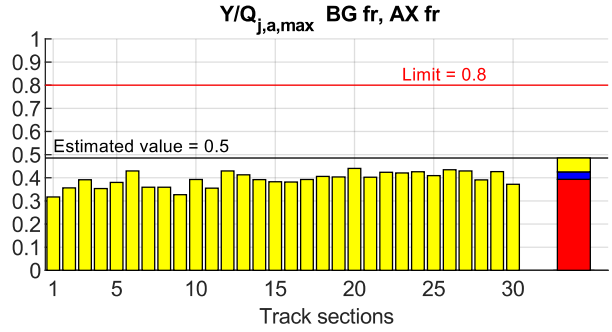

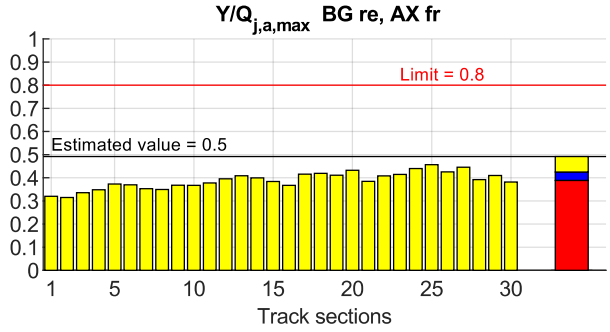

Very small radius curves, AIR 5 kNm	**Running safety**	Mean value Standard deviation

Sum of guiding forces

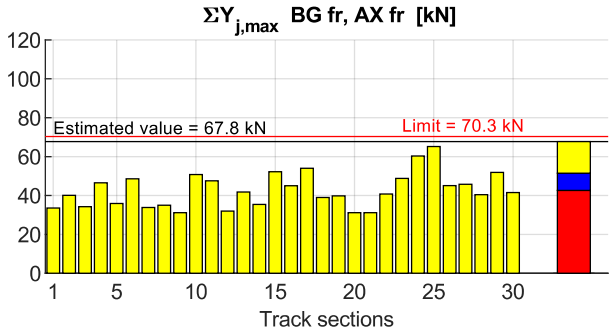

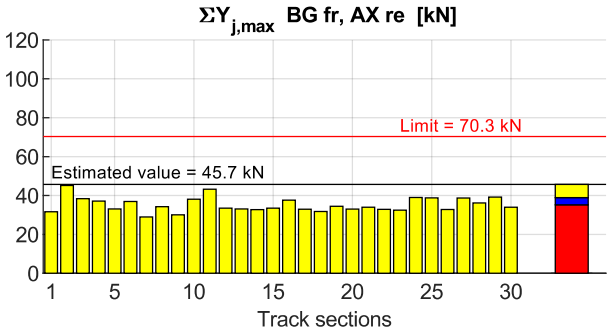

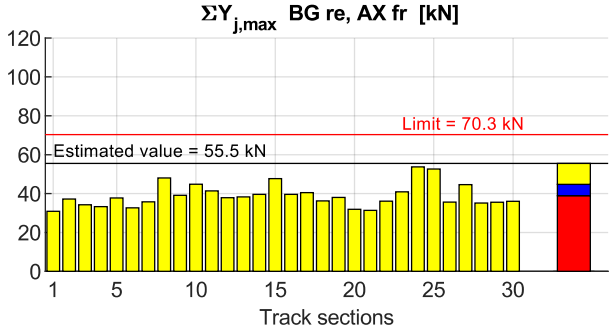

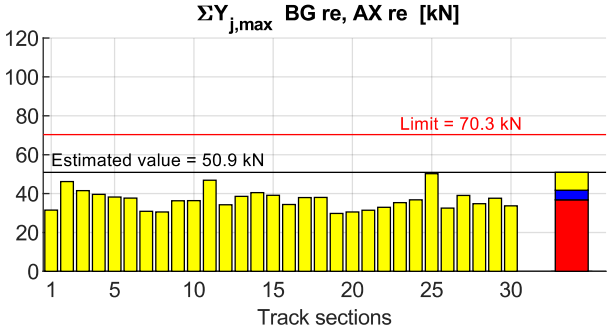

Quotient of lateral and vertical wheel force

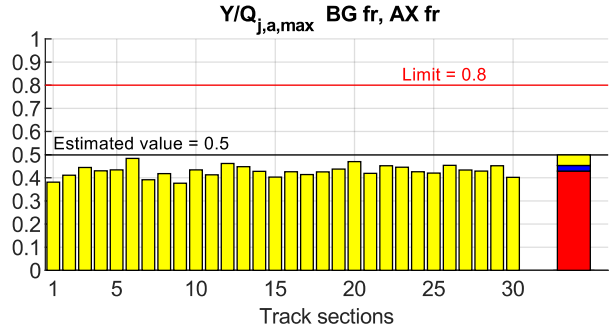

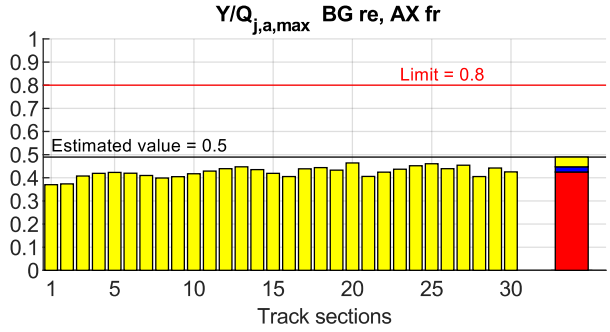

A.5.2 Track Loading Assessment

Tangent Track / Very Large Radius Curves (Test Zone 1)

Tangent track / very large radius curves, tare	**Track loading**	Mean value Standard deviation

Max. vertical wheel force

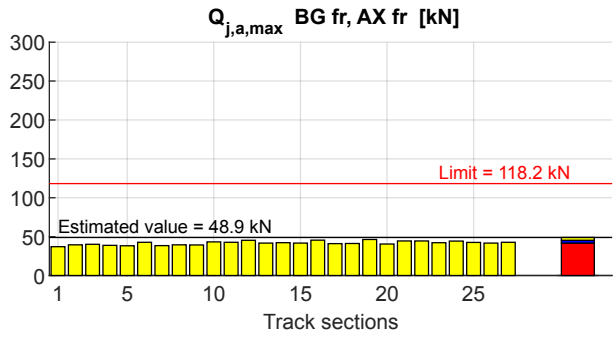

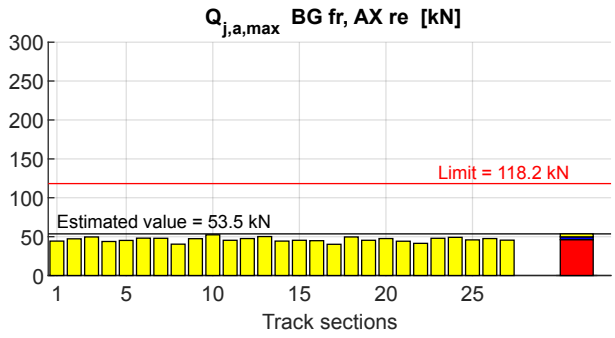

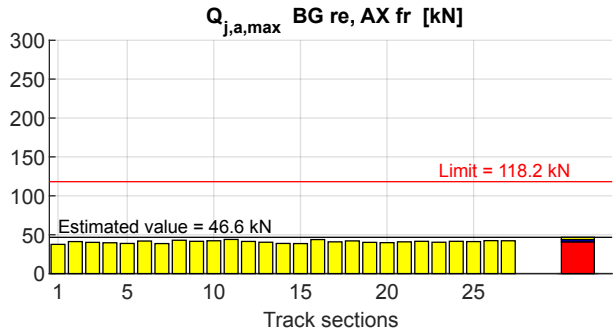

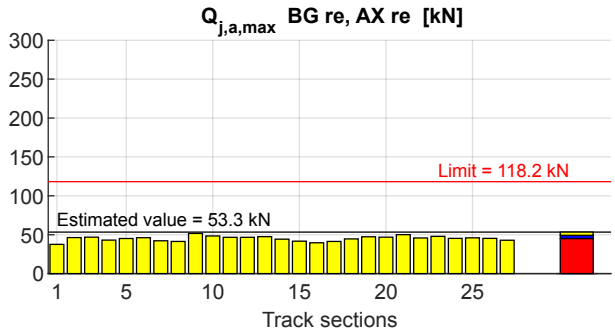

Tangent track / very large radius curves, laden	**Track loading**	Mean value Standard deviation

Max. vertical wheel force

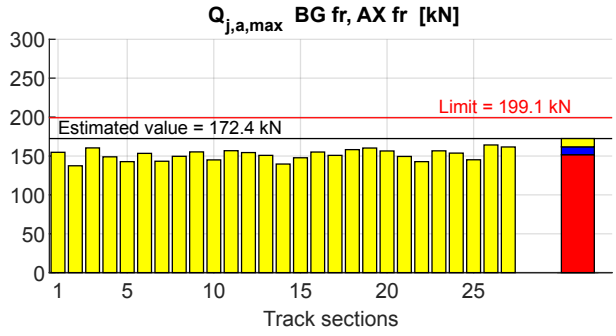

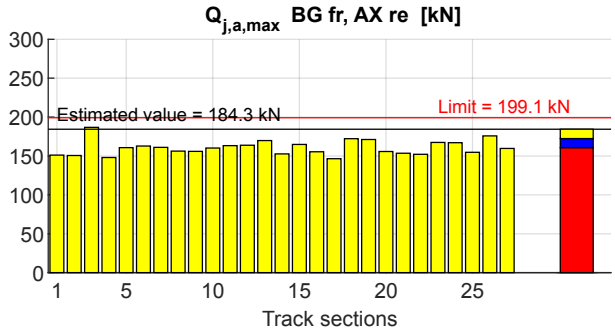

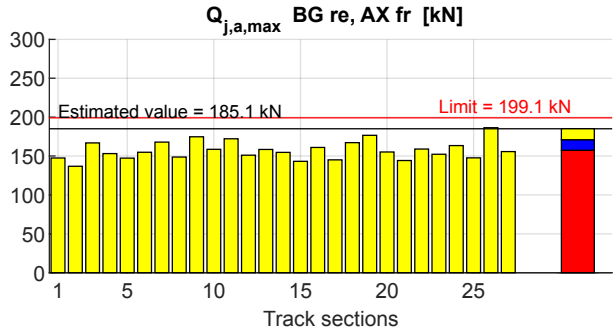

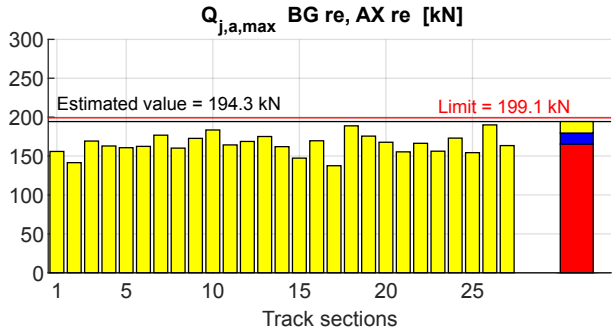

Large Radius Curves (Test Zone 2)

Large radius curves, tare	**Track loading**	Mean value Standard deviation

Quasi-static guiding force

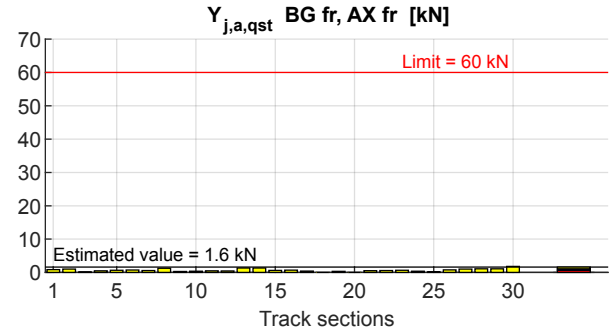

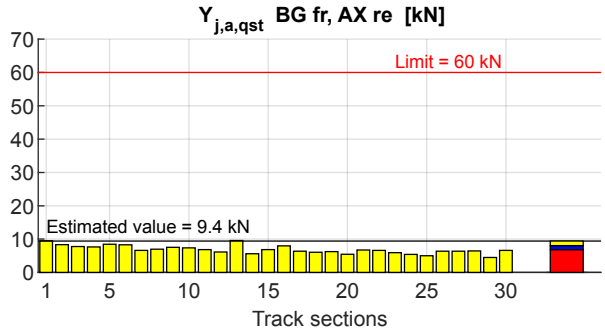

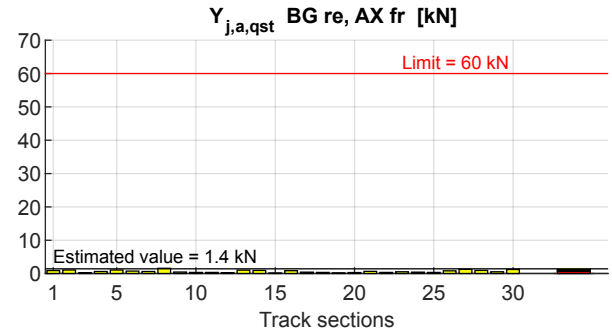

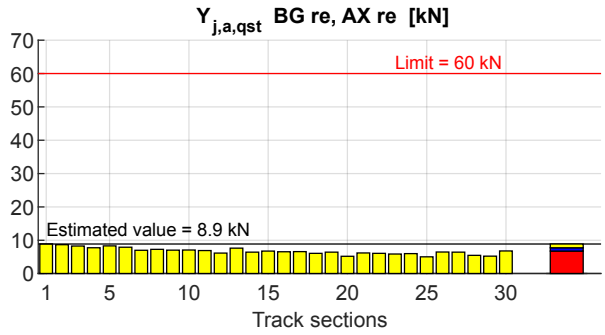

Quasi-static vertical wheel force

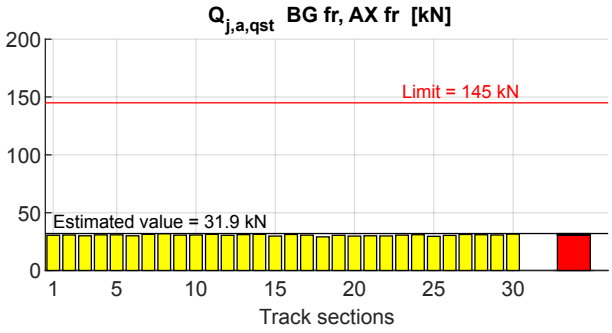

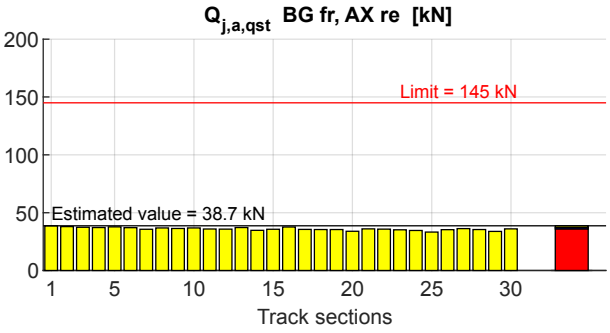

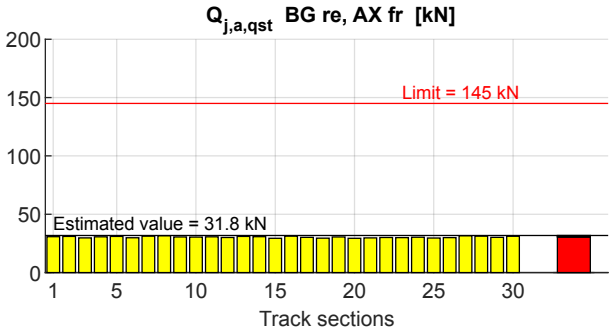

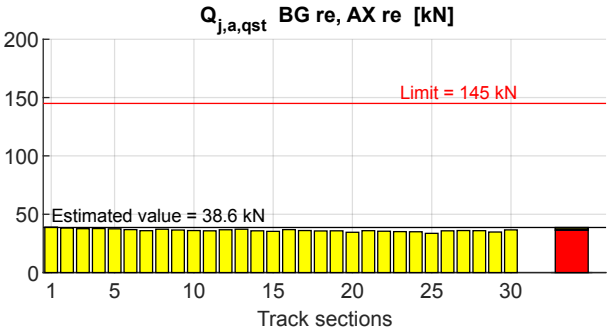

Large radius curves, tare	**Track loading**	Mean value Standard deviation

Max. vertical wheel force

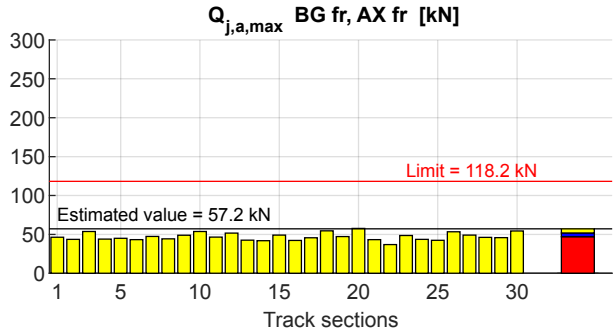

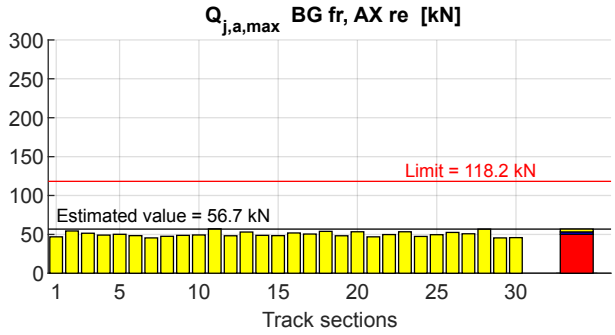

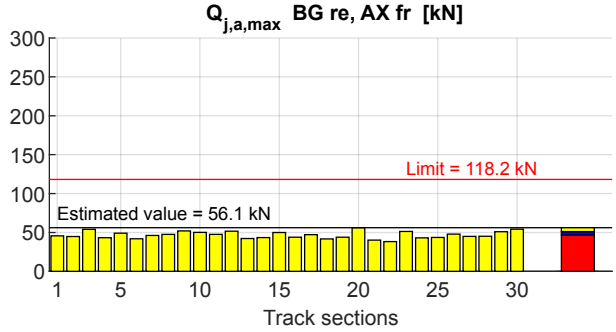

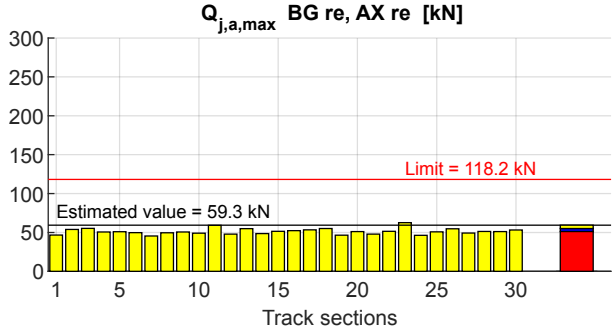

Large radius curves, laden	**Track loading**	Mean value Standard deviation

Quasi-static guiding force

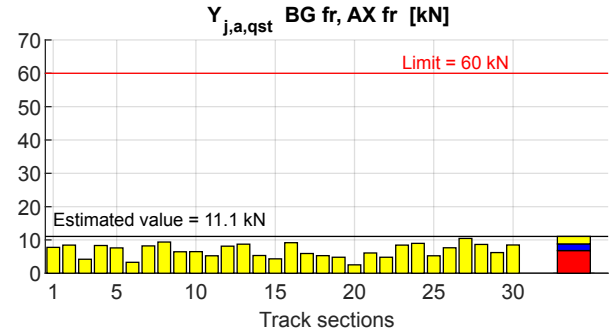

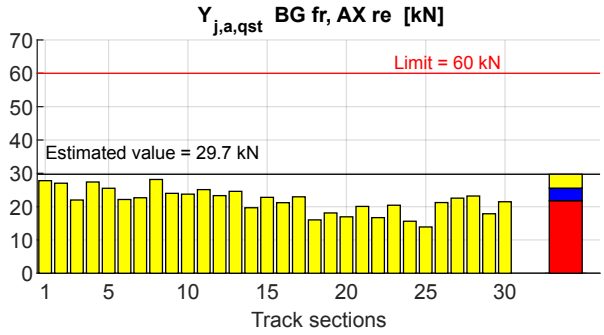

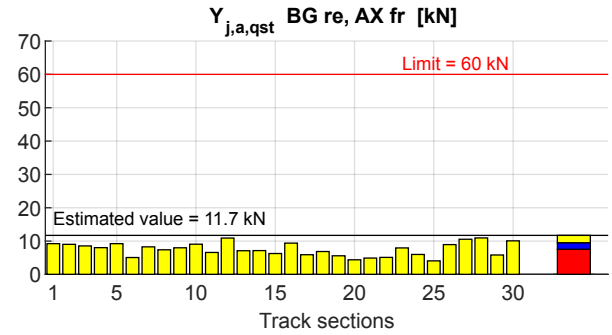

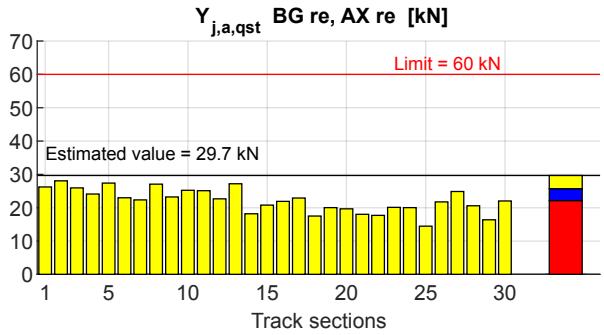

Quasi-static vertical wheel force

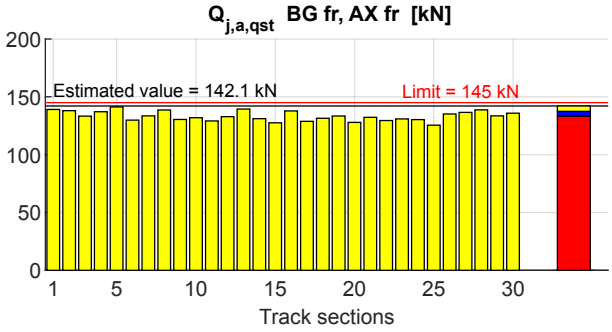

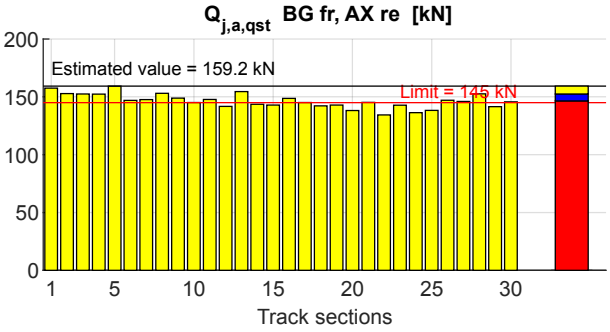

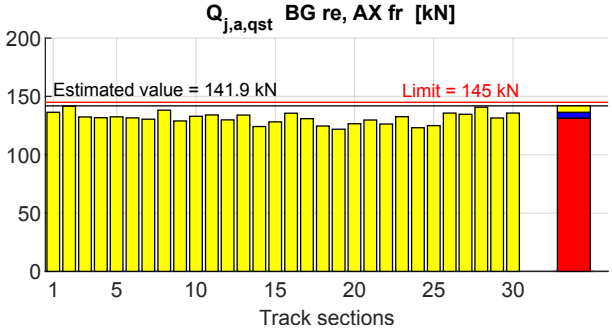

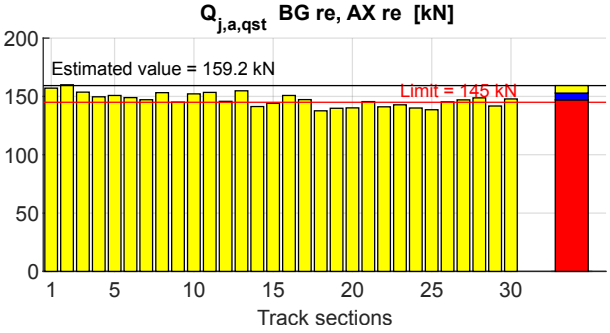

Large radius curves, laden	**Track loading**	Mean value Standard deviation

Max. vertical wheel force

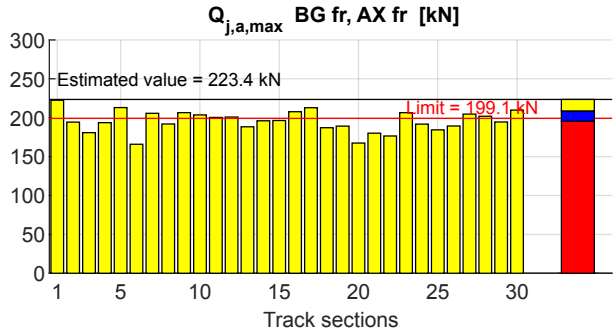

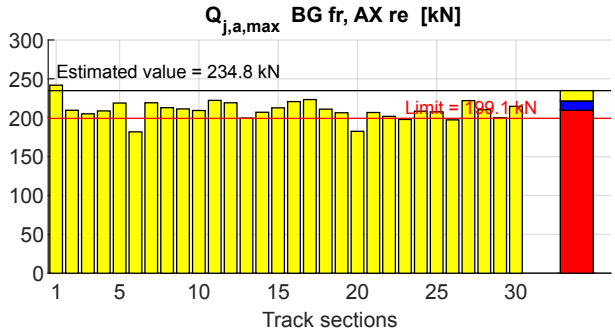

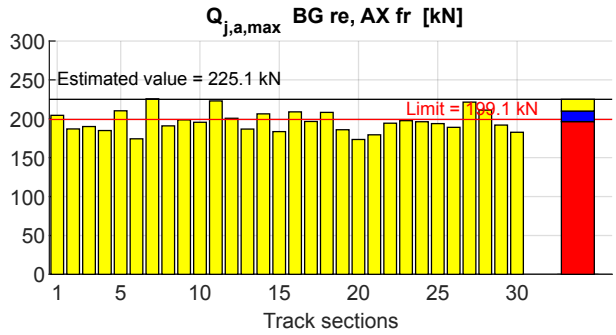

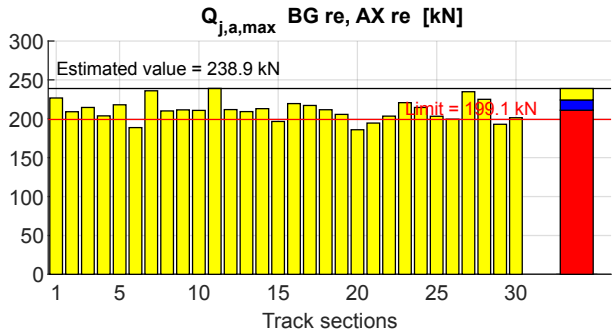

Large radius curves AIR 10 kNm	**Track loading**	Mean value Standard deviation

Quasi-static guiding force

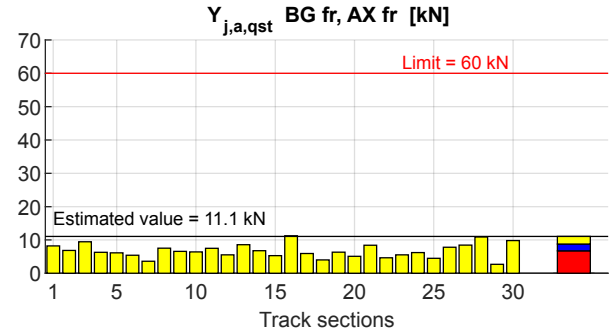

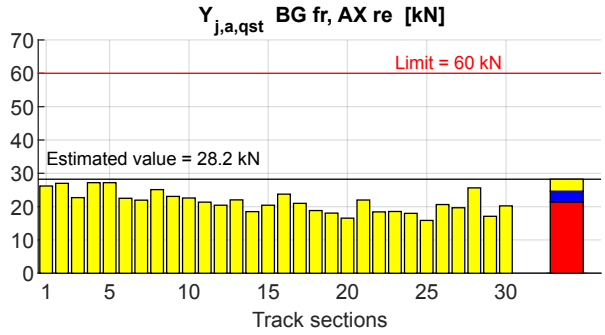

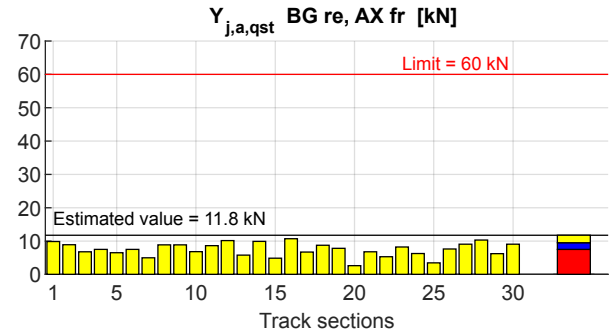

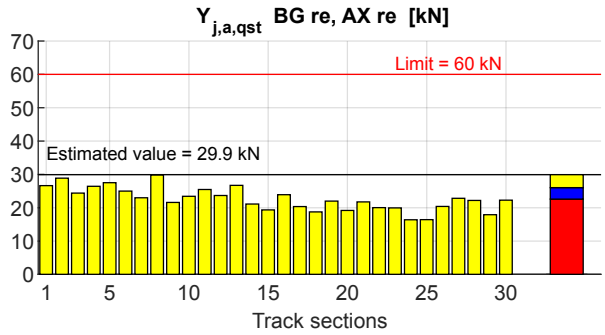

Quasi-static vertical wheel force

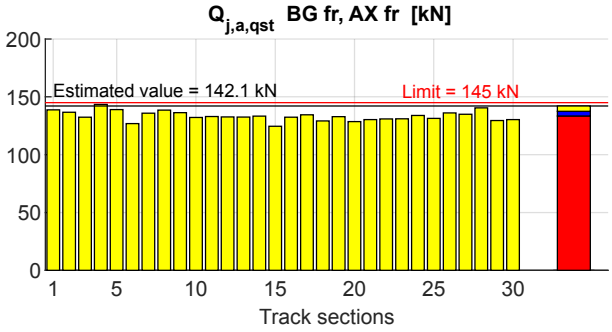

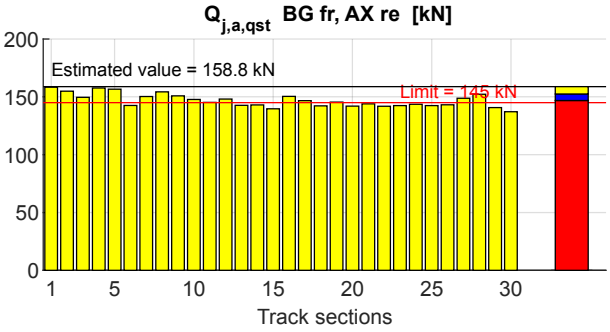

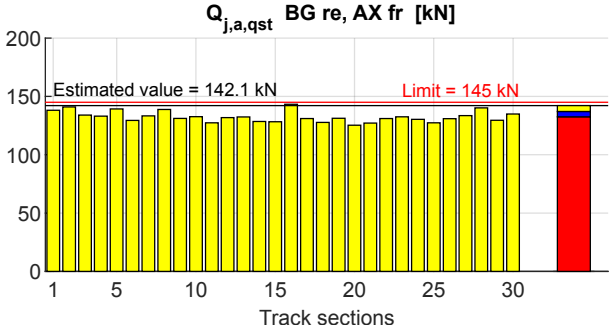

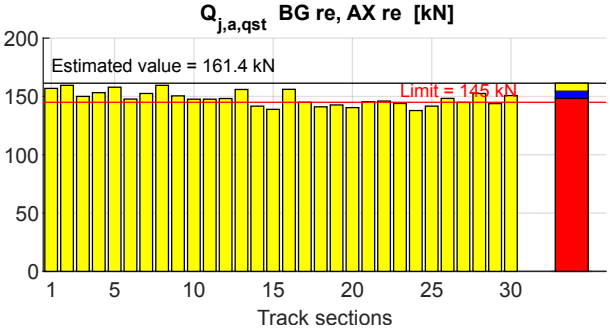

Large radius curves AIR 10 kNm	**Track loading**	Mean value Standard deviation

Max. vertical wheel force

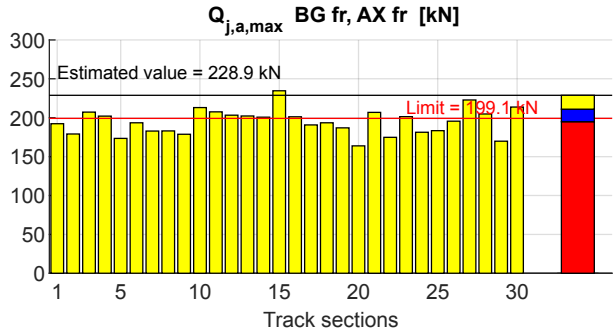

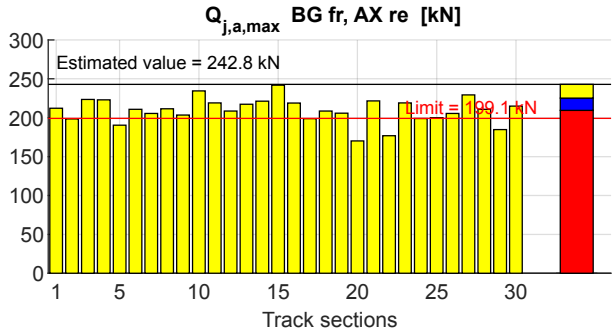

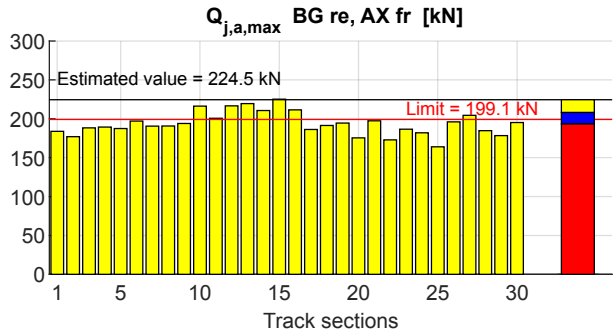

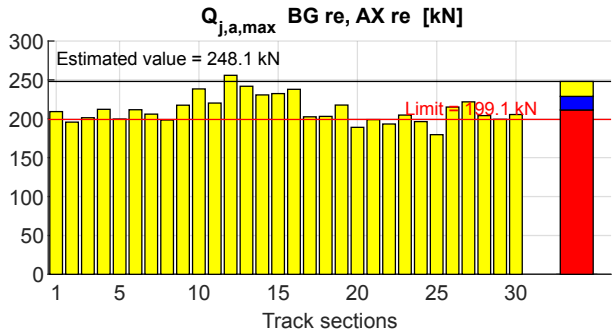

Large radius curves AIR 5 kNm	**Track loading**	Mean value Standard deviation

Quasi-static guiding force

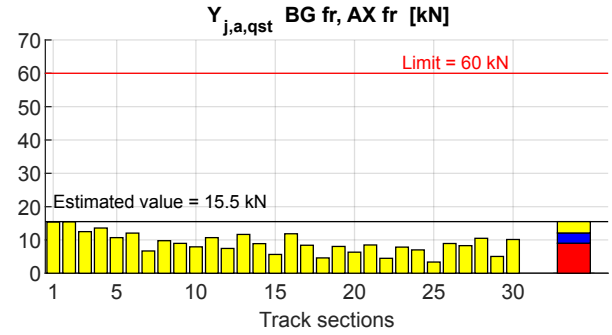

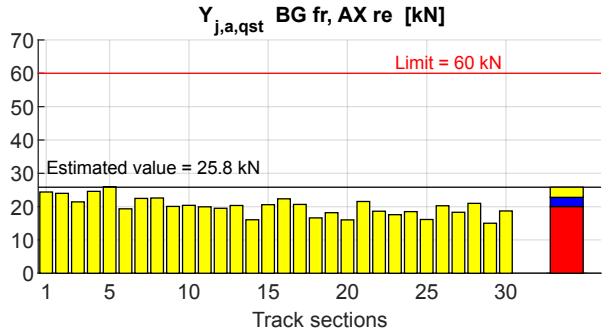

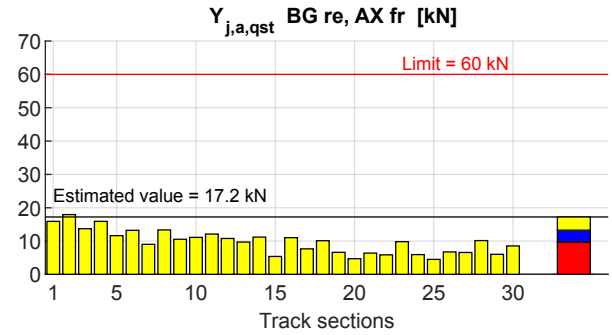

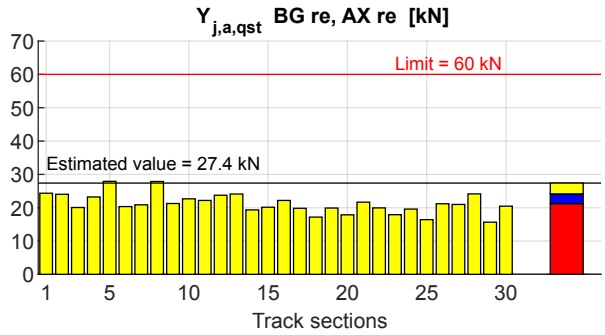

Quasi-static vertical wheel force

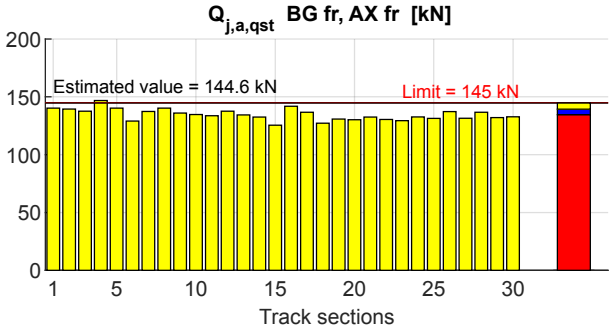

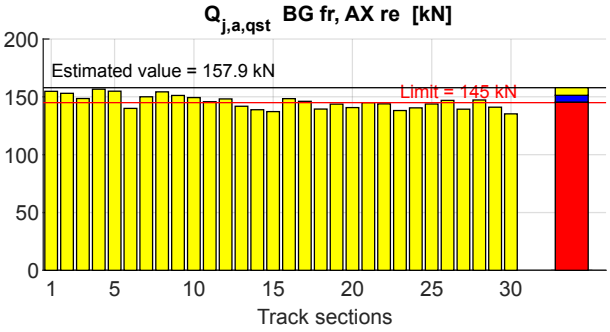

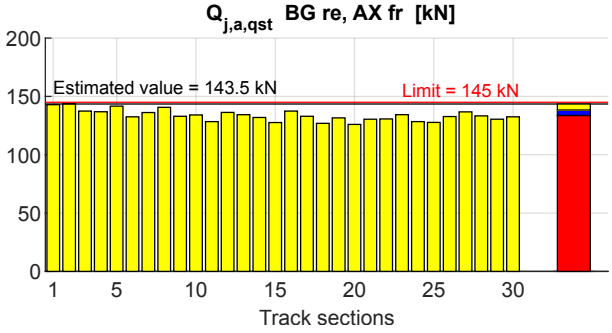

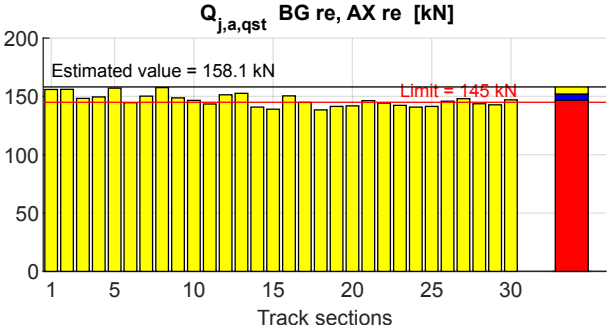

Large radius curves AIR 5 kNm	**Track loading**	Mean value Standard deviation

Max. vertical wheel force

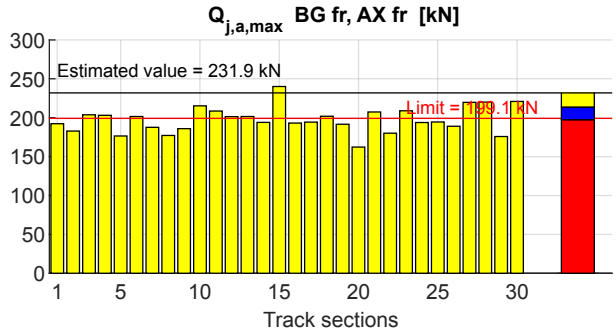

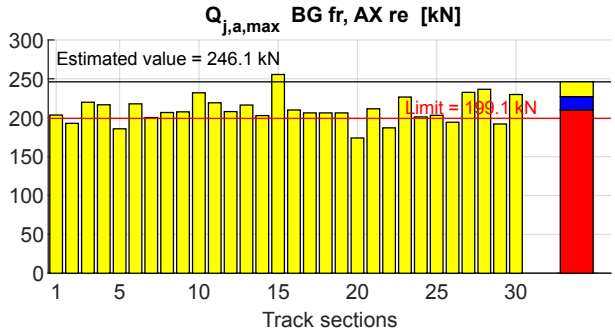

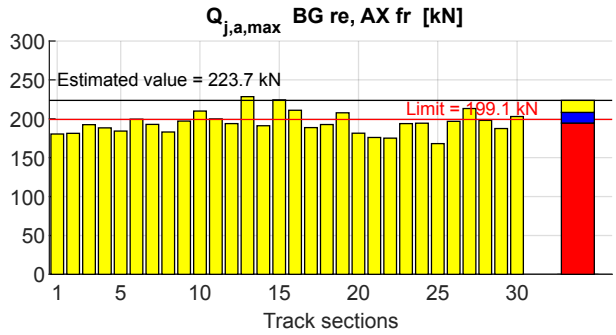

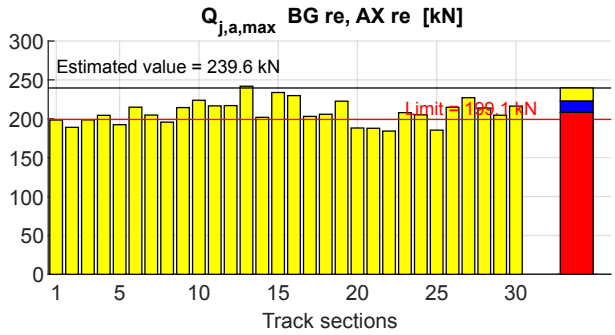

Small Radius Curves (Test Zone 3)

Small radius curves, tare	**Track loading**	Mean value Standard deviation

Quasi-static guiding force

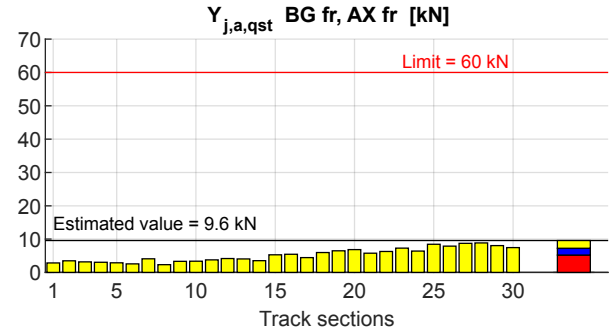

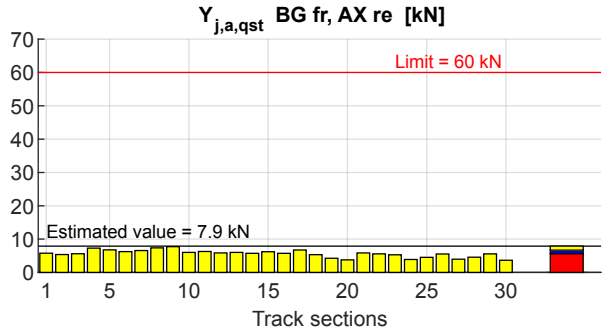

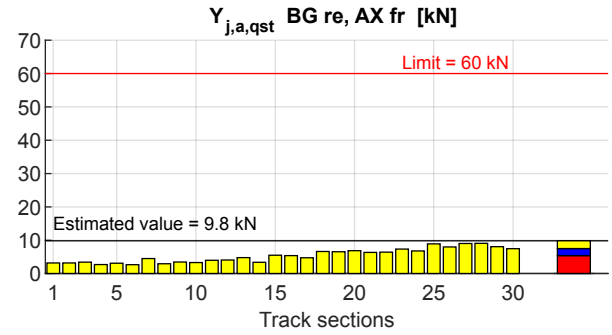

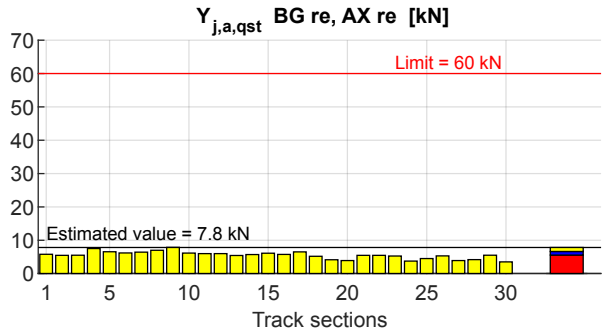

Quasi-static vertical wheel force

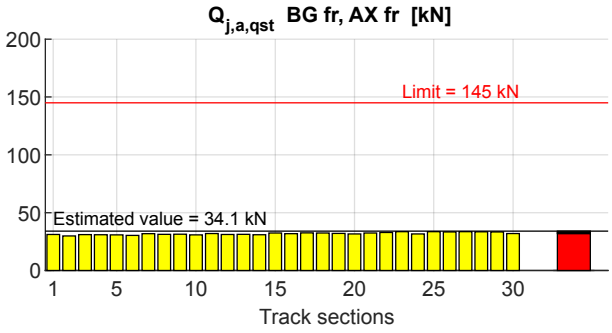

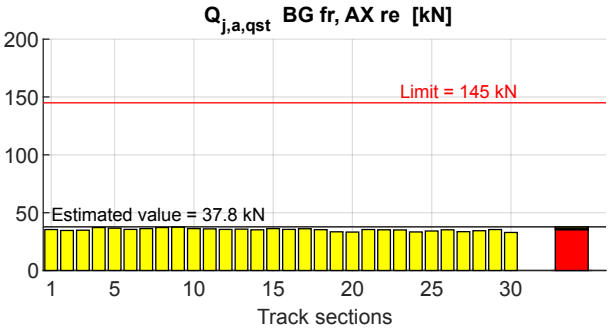

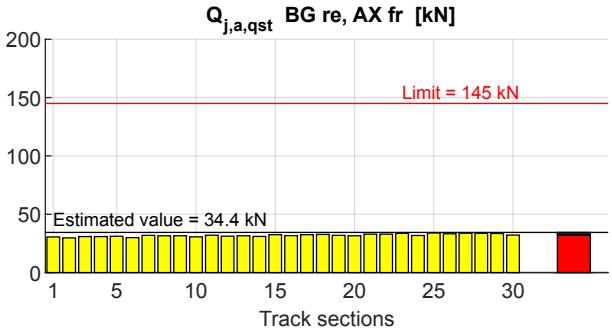

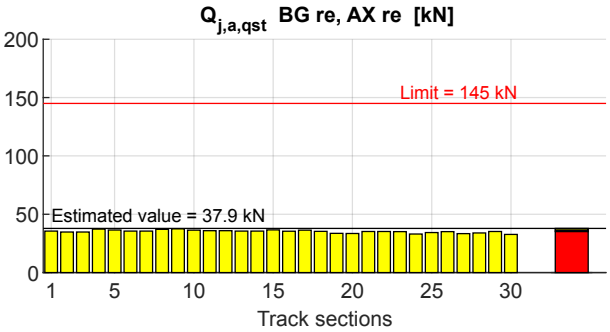

Small radius curves, tare	**Track loading**	Mean value Standard deviation

Max. vertical wheel force

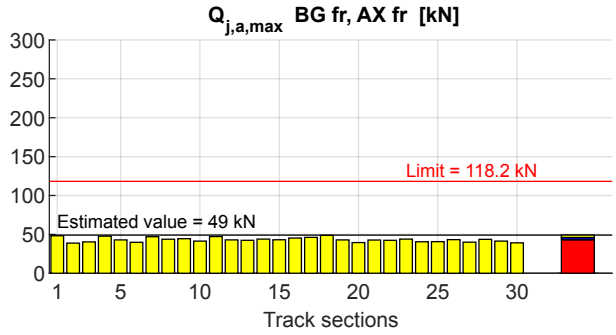

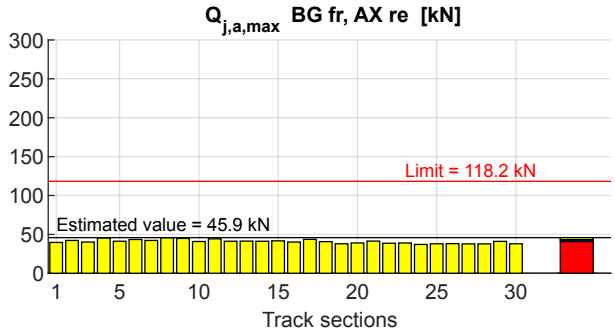

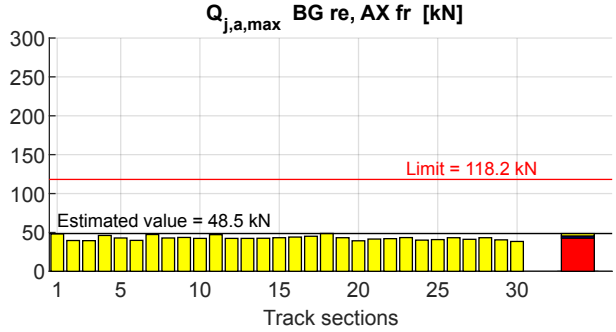

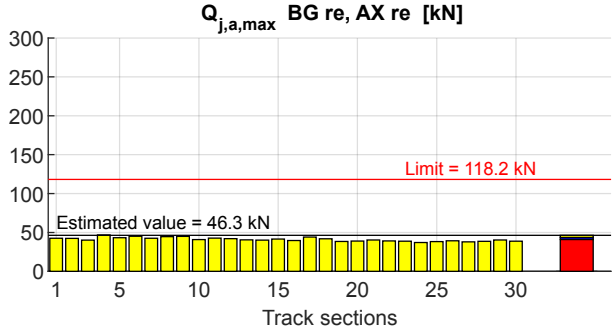

Small radius curves, laden	**Track loading**	Mean value Standard deviation

Quasi-static guiding force

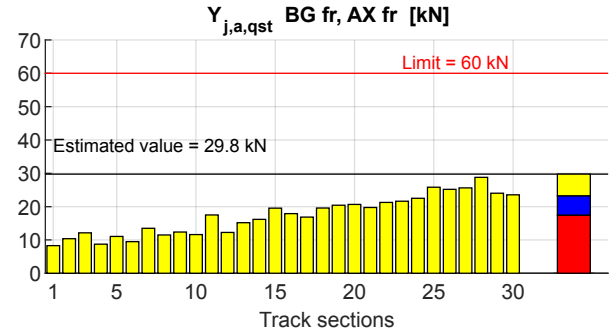

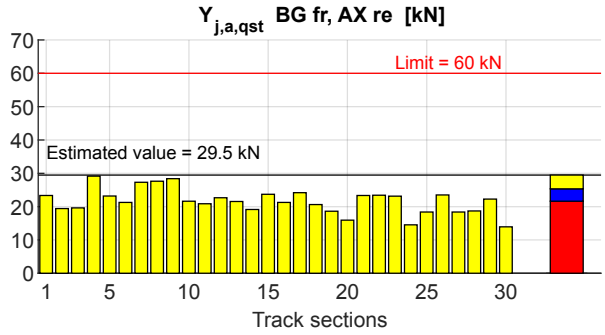

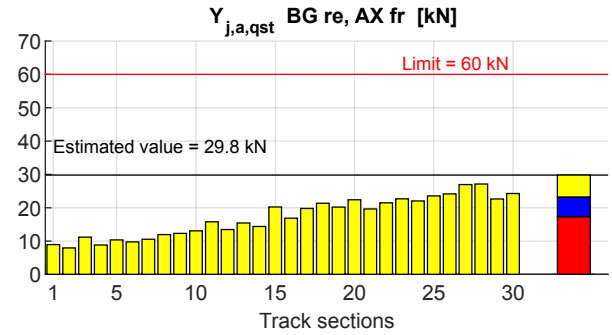

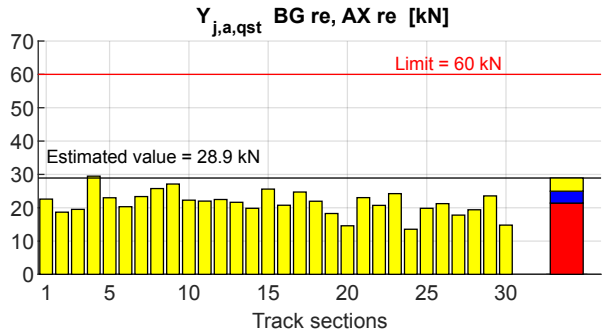

Quasi-static vertical wheel force

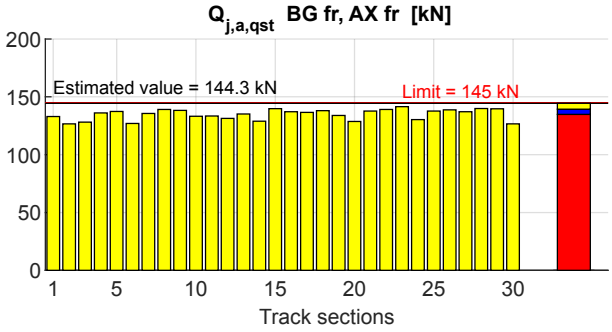

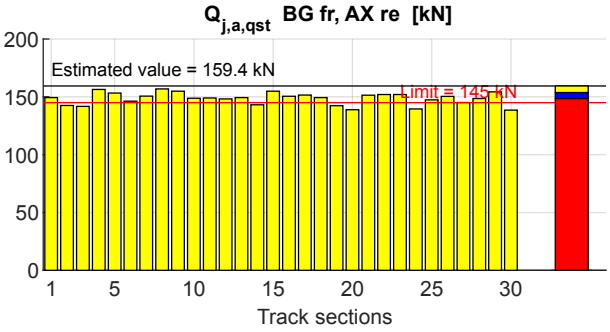

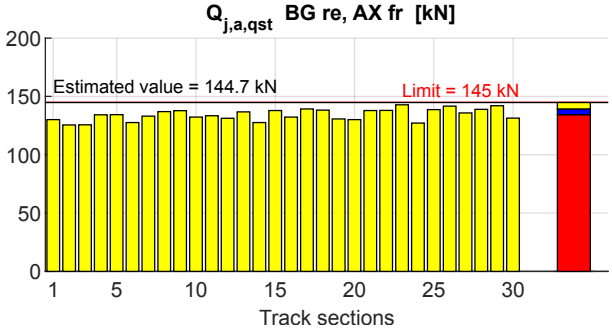

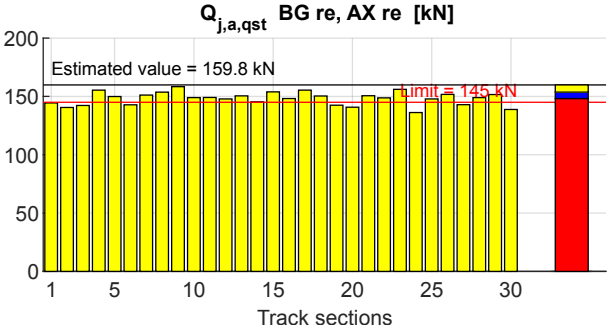

Small radius curves, laden	**Track loading**	Mean value Standard deviation

Max. vertical wheel force

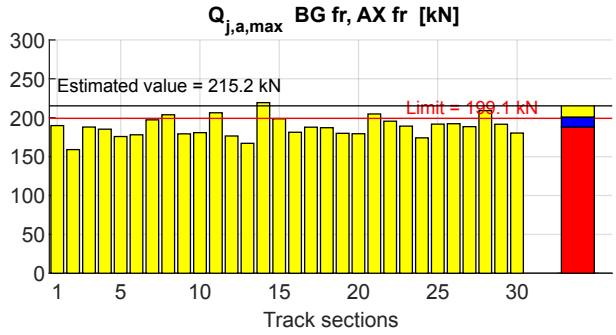

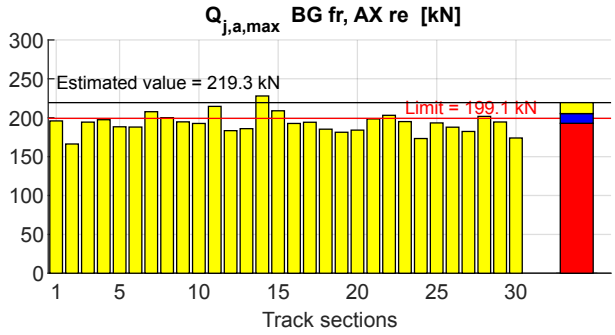

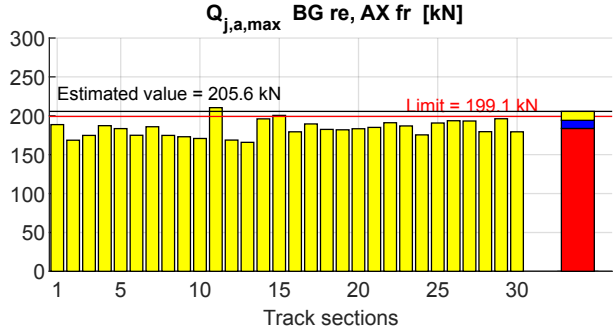

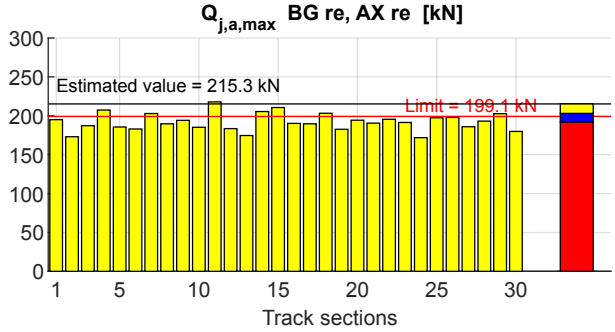

Very Small Radius Curves (Test Zone 4)

Very small radius curves, tare	**Track loading**	Mean value Standard deviation

Quasi-static guiding force

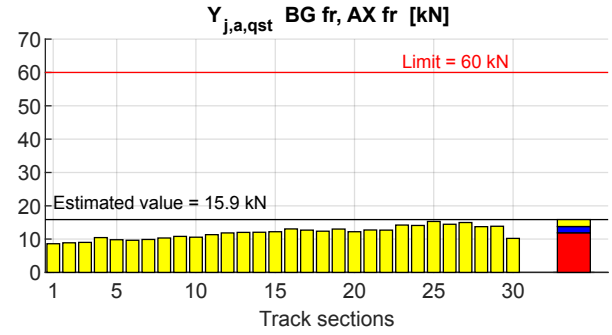

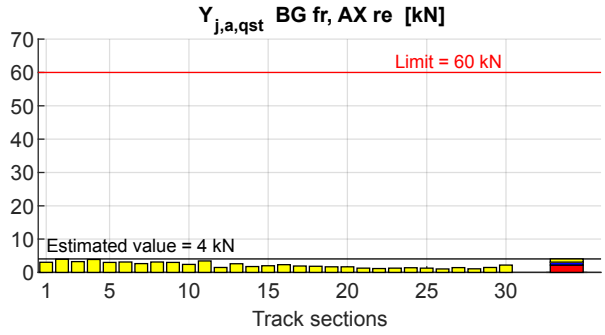

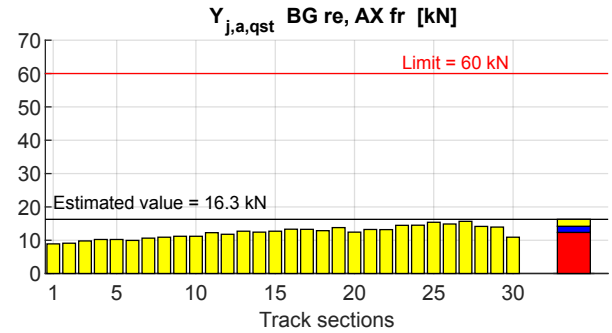

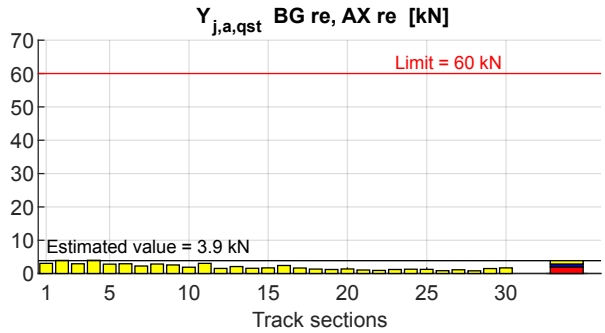

Quasi-static vertical wheel force

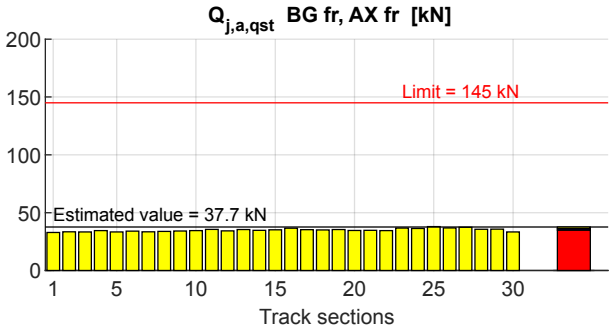

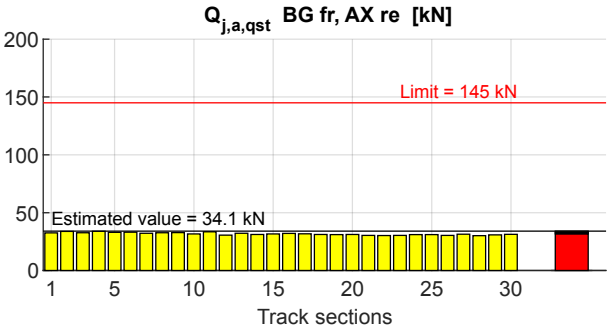

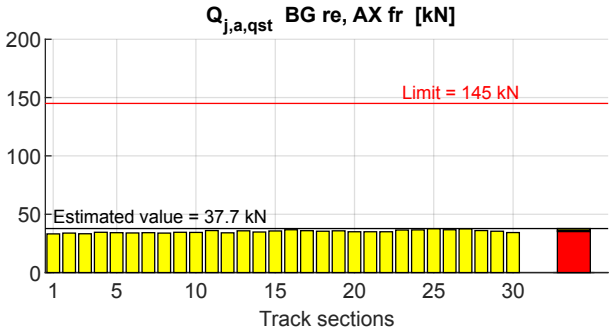

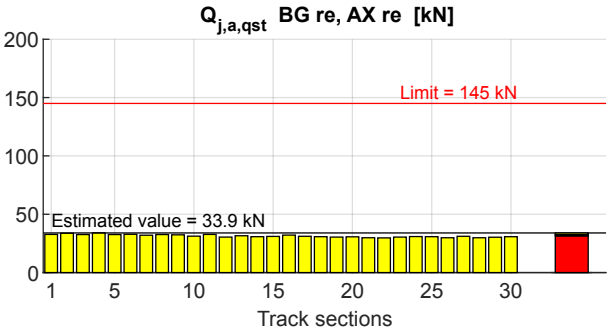

Very small radius curves, tare	**Track loading**	Mean value Standard deviation

Max. vertical wheel force

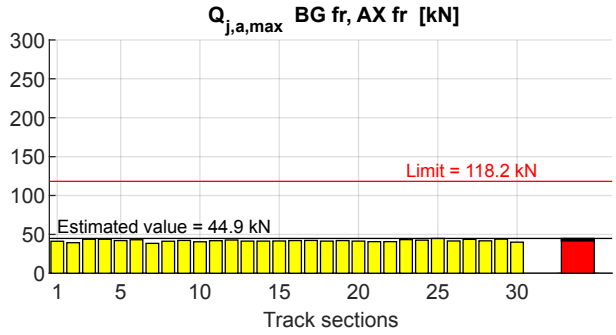

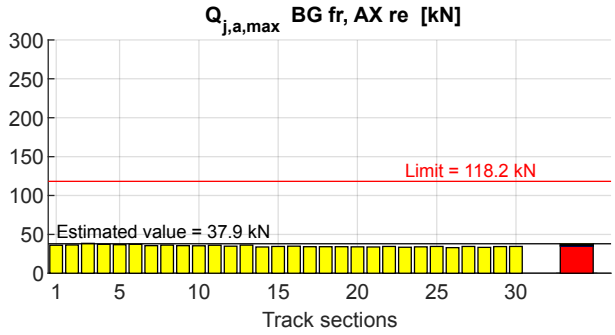

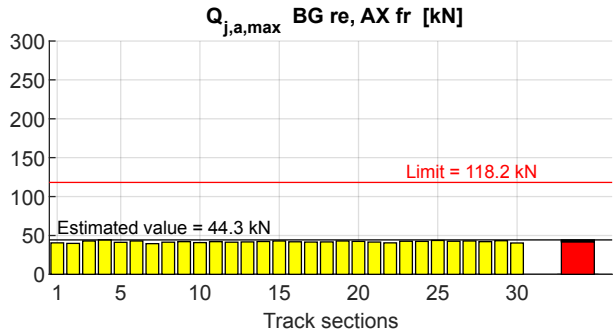

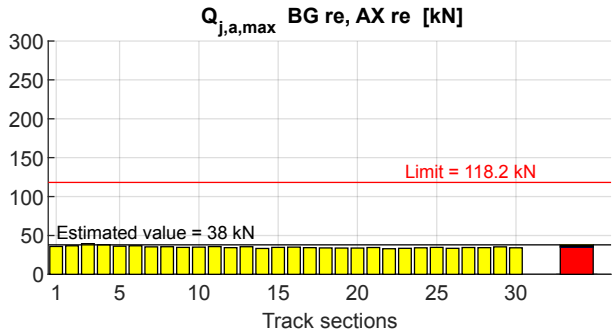

Very small radius curves, laden	**Track loading**	Mean value Standard deviation

Quasi-static guiding force

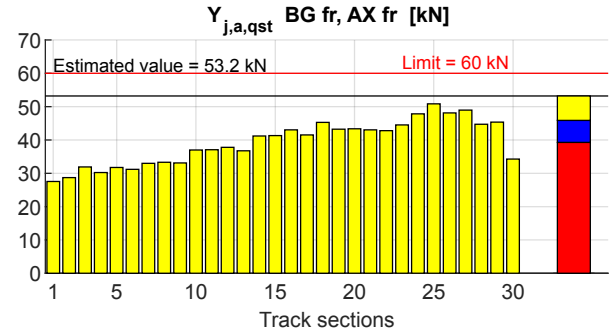

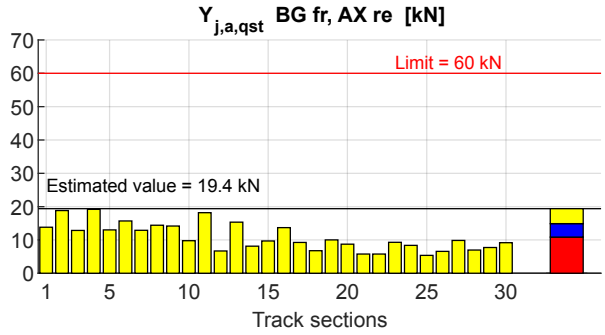

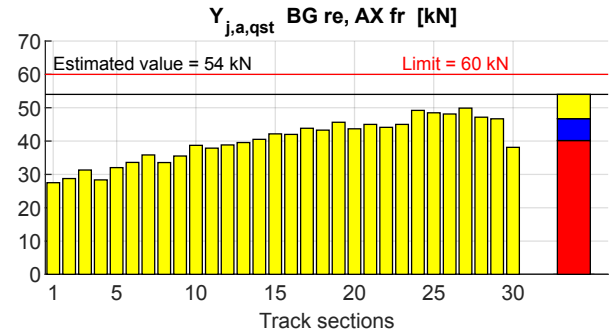

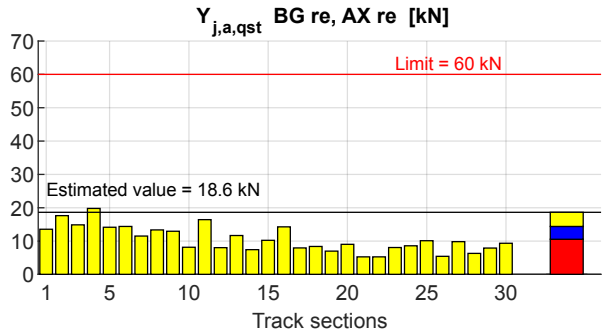

Quasi-static vertical wheel force

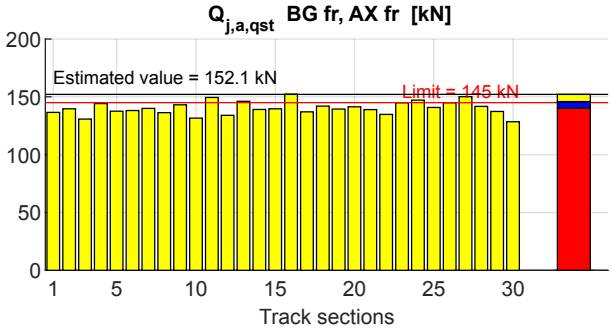

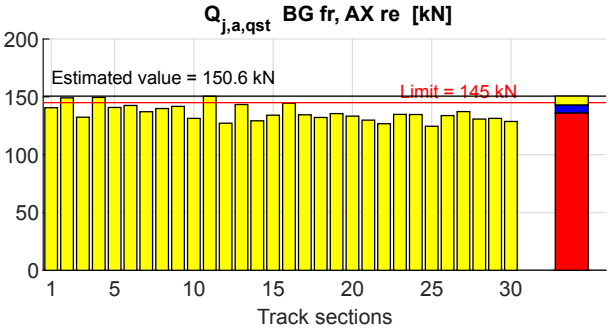

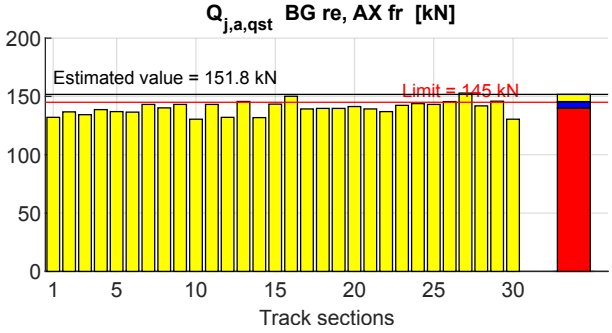

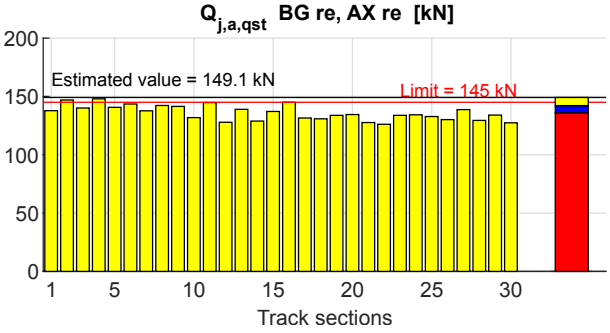

Very small radius curves, laden	**Track loading**	Mean value Standard deviation

Max. vertical wheel force

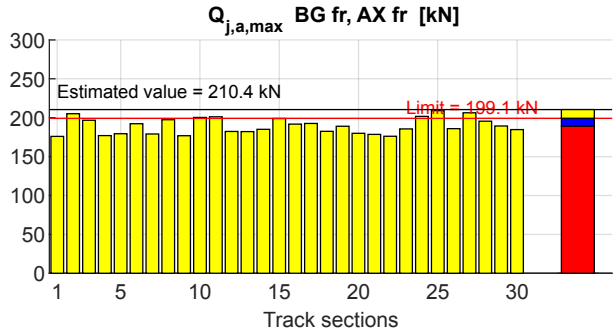

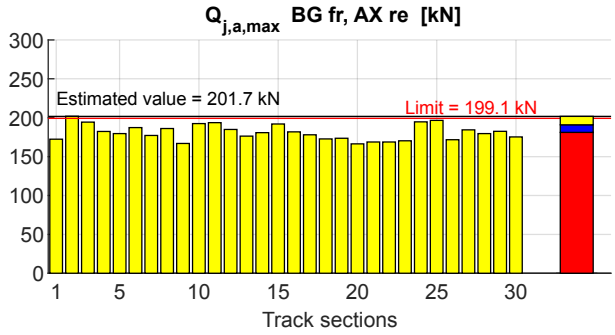

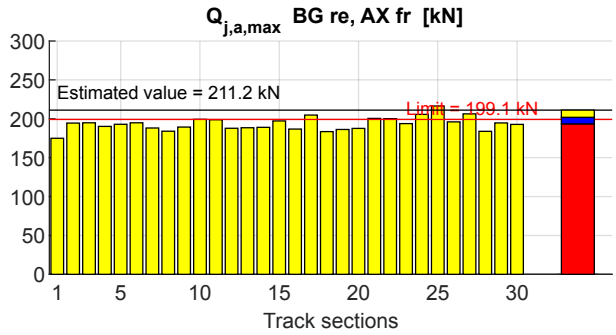

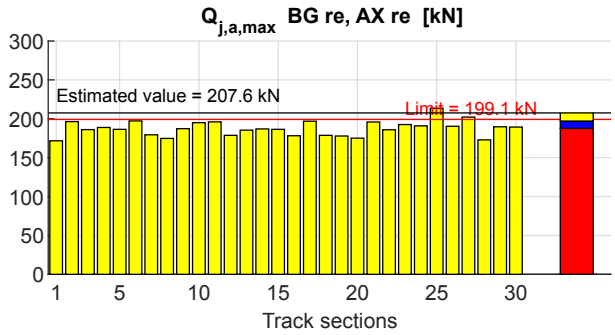

Very small radius curves, AIR 10 kNm	**Track loading**	Mean value Standard deviation

Quasi-static guiding force

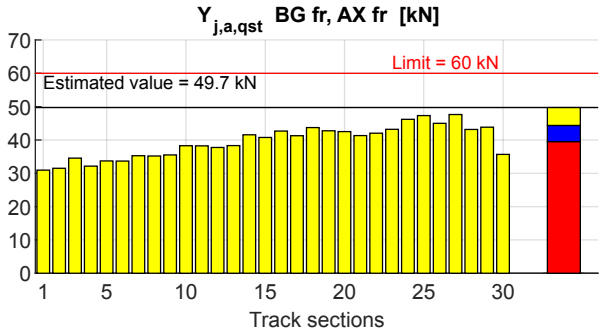

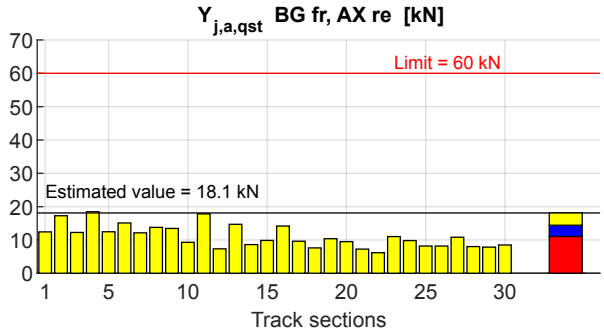

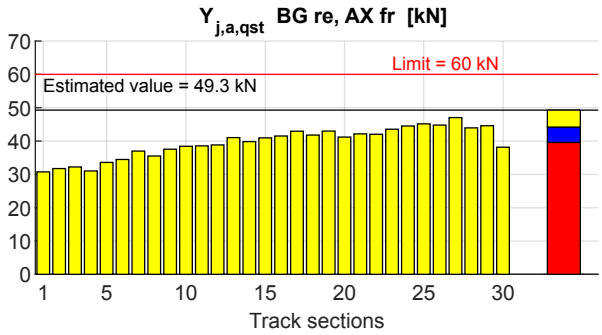

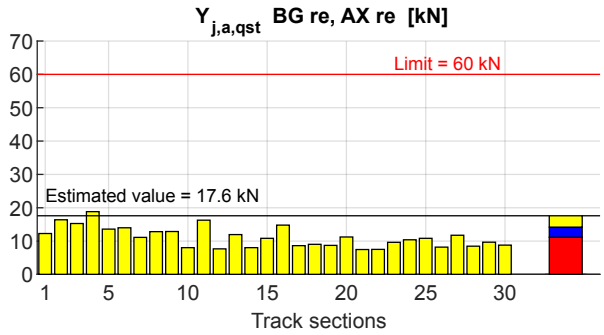

Quasi-static vertical wheel force

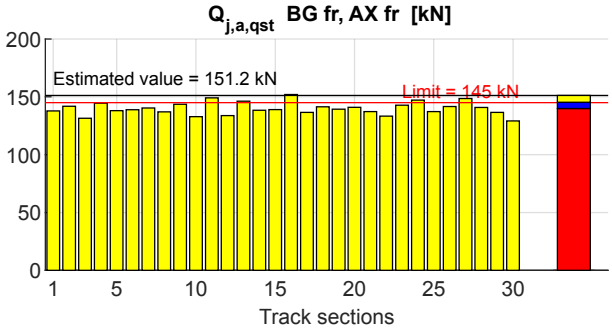

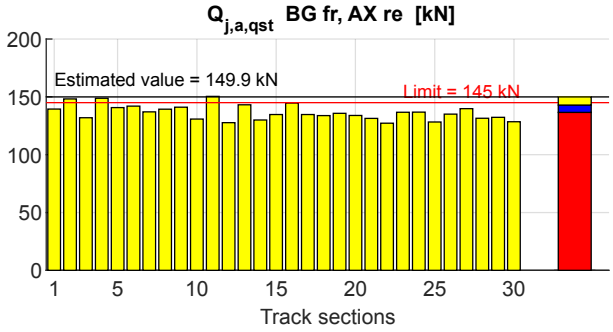

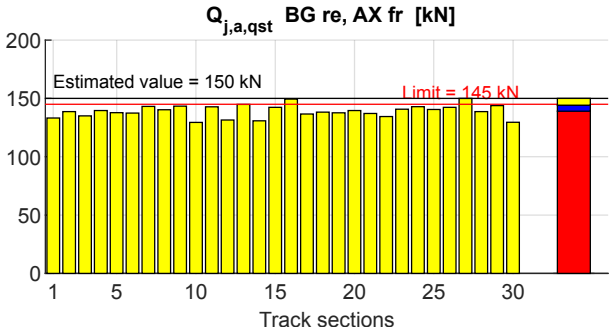

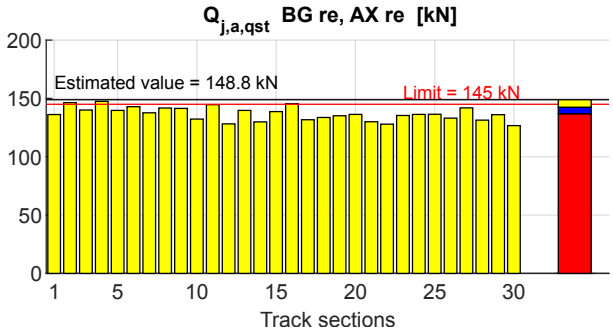

Very small radius curves, AIR 10 kNm	**Track loading**	Mean value Standard deviation

Max. vertical wheel force

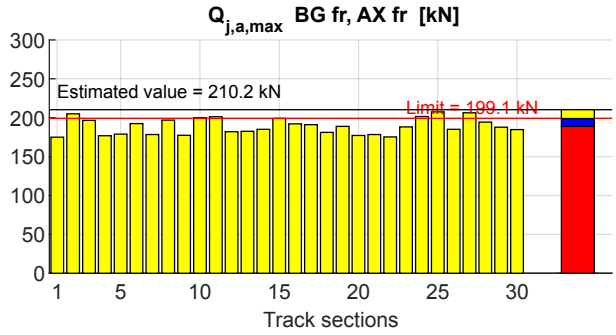

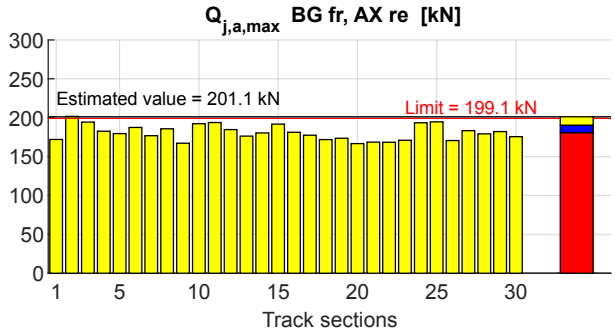

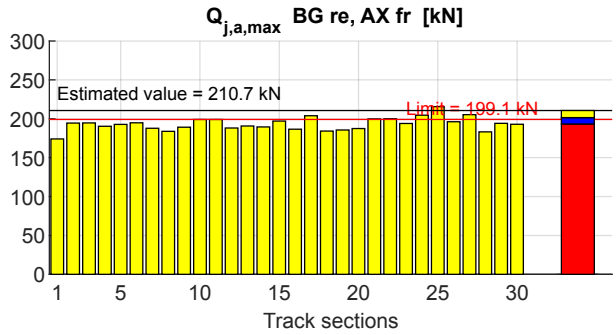

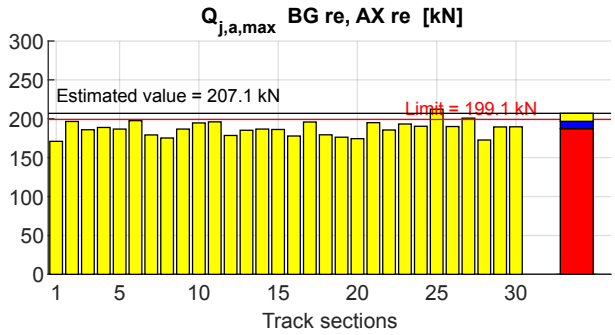

Very small radius curves, AIR 5 kNm	**Track loading**	Mean value Standard deviation

Quasi-static guiding force

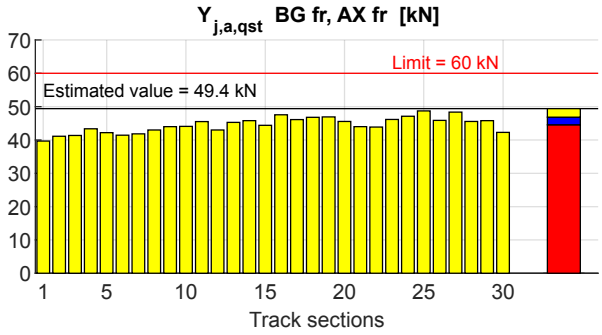

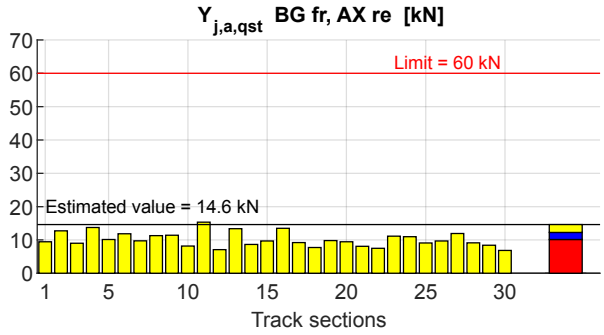

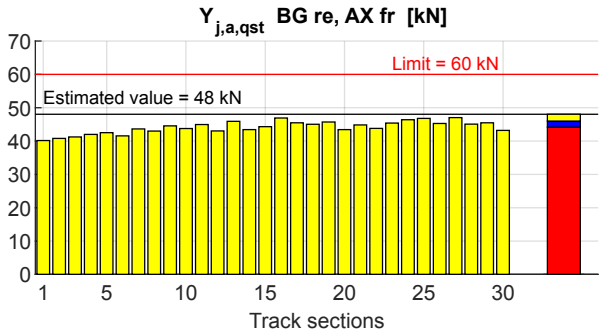

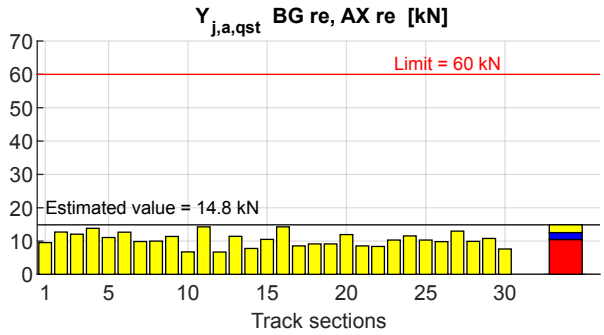

Quasi-static vertical wheel force

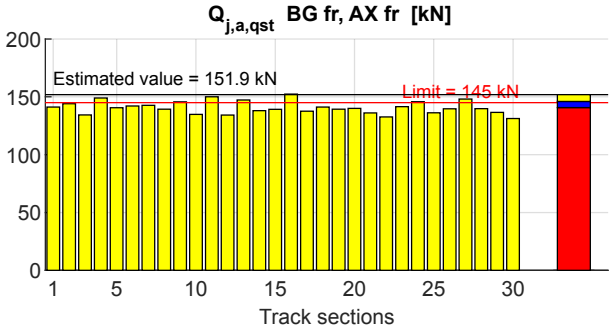

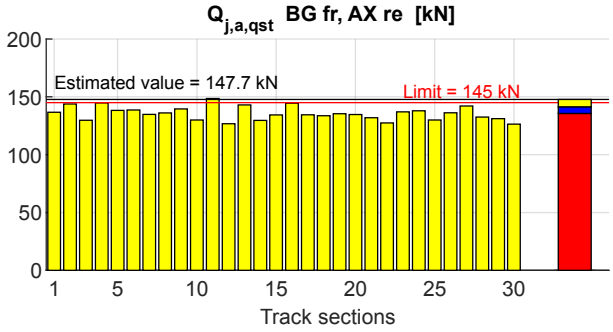

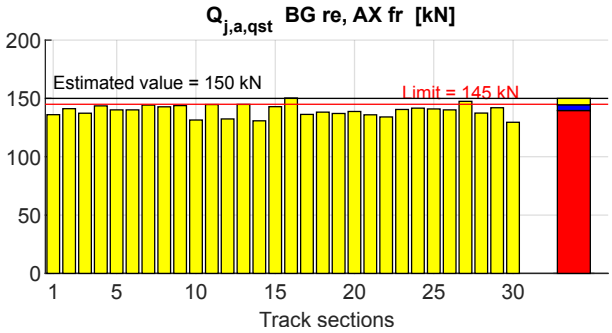

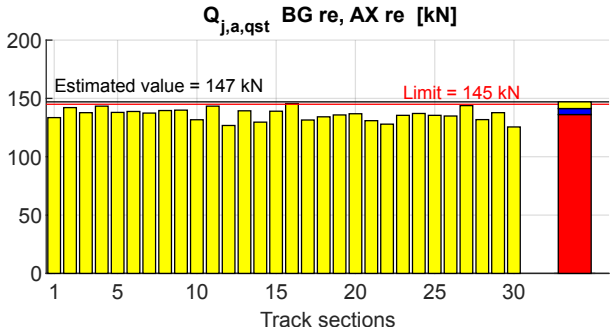

Very small radius curves, AIR 5 kNm	**Track loading**	Mean value Standard deviation

Max. vertical wheel force

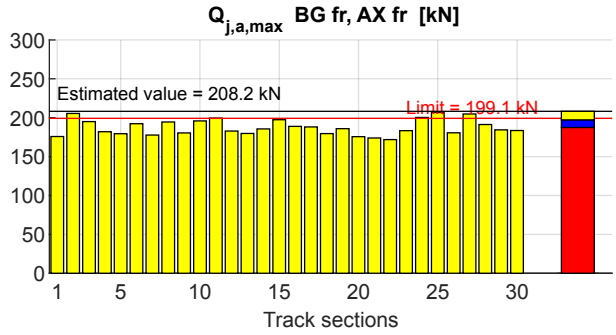

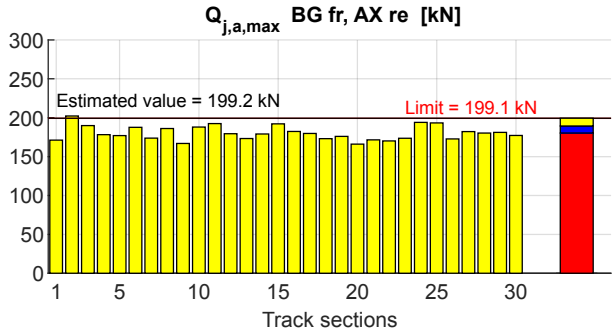

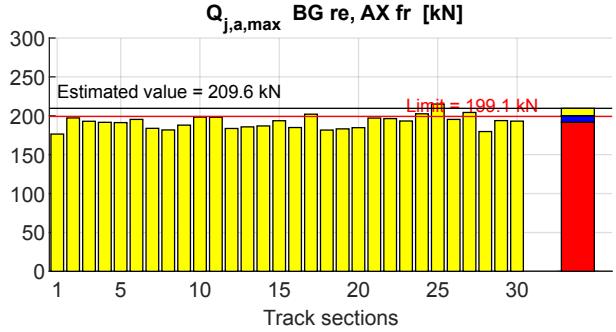

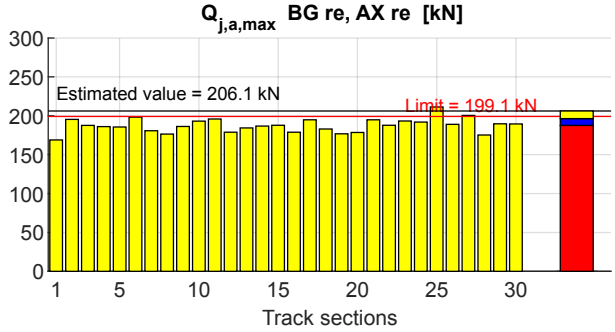

References

[1] R.R. Craig, M.C.C. Bampton: Coupling of substructures for dynamic analyses, AIAA Journal, 6, 1313-1319, 1968.

[2] X. Quost, M. Sebes, A. Eddhahak, J.-B. Ayasse, H. Chollet, P.-E. Gautier, F. Thouverez: Assessment of a semi-Hertzian method for determination of wheel-rail contact patch, Vehicle System Dynamics, Vol. 44, No. 10, 789-814, 2006.

[3] B. Kurzeck: Entwicklung eines modular und flexibel aufgebauten Drehgestellüberwachungs- und Diagonsesystems in Fahrwerken von Schienenfahrzeugen, ZIM-Projekt RailCM Arbeitspaket 6: Simulationsmodellbeschreibung, Institut für Robotik und Mechatronik, DLR, 2011.

[4] P. Shackleton, Y. Bezin, D. Crosbee, P. Molyneux-Berry, A. Kaushal: Development of a new running gear for the Spectrum intermodal vehicle, Proceedings of the 24th IAVSD symposium on dynamics of vehicles on roads and tracks, Graz, Austria, 2015.

[5] A. Bracciali, G. Megna: Contact mechanics issues of a vehicle equipped with partially independenly rotating wheelsets, 10th International conference on contact mechanics CM2015, Colorado Springs, Colorado, USA, 2015.

[6] Deutsches Institut für Normung e.V.: Bahnanwendungen – Versuche und Simulationen für die Zulassung der fahrtechnischen Eigenschaften von Eisenbahnfahrzeugen – Fahrverhalten und stationäre Versuche, DIN EN 14363:2016, 2016.

[7] Knorr Bremse GmbH: Bremszangeneinheit C202772, engineering drawing, 2016.

[8] A. Bracciali, G. Megna: Inside frame bogies & AIR wheelset – a winning marriage, 10th international conference on railway bogies and running gears, Budapest, Hungary, 2016.

[9] A. Bracciali, G. Megna: Track friendliness of an innovative freight bogie, 11th international conference on contact mechanics and wear of rail-wheel systems, Delft, The Netherlands, 2018.

[10] G. Megna, H. Magalhaes, Y. Bezin, A. Bracciali: Running dynamics and contact mechanics comparison of two freight bogies running in plain line and through switches and crossings, Proceedings of the 26th IAVSD symposium on dynamics of vehicles on roads and tracks, Gothenburg, Sweden, 2019.

[11] A. Bracciali, G. Megna: A really innovative freight bogie, Proceedings of the bogie '19 conference, Budapest, Hungary, 2019.

[12] World Intellectual Property Organization: Two-axle railway bogie, WO 2020/115778 A1, 2020.

[13] ANSYS, Inc.: Connecting Bodies to Joints, Ansys Help, 2020: https://ansyshelp.ansys.com/account/secured?returnurl=/Views/Secured/corp/v191/ans_elem/Hlp_E_SOLID187.html

[14] ANSYS, Inc.: SOLID187 Element Description, Ansys Help, 2020: https://ansyshelp.ansys.com/account/secured?returnurl=/Views/Secured/corp/v191/ans_elem/Hlp_E_SOLID187.html

[15] Dassault Systemes Simulia Corp.: Simpack 2021.3 user assistance, software documentation, 2020.